JACS
JOURNAL OF THE AMERICAN CHEMICAL SOCIETY
pubs.acs.org/JACS
Article

Supramolecular Mechanism of Viral Envelope Disruption by Molecular Tweezers

Tatjana Weil,▲ Rüdiger Groß,▲ Annika Röcker,▲ Kenny Bravo-Rodriguez,▲ Christian Heid, Andrea Sowislok, My-Hue Le, Nelli Erwin, Mridula Dwivedi, Stephen M. Bart, Paul Bates, Lukas Wettstein, Janis A. Müller, Mirja Harms, Konstantin Sparrer, Yasser B. Ruiz-Blanco, Christina M. Stürzel, Jens von Einem, Sina Lippold, Clarissa Read, Paul Walther, Marco Hebel, Florian Kreppel, Frank-Gerrit Klärner, Gal Bitan, Michael Ehrmann, Tanja Weil, Roland Winter, Thomas Schrader,* James Shorter,* Elsa Sanchez-Garcia,* and Jan Münch*

Cite This: https://dx.doi.org/10.1021/jacs.0c06400

ABSTRACT: Broad-spectrum antivirals are powerful weapons against dangerous viruses where no specific therapy exists, as in the case of the ongoing SARS-CoV-2 pandemic. We discovered that a lysine- and arginine-specific supramolecular ligand (CLR01) destroys enveloped viruses, including HIV, Ebola, and Zika virus, and remodels amyloid fibrils in semen that promote viral infection. Yet, it is unknown how CLR01 exerts these two distinct therapeutic activities. Here, we delineate a novel mechanism of antiviral activity by studying the activity of tweezer variants: the "phosphate tweezer" CLR01, a "carboxylate tweezer" CLR05, and a "phosphate clip" PC. Lysine complexation inside the tweezer cavity is needed to antagonize amyloidogenesis and is only achieved by CLR01. Importantly, CLR01 and CLR05 but not PC form closed inclusion complexes with lipid head groups of viral membranes, thereby altering lipid orientation and increasing surface tension. This process disrupts viral envelopes and diminishes infectivity but leaves cellular membranes intact. Consequently, CLR01 and CLR05 display broad antiviral activity against all enveloped viruses tested, including herpesviruses, Measles virus, influenza, and SARS-CoV-2. Based on our mechanistic insights, we potentiated the antiviral, membrane-disrupting activity of CLR01 by introducing aliphatic ester arms into each phosphate group to act as lipid anchors that promote membrane targeting. The most potent ester modifications harbored unbranched C4 units, which engendered tweezers that were approximately one order of magnitude more effective than CLR01 and nontoxic. Thus, we establish the mechanistic basis of viral envelope disruption by specific tweezers and establish a new class of potential broad-spectrum antivirals with enhanced activity.

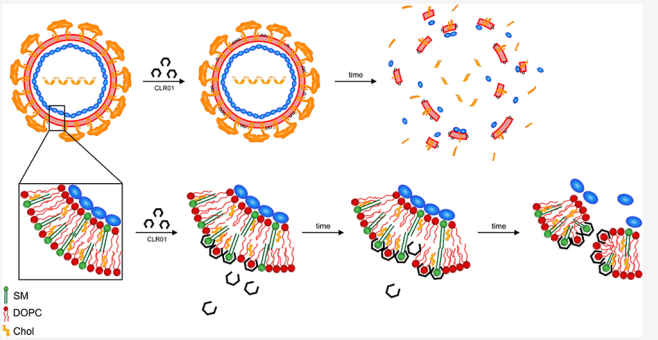

INTRODUCTION

Classical therapeutic strategies against viral infections focus primarily on inhibiting viral replication; in a "one bug−one drug" concept, a specific protease and polymerase inhibitor is developed for each virus. However, for an increasing number of new viruses, no treatment is available, and there is an urgent need for innovation. A new approach has recently emerged which targets the virions themselves. This strategy has the potential to achieve broad antiviral activities especially against the constant threat of zoonoses, which are a major issue as evidenced by the newly emerged coronavirus, SARS-CoV-2. It involves external interference with the membrane fusion process which is essential for all enveloped viruses.[1,2] Major avenues comprise inhibition of fusion proteins[3] (e.g., by antiviral peptides [AVPs][4] or protein disulfide isomerase [PDI] inhibitors[5]) and modulation of membrane properties such as integrity (e.g., by virolytic peptides[6]), fluidity (e.g., by polyunsaturated ER-targeting liposomes [PERLs][7]), or curvature (e.g., by rigid amphipathic fusion inhibitors [RAFIs][8]). Finally, membrane properties essential for fusion are influenced by lipid oxidation which can be brought about by type II photosensitizers that oxidize unsaturated phospholipids (e.g., certain amphiphilic thiazolidines[9]). The "molecular tweezers" described in this work also modulate membrane integrity, albeit in a very subtle way: they specifically recognize lipid head groups

Received: June 12, 2020
Published: September 14, 2020

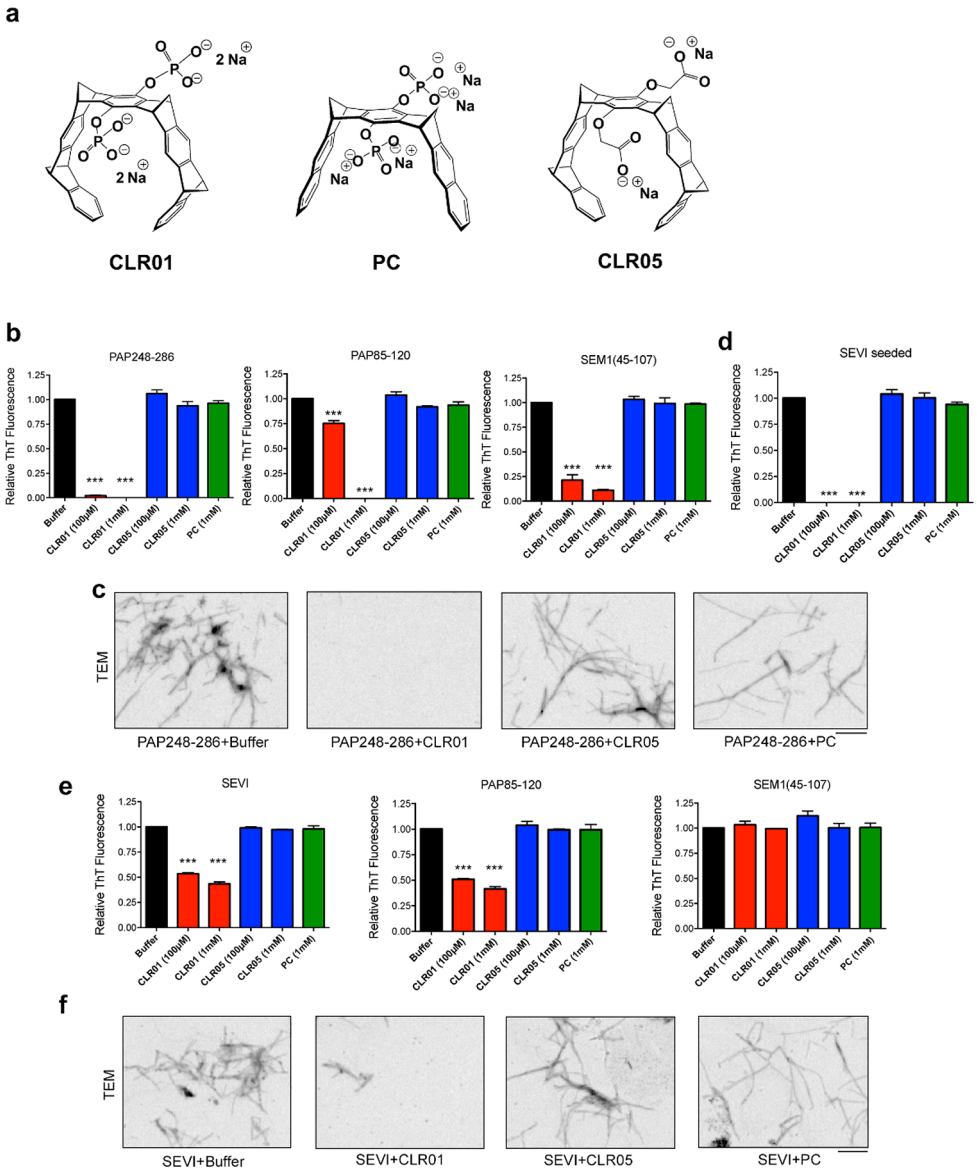

Figure 1. The molecular tweezer CLR05 and the clip PC neither inhibit amyloid assembly nor remodel amyloid fibrils. (a) Chemical structures of the hydrogen phosphate tweezer CLR01, methylene carboxylate tweezer CLR05, and the naphthalene phosphate clip PC. (b, c) CLR05 and PC do not inhibit amyloid fibril formation. (b) PAP248−286 (1 mM), PAP85−120 (1 mM), and SEM1(45−107) (0.5 mM) peptides were incubated with the indicated concentrations of CLR01, CLR05, PC, or buffer and agitated at 1400 rpm at 37 °C. After 24 h (PAP85−120) or 72 h (PAP248−286 and SEM1(45−107)), fibrillization was assessed using the amyloid-binding dye Thioflavin-T (ThT). Values represent means ± SEM (n = 3). (c) PAP248−286 (1 mM) was incubated with CLR01 (1 mM), CLR05 (1 mM), PC (1 mM), or buffer and agitated at 1400 rpm at 37 °C. After 72 h, fibrillization was assessed by transmission electron microscopy (TEM). Bar, 250 nm. (d) PAP248−286 (1 mM, plus 2 wt %/wt SEVI fibrils) was incubated with the indicated concentrations of CLR01, CLR05, PC, or buffer and agitated at 1400 rpm at 37 °C. After 48 h, fibrillization was assessed using the amyloid-binding dye Thioflavin-T (ThT). Values represent means ± SEM (n = 3). (e) CLR05 and PC do not remodel preformed fibrils. SEVI, PAP85−120 fibrils, or SEM1(45−107) fibrils (20 μM) were incubated with the indicated concentrations of CLR01, CLR05, or PC. After 2 h at 37 °C, ThT fluorescence was measured. Values represent means ± SEM (n = 3). (f) SEVI fibrils (20 μM) were incubated with CLR01 (1 mM), CLR05 (1 mM), or PC (1 mM). After 2 h at 37 °C, reactions were processed for TEM. Bar, 250 nm. For b, d, and e, one-way ANOVA (nonparametric, grouped) and Dunnett's multiple comparison tests were applied to compare the compound-treated samples to the respective buffer control.

and increase surface tension—a truly supramolecular mechanism which operates on all enveloped viruses. The molecular tweezer CLR01 (Figure 1a) is an inhibitor of aggregation and toxicity of amyloidogenic polypeptides containing arginine or lysine residues.[10−13] Through specific binding to lysine and arginine residues, CLR01 prevents polypeptide assembly into amyloid and even remodels mature fibrils.[12] We established that CLR01 also inhibits the assembly of seminal amyloids formed by specific proteolytic fragments of prostatic acid phosphatase (PAP) and semenogelins (SEM).[14] These fibrils are naturally present in human semen and markedly enhance the infectivity of sexually transmitted viruses such as human immunodeficiency virus type 1 (HIV-1),[15−19] herpesviruses,[20] and Ebola virus (EBOV).[21] CLR01 also remodels preformed PAP248−286 fibrils (termed SEVI for semen-derived enhancer of virus infection) and PAP85−120 fibrils.[14] Semen amyloids are polycationic due to several arginine and lysine residues and bind to the negatively charged membranes of viral particles and cells, which increases viral attachment and augments fusion.[15,17,22,23] Unexpectedly, we previously found that

https://dx.doi.org/10.1021/jacs.0c06400
J. Am. Chem. Soc. XXXX, XXX, XXX−XXX

CLR01 not only antagonizes the infectivity-enhancing activity of seminal amyloids but also exerts a direct antiviral activity against several enveloped viruses such as HIV-1, hepatitis c virus (HCV), herpes simplex virus type 2 (HSV-2), human cytomegalovirus (HCMV), Zika virus (ZIKV), and Ebola virus.[14,24] The antiviral activity is a consequence of the direct interaction of CLR01 with the membrane of the enveloped viral particle, which ultimately results in the loss of virion integrity and hence infectivity.[14,24] However, the precise antiviral mechanism of CLR01 remains unclear.

Due to their broad antiviral activity, CLR01 and its enhanced variants defined here are promising leads for the development of a new class of potential antiviral drugs that specifically destroy the structural integrity of enveloped viruses.[14,24] Yet, although it is essential for future therapeutic applications, the underlying mechanism of viral membrane destabilization is still unknown.[14] To address this issue and to identify the structural requirements for suppressing amyloid formation, we investigated how molecular tweezers, and a related clip-like molecule with known supramolecular behavior, affect amyloidogenesis and viral membrane integrity. In addition to the "phosphate tweezer" CLR01, we analyzed the "carboxylate tweezer" CLR05 and the "phosphate clip" PC (Figure 1a). These three scaffolds were selected for this mechanistic study because they represent prototypes that display different binding profiles. Tweezers with phosphate, phosphonate, or sulfate anions behave very similarly, but CLR01 is the least toxic among them. The carboxylate tweezer, CLR05, has a cavity (Figure 1a) but displays reduced affinity for lysine or arginine, and thus, we hypothesized it might have reduced ability to antagonize protein aggregation. The phosphate clip, PC, differs from CLR01 only in its cavity shape, which is more open due to the planar naphthalene side walls (Figure 1a). With these characteristic supramolecular host structures, we hoped to probe and separate the different mechanistic paths of antiviral and antiamyloid action. Using a synergistic approach combining computational chemistry, cell biology, virology, supramolecular binding studies, and biophysics, we elucidated both the antiamyloid and antiviral mechanisms. We found that lysine complexation inside the tweezer cavity is required to antagonize amyloidogenesis. The formation of inclusion complexes with lipid head groups of the viral membrane increases surface tension and disrupts the viral membrane, resulting in diminished infectivity. Our findings explain the origin of viral envelope destabilization by tweezers. With the identification of CLR05 as an antiviral agent, in addition to CLR01, we establish these supramolecular ligands as a new class of broadly active antiviral compounds. Based on these mechanistic insights, a series of advanced new tweezer derivatives was designed with additional lipid anchors. These novel tweezers exhibited potentiated antiviral activity compared to the parental CLR01 scaffold.

RESULTS

CLR05 and PC Have No Antiamyloid Activity. To define the mechanism of CLR01 action, we first established the activity of CLR05 and PC. The tweezers (CLR01 and CLR05) and the clip (PC) share the same central unit but carry distinct sidewalls, which form cavities with typical shapes, thus enabling their specific binding profiles (Figure 1a, Table 1). CLR01 forms inclusion complexes with lysine residues and to a lesser extent with arginine.[25] CLR05 is structurally similar to CLR01, but the hydrogen phosphate substituents are replaced with methylene carboxylate groups (Figure 1a). The phosphate clip, PC, with its almost parallel naphthalene sidewalls, was designed for planar aromatic guests such as cationic cofactors, which are preferentially accommodated inside its cavity[26,27] (Figure 1a). In sharp contrast, inclusion of aliphatic cationic guests such as Lys or Arg inside PC is less favored and occurs only with low affinity[28] (Table 1).

Table 1. Lysine and Arginine Affinities of the Three Host Molecules (CLR01, CLR05, and PC) Determined by Fluorescence Titrations in 75 mM Phosphate Buffer (pH 7.4)

host	K_d (μM) Ac-Lys-OMe	Ac-Arg-OMe
CLR01[25]	17	22
PC[29]	4670	1760
CLR05[25]	1160	1390

In solution, CLR05 forms both chelates and inclusion complexes with Lys/Arg residues[25] (Supplementary Figure 1a). However, it is important to clarify CLR05 behavior in a protein environment. In line with its experimentally determined low Lys and Arg affinities in solution[25] (Table 1), our computational studies of the CLR05 interaction with the prototype amyloidogenic peptide in semen, PAP248−286, showed that CLR05 has a reduced ability to form inclusion complexes with Lys or Arg, as compared to CLR01 (Supplementary Figures 1b and 1d). The global minima on the peptide-tweezer free energy surfaces obtained with extended-system adaptive biasing force (eABF) calculations indicate that binding of CLR05 to residues at the N-terminal (K251) and C-terminal (K281 and K282) regions of PAP248−286 is not favored, whereas K253 and R257 form distorted, unstable inclusion complexes (Supplementary Figure 1b and 1c). In addition, free energy perturbation calculations indicate that CLR01 forms more stable inclusion complexes with almost all Lys or Arg residues in PAP248−286, as compared to CLR05 (Supplementary Figure 1d). The only exception was R273, which formed a more stable inclusion complex with CLR05 than with CLR01 (Supplementary Figure 1d). However, R273 is not located in any of the hexapeptides predicted to form self-complementary β-sheets, termed steric zippers, which are anticipated to contribute to SEVI fibril formation.[14,19] Importantly, unlike CLR01,[14] CLR05 fails to interact effectively with K281 and K282, which are located in two potent steric zippers at the C-terminal end of PAP248−286[19] and form part of the stable cross-β SEVI fibril core defined by hydrogen−deuterium exchange.[30] Collectively, these findings predict that CLR05 would lack the antiamyloid activity of CLR01. Similarly, we expected that PC would not show antiamyloid activity because its affinity for Lys/Arg is even lower than that of CLR05 (Table 1).

For the experimental evaluation of these predictions, we investigated the effects of CLR01, CLR05, and PC on the formation of semen amyloid fibrils. Indeed, unlike CLR01, neither CLR05 nor PC inhibit spontaneous assembly of PAP248−286, PAP85−120, and SEM1(45−107) fibrils (Figure 1b, c). Moreover, CLR05 and PC did not inhibit fibrillization of PAP248−286 that was seeded by preformed SEVI fibrils (Figure 1d). Likewise, CLR05 and PC were unable to remodel preformed SEVI or PAP85−120 fibrils (Figure 1e, f), and none of the scaffolds could remodel SEM1(45−107) fibrils (Figure 1e).[14] Thus, in contrast to CLR01, CLR05 has no antiamyloid activity. As expected, due to its architecture, PC does not bind aliphatic guests and did not affect fibril formation by any of the peptides.

https://dx.doi.org/10.1021/jacs.0c06400
J. Am. Chem. Soc. XXXX, XXX, XXX−XXX

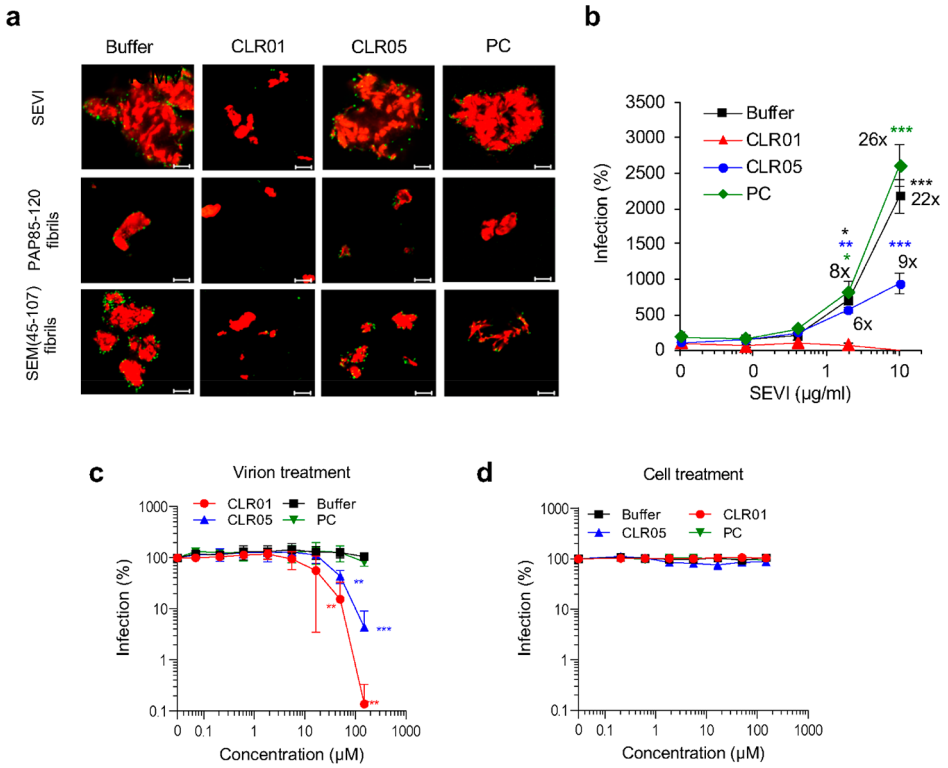

Figure 2. CLR05 anti-HIV-1 activity. (a) CLR05 and PC do not prevent formation of virus-fibril complexes. Fibrils (200 μg/mL) were incubated with buffer, CLR01, CLR05 or PC in 20-fold molar excess for 5 min and stained with Proteostat Amyloid Plaque Detection Kit. MLV-Gag-YFP particles (green) were added 1:2 and incubated with the stained fibrils (red) for 5 min before samples were analyzed via confocal microscopy. Scale bar: 5 μm. (b) CLR05 but not PC decreases the HIV-1 enhancing activity of SEVI. Fibrils were incubated with buffer or a 20-fold molar excess of CLR01, CLR05 or PC for 10 min at room temperature. After preparing 5-fold dilution series of the mixtures, HIV-1 was added and TZM-bl cells were inoculated with these samples. Values represent % β-galactosidase activities (mean) compared to cells infected with virus only and are obtained from triplicate infections ± SEM (n = 9). Numbers above the symbols indicate n-fold enhancement of infection. (**c, d**) CLR05 blocks HIV-1 infection by targeting the virus. (**c**) HIV-1 was incubated with CLR01, CLR05, PC or buffer for 10 min at 37 °C before it was added to TZM-bl cells. Three days post infection (dpi), infection rates were quantified by measuring β-galactosidase activity in cellular lysates. Values represent % infection (mean) compared to buffer control ± SD (n = 3). (**d**) TZM-bl cells were incubated with the indicated concentrations of CLR01, CLR05, PC or buffer for 1 h at 37 °C. Cell supernatants were discarded, and cells were infected with CCR5-tropic HIV-1 NL4−3. Values represent % infection (mean) compared to buffer control ± SD (n = 3).

CLR05 and PC Do Not Prevent the Formation of Virus−Fibril Complexes nor Abrogate Viral Infection Enhancement. CLR01 not only has antiamyloid activity but also prevents the formation of complexes between seminal fibrils and HIV-1 particles.[14] In contrast, we discovered that CLR05 and PC do not inhibit complexation of YFP-tagged virions with the three types of seminal amyloids (Figure 2a). We next determined the effect of CLR05 and PC on cell growth and found that concentrations of up to 250 μM were well-tolerated (Supplementary Figure 2a). Thus, all subsequent experiments were performed with CLR05 and PC concentrations ≤150 μM to exclude any confounding effects caused by residual cytotoxicity. To determine the effect of CLR05 and PC on amyloid-mediated infectivity enhancement, SEVI fibrils were incubated with PBS or with a 20-fold molar excess of each tweezer/clip, then mixed with HIV-1 and this solution was used to inoculate target cells. SEVI fibrils increased HIV-1 infection in a dose-dependent manner as described previously,[15] and CLR01 eradicated this effect[14] (Figure 2b). In the presence of CLR05, however, the infectivity enhancing activity of the fibrils was reduced but not abrogated. PC was completely inactive in antagonizing the infection enhancing effects of SEVI (Figure 2b). The experiment was also performed with PAP85−120 and SEM1(45−107) fibrils. Again, CLR01 abrogated infectivity enhancement, CLR05 showed an intermediate effect and PC was inactive (Supplementary Figure 2b-d). Since CLR05 has no antiamyloid activity (Figure 1b-1d), these data suggest that reduced infection rates are due to a direct antiviral activity of CLR05.

CLR05 has direct anti-HIV activity. Next, we tested CLR01, CLR05 and PC for a direct effect on virus infection. First, HIV-1 particles were incubated with tweezers, clip or buffer, and then used for infection. PC did not exert any antiviral activity whereas CLR05 inhibited HIV-1 infection with a half-maximal inhibitory concentration (IC_{50}) of ~41 μM, which is ~2.4-fold higher than the IC_{50} of CLR01 (~17 μM) (Figure 2c, Supplementary Figure 2e). Like CLR01, CLR05 did not inhibit HIV-1 infection if target cells were pre-exposed to the tweezer, demonstrating that both tweezers target the virus itself (Figure 2d).

Tweezers and clip form inclusion complexes with lipid head groups. To understand the antiviral effects of CLR01 and CLR05 at the molecular level, we investigated if the tweezers and the clip directly interact with the lipid head groups in the viral envelope, first by molecular dynamics simulations, then by NMR titration. The composition of viral envelopes greatly varies with the type of virus, the host cell membrane and the cell type. Generally, however, viral membranes tend to be enriched in

https://dx.doi.org/10.1021/jacs.0c06400
J. Am. Chem. Soc. XXXX, XXX, XXX−XXX

lipids found in lipid rafts (lipid microdomains enriched in glycosphingolipids and cholesterol) such as sphingomyelin (SM),[31,32] because viruses bud directly from lipid-raft domains of cell membranes.[33] Thus, lipidomics analyses provide experimental evidence of a special enrichment of HIV-1 viral membranes in SM and Cholesterol (Chol), phosphatidylserine (PS) and plasmalogen-phosphatidylethanolamine (pl-PE), all leading to more rigid membranes characteristic of lipid rafts.[31] A similar case can be made for the influenza virus, which is likewise enriched in SLs (sphingolipids) and cholesterol, irrespective of the investigated producer cell line.[32] Thus, viral membranes tend to resemble the lipid-raft microdomains from whence they originate.[31,34−37]

For our calculations, we selected three abundant lipids which occur in both eukaryotic cells and virions: dipalmitoylphosphatidylcholine (DOPC), sphingomyelin (SM) and cholesterol (Chol). To account for the different degree of lipid rafts, we composed a simple bilayer containing 120 DOPC lipids per leaflet, and a mixed bilayer containing 54, 30, and 36 molecules per leaflet of DOPC, sphingomyelin (SM) and cholesterol (Chol), respectively. We then studied the interaction of CLR01, CLR05 and PC with these model membranes using unbiased molecular dynamics simulations. Our simulations contained nine molecules of tweezers or clip, initially placed 4 Å above the membrane (example shown for CLR01 in Supplementary Figure 3a). Our results indicate that CLR01, CLR05 and PC form inclusion complexes with the head groups of DOPC and SM lipids, in both the DOPC and the mixed bilayer (Supplementary Tables 1−4, Supplementary Figures 4a-c). Importantly, after forming an inclusion complex, CLR01 and CLR05 induce preferential orientations of the complexed lipid head groups (Figure 3a and 3b), unlike PC (Figure 3a and 3c). Upon inclusion inside CLR01 or CLR05, the lipid head groups adopt an orientation nearly perpendicular to the normal of the membrane (*z*-axis) (the angle with respect to the *z*-axis is ∼90°, Figure 3b). This distortion is dictated by the upright orientation of the amphiphilic tweezer inside the membrane whose cavity must be entered from the side. Consequently, the whole tweezer is inserted in the most external layer of the membrane, formed by the polar ammonium and phosphate groups of its phospholipid components (Figure 3b). This tweezer orientation likely induces local stress around the binding site thus weakening the bilayer. By contrast, in the presence of PC, the lipid head group remains aligned nearly parallel to the normal of the membrane (*z*-axis) (Figure 3c). This alignment can occur because the clip cavity is more open than the tweezer cavity, which enables facile lipid inclusion into the clip cavity by vertical entry.

To further explore the finding that the tweezers encapsulate lipid head groups and do not penetrate into the membrane interior, the free energy changes for the insertion of CLR01, CLR05 and PC into a DOPC or a mixed bilayer were calculated using the eABF scheme (Supplementary Figure 3 shows CLR01 as a representative case). For both bilayers, the minimum in the one-dimensional Potential of Mean Force (PMF) profile corresponds to the tweezers forming an inclusion complex with a head group of a lipid located at the surface of the membrane (as indicated by position 2 in Supplementary Figure 3b) rather than inside the bilayer where the free energy is much higher (position 3, Supplementary Figure 3b). Although the free energy differences between the tweezers in solution (position 1, Supplementary Figure 3b) and the complex at the surface of the membrane (position 2, Supplementary 3b) are very small, the MD simulations indicate that the tweezer-lipid complexes do

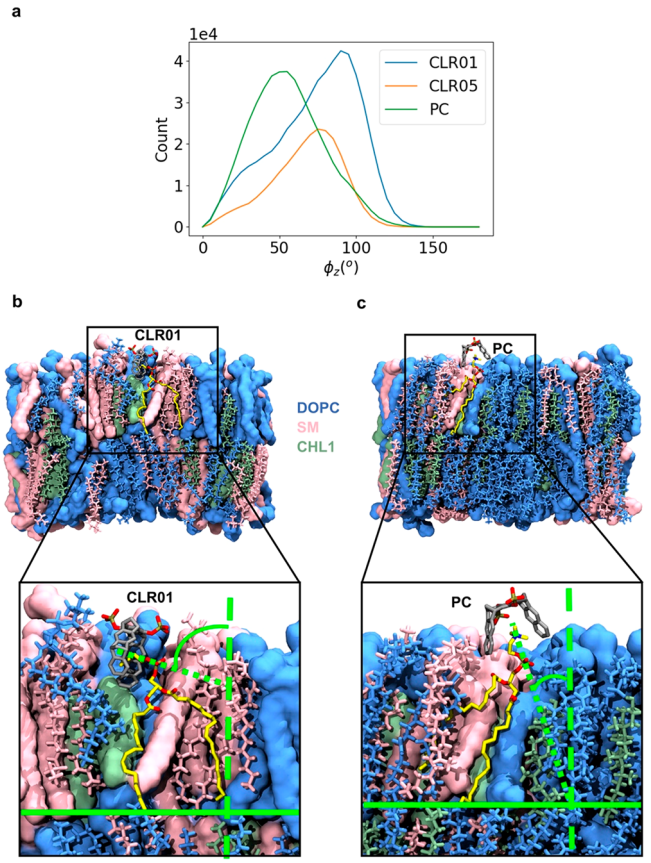

Figure 3. Computational modeling of the interactions of the tweezers and clip with lipid membranes. (a) The distribution of the values adopted by the angle indicating the relative orientation of the lipid head group with respect to the normal of the membrane model (*z* axis) provides evidence that the orientations of the lipids are different upon interaction with the tweezers with respect to the clip. (b) Upon binding to a lipid in the bilayer, the tweezers (CLR01 is shown here as representative case) enforce a conformation of the lipid head group almost parallel to the bilayer surface, raising surface tension. (c) By contrast, the lipid head group bound to PC remains nearly perpendicular to the bilayer surface in a tension-free conformation. An enlargement of the binding region is shown for both b) and c). CLR01 and PC are depicted as sticks with carbon atoms in gray, oxygen in red and phosphorus in tan. DOPC is shown in blue, PSM in pink and CHL1 in green. The lipid bound to CLR01 or PC is highlighted in yellow. The dotted line is traced along the vector between the centers of the phosphate and the ammonium groups in the lipid head. The solid line indicates the plane of the membrane and the dashed line corresponds to the direction of its normal vector (z-axis).

form, albeit not as efficiently as the PC−lipid complexes (Supplementary Table 1). Importantly, the free-energy calculations establish that CLR01, CLR05 and PC are unlikely to penetrate deep inside or cross the bilayers. The key to the antiviral activity of the tweezers most likely relates to their effect on the lipid orientation, as discussed above, and/or a preference of the tweezers toward lipids like SM, which are characteristic of viral membranes.

Here, to explore if CLR01 has a certain preference for raft-forming lipids, we performed quantum mechanics/molecular mechanics (QM/MM) calculations. Our results indicate that the CLR01-SM complex is indeed more stable (in terms of electronic energy) than the CLR01-DOPC complex (Supplementary computational details, Supplementary Figure 5a and 5b). To clarify if this selective stabilization of the CLR01-SM

https://dx.doi.org/10.1021/jacs.0c06400
J. Am. Chem. Soc. XXXX, XXX, XXX−XXX

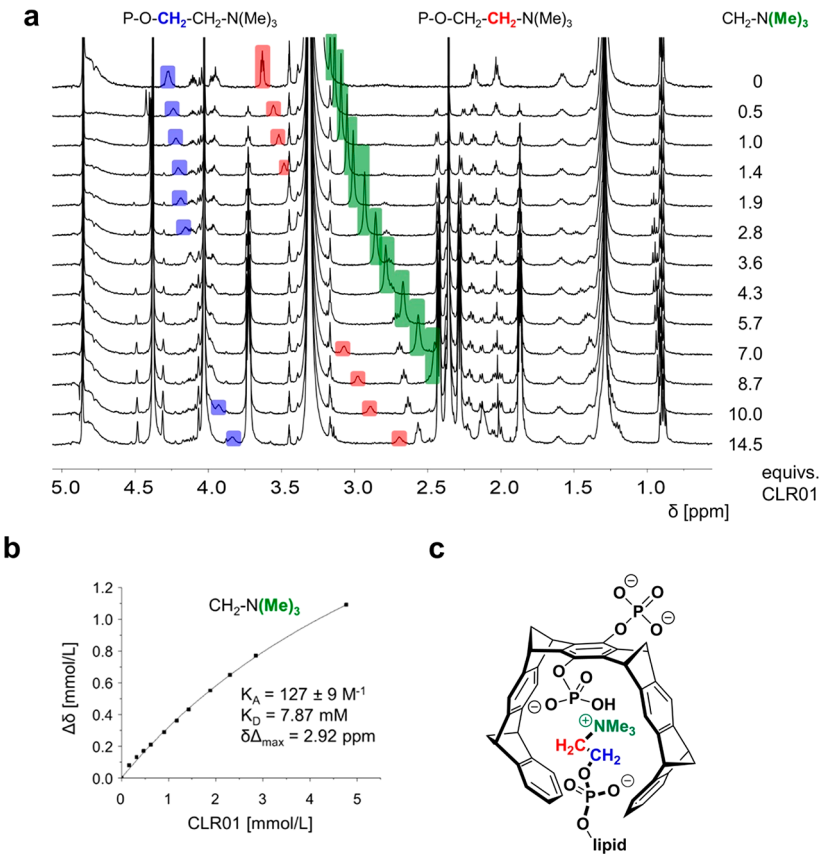

Figure 4. Tweezers and clip form inclusion complexes with lipid head groups. (a) Complex formation between CLR01 and sphingomyelin (SM) monitored by NMR spectroscopy: stacked plot of ^{1}H NMR spectra showing SM with increasing amounts of added CLR01. Colored signals represent the choline head group inserted into the tweezer cavity. (b) Corresponding binding curve for the $N(Me)_3^+$ signal with the resulting affinity (K_A/K_D) and $\Delta\delta_{max}$ value obtained from nonlinear regression. (c) Lewis structure of CLR01 with inserted choline moiety from PSM inside; CH_2/CH_3 groups inside the tweezer cavity are color-coded because they undergo large upfield shifts.

complexes is related to the disruption of interactions between the lipid molecules and the solvent or due to the membrane environment, we also calculated CLR01-SM and CLR01-DOPC inclusion complexes in an explicit water environment using the same computational protocol as in the membrane simulations. We found that the CLR01-SM complex is more stable than the CLR01-DOPC complex also in solution (Supplementary Figure 5b). Our results suggest that the hydration of the lipid polar head groups is the main determinant of the higher affinity of the tweezers for SM. This finding can be rationalized by the fact that the lipid bilayer is commonly hydrated at its most external regions composed of quaternary ammonium and phosphate groups. The binding of the tweezers implies desolvation of the ammonium moiety and partial desolvation of the phosphate group of the lipid. Hence, the stabilization of the inclusion complex is determined by competing forces between electrostatic and dispersion interactions with the tweezers and the solvation of the polar groups of the lipid. Notably, the phosphate group of SM establishes a stabilizing intramolecular hydrogen bond with the hydroxyl group next to it (Supplementary Figure 5c), unlike DOPC. This interaction diminishes the desolvation cost in SM thereby stabilizing the CLR01-SM complex. Conversely, the DOPC molecules depend completely on the surrounding water to stabilize the phosphate group, resulting in a higher desolvation cost for the formation of CLR01-DOPC inclusion complexes. Although lipid rafts are composed of various different rigid lipids, such effects may contribute to a preferred complexation of prominent raft lipids by the tweezers, and contribute to their low toxicity toward cells relative to enveloped viruses. Taken together, our modeling experiments suggest an explanation for the preferential destabilization of viral membranes by molecular tweezers: they reveal that lipid head groups are included in the tweezer cavity, which causes alterations in lipid orientation that destabilize the membrane. Indeed, the formation of a supramolecular complex allows for the insertion of the tweezers in the hydrophilic region of the outer membrane leaflet. Consequently, membrane tension will increase in both cellular and viral membranes. However, if viral membranes are enriched in lipid rafts, this effect will elevate their tension above a tolerable threshold and lead to membrane rupture.

NMR titrations corroborate the formation of inclusion complexes with lipids. To complement the computational studies, we proceeded to structural investigations. ^{1}H NMR spectra of the 1:1 complexes (0.33 mM) between hosts (tweezers and clip) and lipids (SM, DOPC) revealed significant complexation-induced upfield shifts for the protons of the entire trimethylammonium choline head group, indicating at least partial inclusion inside the host cavities (Figure 4a). Figure 4 shows the example of phosphosphingomyelin interacting with CLR01. All the other combinations are presented in Supplementary Figures 6a-f. Attempted fluorescence titrations in methanol gave very small changes in host emission intensity, too small for reliable quantification. After careful optimization, a comparative NMR study was executed in d_4 methanol (due to the low lipid solubility in water), with all three host molecules

https://dx.doi.org/10.1021/jacs.0c06400
J. Am. Chem. Soc. XXXX, XXX, XXX−XXX

and DOPC as well as SM as guests. Binding isotherms produced excellent fits by nonlinear regression (Figure 4b) and revealed weak affinities resulting from K_d values in the low millimolar regime (Table 2). Maximum complexation-induced ^{1}H NMR chemical upfield shifts reached remarkable $\Delta\delta$ values of up to 4 ppm and demonstrated the efficient inclusion of the entire choline lipid head group inside the respective host cavities (Figure 4c).

Table 2. Maximum Complexation-Induced Chemical ^{1}H NMR Shift Changes ($\Delta\delta_{max}$ [ppm]) of the $N(Me)_3^+$ Protons and Dissociation Constants K_D Obtained From NMR Titrations of Lipids (PSM, DOPC) with Hosts (CLR01, CLR05, PC)[a]

	$\Delta\delta_{max}$ (ppm)		K_d (1:1)	
host	SM	DOPC	SM (mM)	DOPC (mM)
CLR01	2.92	4.36	7.9	14
PC	0.89	1.45	7.0	13
CLR05	1.73	0.96	61	37

[a]Lipid concentration was 0.33 mM in d_4-methanol.

We asked if the weak affinities originate from the steric bulk of the trimethylammonium head group and turned to trimethyllysine: NMR spectra for CLR01 with this related guest molecule reached comparable upfield shifts for the NMe_3^+ cation, but titrations maintained the high lysine affinity ($K_d \sim 10\ \mu M$). We conclude that the close proximity between the choline phosphate ester anion and the anionic substituents of the tweezers or clip severely limits lipid affinities, whereas the extended alkylammonium arms of Lys or Arg fit well into the tweezer cavity, and most likely benefit from large dispersive and electrostatic attraction. CLR01 and PC produce comparable affinities toward both lipids (SM ~ 7 mM; DOPC~ 14 mM) (Table 2). By contrast, CLR05 is a much weaker lipid binder (~40−60 mM), most likely because it also chelates the choline head group externally, as evidenced by the modest complexation-induced ^{1}H NMR upfield shifts compared to CLR01 (Figure 4, Supplementary Figure 6). This finding agrees well with poor lysine inclusion by CLR05[21] and with the simulations (binding events and free energy calculations).

CLR05 Selectively Disrupts Raft-Rich Membranes. To further investigate the consequences of the tweezer/clip interaction with lipid bilayers, we took advantage of two types of engineered giant unilamellar vesicles (GUVs) of ~5−40 μm in diameter. In parallel with the calculations, one type of GUVs consisted only of DOPC. The other type of GUVs was composed of a 45/25/30 mol % mixture of DOPC, SM, and Chol as a membrane model with a large content of lipid rafts. These models are not intended to exactly recreate viral or eukaryotic cell membranes per se, whose lipid composition greatly varies and is much more complex. Instead, they aim at testing whether an elevated lipid raft content of representative lipids enriched in viral membranes renders them more susceptible to disruption by tweezers.

The different lipid phases were marked with fluorescent lipid analogs that segregated into the liquid-disordered (l_d) (red channel) or the liquid-ordered (l_o) (green channel) phase when viewed via fluorescence microscopy (Figure 5a and b). In addition, the GUVs were loaded with the water-soluble dye ATTO 647 (blue channel). Exposure of DOPC vesicles to CLR05 (Figure 5a, bottom panel) or PC (Figure 5b, bottom panel) did not affect vesicle morphology and did not elicit dye leakage. However, when CLR05 was added to DOPC/SM/Chol vesicles, the l_o domains started to bud from the GUVs, and most of them had pinched off after ~15−30 min of incubation with concomitant dye leakage from the GUVs (Figure 5a, top panel). However, in contrast to CLR01, which destroys the mixed vesicles,[14] CLR05 partially preserved GUV membrane integrity (Figure 5a, top panel). In sharp contrast, the clip did not permeabilize either of the GUV species even after 60 min of incubation (Figure 5b). Under identical conditions, CLR01 had a much more drastic effect: While the DOPC vesicles remained all intact, already after 5 min all membranes of mixed vesicles were disrupted, and the dye was lost completely.[14]

To study membrane disruption in the context of virus-like vesicles, mixed-lipid (DOPC/SM/Chol, 45/25/30 mol %) liposomes were prepared and loaded with carboxyfluorescein at a self-quenching concentration of 50 mM. In this setup, an increase in fluorescence indicates membrane disruption due to dye leakage and dilution below self-quenching concentrations in the surrounding medium. CLR05 and CLR01 but not PC induced dye leakage in a dose-dependent manner within few minutes (Figure 5c). CLR05 was less potent than CLR01 (Figure 5c). CLR01 rapidly induced full leakage of liposomes at 150 μM concentration, whereas CLR05 resulted in a maximal leakage of only 78% after 30 min of coincubation at the same concentration (Figure 5c, Supplementary Figure 7a). The previously reported antivirally inactive spacer molecule CLR03[14] behaved similarly to PC and did not induce leakage (Supplementary Figure 7a−c).

Atomic force microcopy (AFM) of the heterogeneous model biomembrane confirmed that the line tension at the phase interface is increased in the presence of CLR05 (Figure 5d). As a result, the size of the l_o domains increased, which is accompanied by a slight increase in the difference in domain height thickness. This effect is likely due to an increased line tension at the boundary between the ordered and disordered domains induced by CLR05 attachment. AFM experiments demonstrated that addition of PC produced a small increase in height difference between the l_o and l_d phase as well; however, changes in the lateral membrane organization were small (Figure 5d). This finding further confirms that PC binds to the lipid bilayer although it does not disrupt it, pointing to a subtle but profound difference in its mode of action compared to the tweezers, CLR05 and CLR01, which disrupt membranes enriched in SM and Chol, such as those of enveloped viruses, as predicted by the biomolecular simulations (Figure 3).

We conclude that experiments on model membranes strongly support the suggested mechanism of membrane destabilization by supramolecular docking of designed ligands to the lipid head groups and subsequent increase in surface tension. Importantly, lipid rafts are enriched in viral membranes, which makes them more susceptible to disruption by tweezers. Indeed, a single rupture of the viral membrane destroys the virus irreversibly. By contrast, cells can actively repair their membranes after lipid-raft disruption.

CLR01 Induces Distortions in Viral Membrane. We next visualized the effect of the tweezers on the envelope of virus particles. We first analyzed HIV-1 and ZIKV by cryo-transmission electron microscopy (cryo-TEM) but encountered problems at detecting a sufficient number of the relatively small virions (data not shown). We therefore switched to HCMV, a relatively large virus, which is antagonized by CLR01.[14] Cryo-TEM analysis of untreated HCMV virions showed ~200 nm-sized particles with a protein-rich tegument and an intact

https://dx.doi.org/10.1021/jacs.0c06400
J. Am. Chem. Soc. XXXX, XXX, XXX−XXX

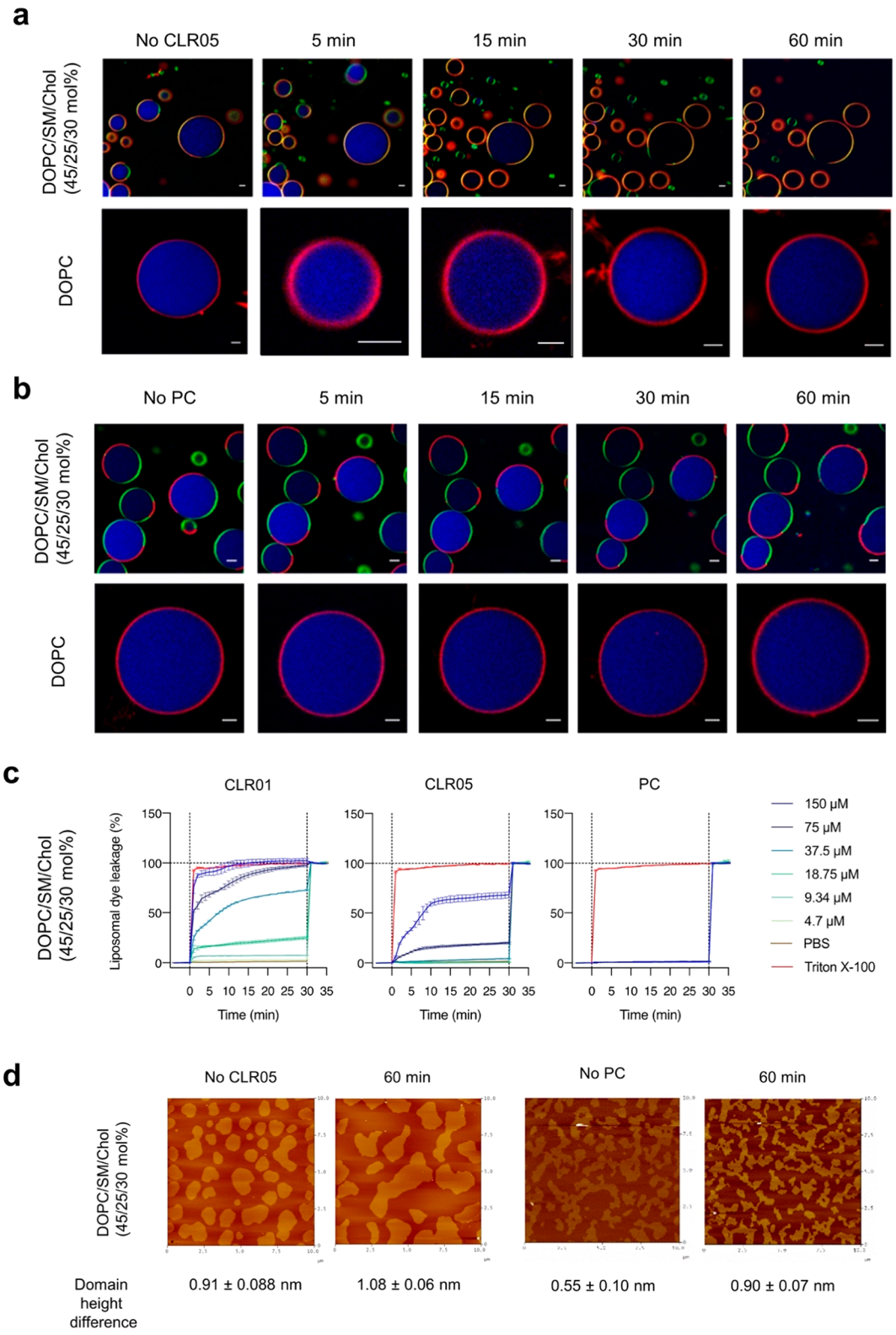

Figure 5. CLR05 destroys raft-like lipid vesicles. (a, b) Confocal fluorescence microscopy images of lipid raft enriched GUVs consisting of pure DOPC (lower panel) or a DOPC/SM/Chol (45/25/30 mol %) lipid mixture (upper panel) labeled with N−Rh-DHPE (l_d lipid phase, red channel) and Bodipy-Chol (l_o lipid phase, green channel) and filled with Atto 647 dye (blue channel). CLR05 (a) or PC (b) (150 μM) was added and incubated for the indicated times. Scale bar: 5 μm. (c) Liposome dye leakage assay of DOPC/SM/Chol (45/25/30 mol %) liposomes extruded to 200 nm size filled with 50 mM carboxyfluorescein. Compounds were added after measuring baseline fluorescence for 5 min (first dotted line), and after 30 min of incubation with compounds, Triton X-100 was added to 1% final concentration to measure fluorescence intensity after full leakage in each well (second dotted line). Fluorescence values were baseline-subtracted (before addition of compounds) and normalized to maximum fluorescence obtained after addition of Triton X-100. Values represent means ± SD (n = 3). (d) AFM images of a DOPC/SM/Chol (45/25/30 mol %) lipid membrane on mica before injection (0 min) and after injection of 150 μM CLR05 (left) or PC (right) in 10 mM NaH_2PO_4, pH 7.6 into the AFM fluid cell.

https://dx.doi.org/10.1021/jacs.0c06400
J. Am. Chem. Soc. XXXX, XXX, XXX−XXX

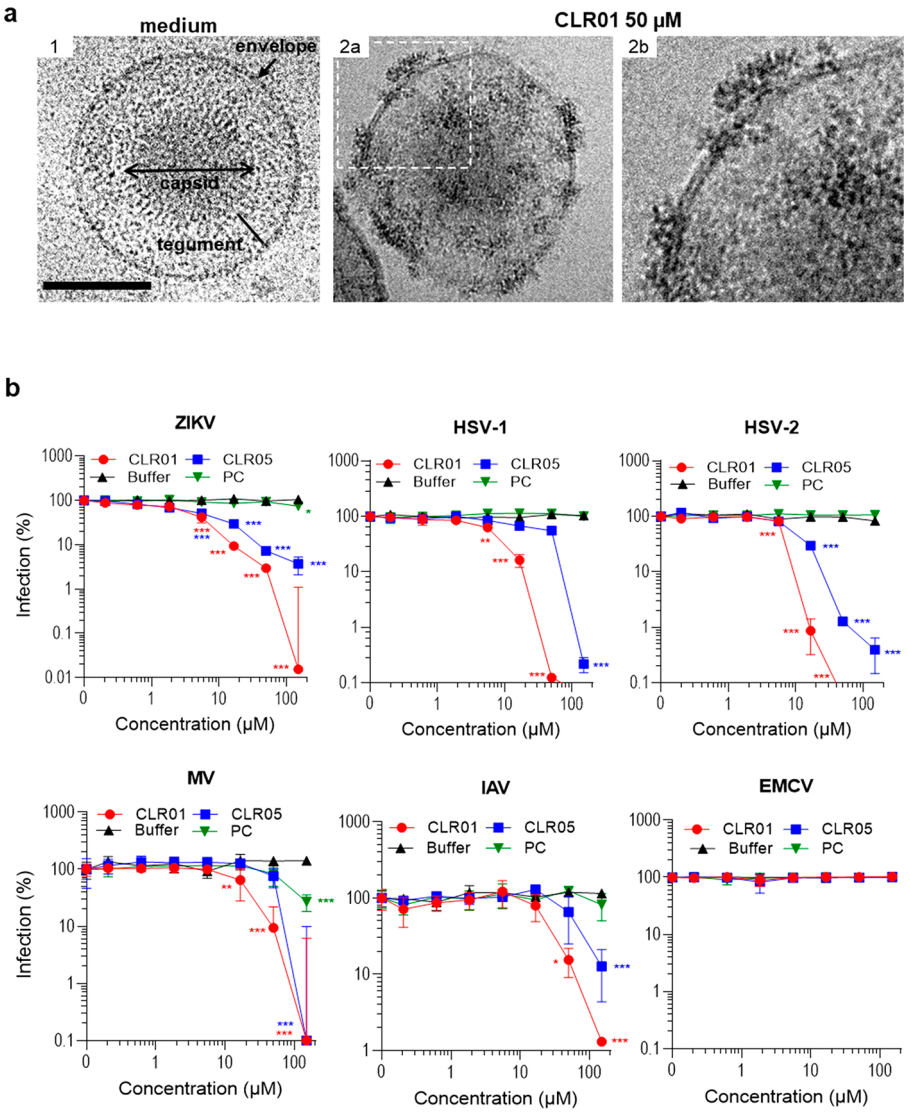

Figure 6. CLR01 destroys the HCMV envelope and exerts broad antiviral activity against enveloped virus infection. (a) Cryo-TEM of HCMV virions after treatment with medium (1) or 50 μM CLR01 (2a-b) for 30 min at 37 °C. Important virion structures are indicated in image 1. CLR01-treated virion in 2a-b shows a discontinuous envelope and is decorated with electron-dense material at these sites (white arrowhead). Scale bar is 100 nm. (b) Antiviral activity of tweezers and clip against enveloped (ZIKV, HSV-1, HSV-2, HCMV, MV, IAV) and nonenveloped virus infection (EMCV). ZIKV MR766 was incubated for 30 min at 37 °C with buffer or 0.2−150 μM CLR01, CLR05, or PC before these mixtures were added to Vero E6 cells. After 2 dpi, cell-based ZIKV immunodetection was performed. Values represent means ± SEM (n = 3). HSV-1 and HSV-2 were incubated for 30 min with compounds and then added to Vero E6 cells. After 1 h incubation, media were changed; 12 h post infection, cells were fixed, and infection rates were quantified via staining for the HSV protein ICP0. Values represent means of % infection ± SD (n = 3). Measles virus was exposed to compounds for 30 min at 37 °C before these mixtures were added to A549 cells. After 4 h, cells were washed, and medium was replaced. After 2 dpi, infection rates were quantified by staining with an FITC-coupled MV antibody and mean fluorescence intensities were measured on a plate reader. Values represent means ± SD (n = 6). Influenza strain A/PR/8/34 was incubated with 0−150 μM CLR01, CLR05, or PC for 30 min at 37 °C before the mixtures were used to infect A549 cells. After 1 h, cells were washed, and medium was changed. After 48 h, infectivity rates were determined by measuring neuraminidase activity in cellular lysates (MUNANA assay). Values represent means ± SD (n = 3). EMCV was incubated for 30 min at 37 °C with buffer or different concentrations of CLR01, CLR05, or PC before it was added to HFF cells. Two days later, the cytopathic effect (percentage of detached cells) was quantified by MTT assay and used to calculate infection rates. Values represent means ± SD (n = 3).

membrane in 78.1% of all analyzed images (n = 32) (Figure 6a, Supplementary Figure 8a and Supplementary Table 5). Upon incubation of HCMV with CLR01 for 30 min, we observed distortions in the viral membrane in 84.6% of the analyzed samples (n = 39) (Figure 6a, Supplementary Figure 8a and Supplementary Table 5). Interestingly, these distortions resulted in the leakage of the gel-like tegument to the outside of the virus, but not an entire loss of the structural integrity of the viral particle. Viral DNA release assays confirmed that CLR01 does not cause an entire destruction of the HCMV particle (Supplementary Figure 8b). These data are in contrast to those obtained with HIV-1 and ZIKV,[14,24] where CLR01 and CLR05 resulted in complete destruction of the virions (Supplementary Figure 9). However, this discrepancy is likely explained by the fact that HCMV is a relatively stable virus because of the numerous interactions of the viral glycoproteins with the tegument, explaining its partial resistance even against detergents (Supplementary Figure 8b). To assess whether CLR01 or CLR05 might induce virus aggregation, we utilized fluorescent nanoparticle tracking of virus-like particles. We did

https://dx.doi.org/10.1021/jacs.0c06400
J. Am. Chem. Soc. XXXX, XXX, XXX−XXX

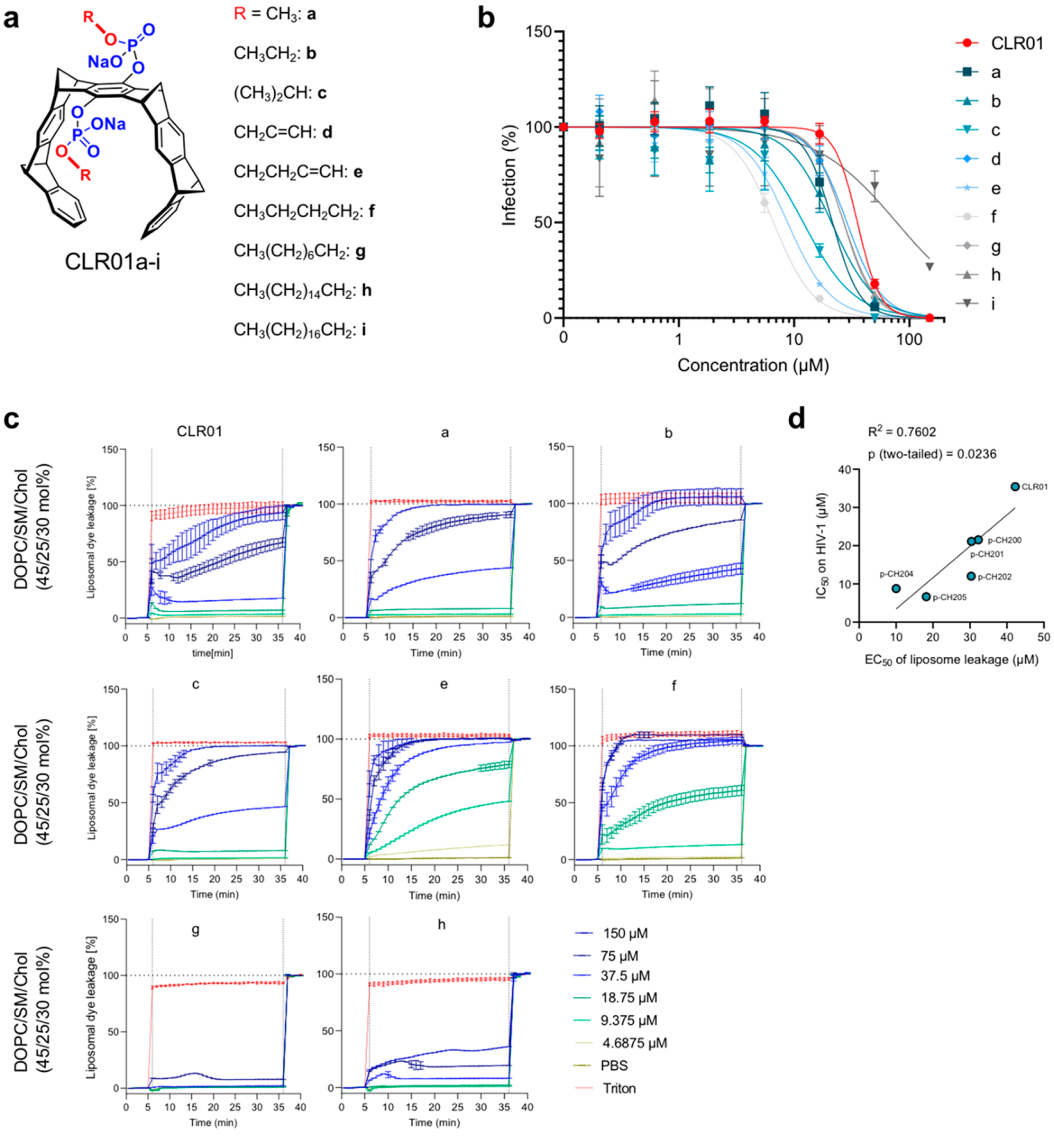

Figure 7. Advanced molecular tweezer derivatives with two aliphatic ester arms display improved activity against HIV-1 infection. (a) Chemical structures of the new two-armed tweezer derivatives developed from the parent phosphate tweezer CLR01. (b) Effect of the new tweezers on HIV-1 infection. HIV-1 was exposed to tweezer at indicated concentrations and then used to infect TZM-bl cells. Infection rates were determined 2 days later by quantifying β-galactosidase activity. Shown are mean values derived from 1−3 experiments each performed in triplicates ± SEM. (c) Liposome dye leakage assay of DOPC/SM/Chol (45/25/30 mol %) liposomes filled with 50 mM carboxyfluorescein. Compounds were added after measuring baseline fluorescence for 5 min (first dotted line) and after 30 min incubation with compounds, Triton X-100 was added to 1% final concentration to measure fluorescence intensity after full leakage in each well (second dotted line). Fluorescence values were baseline-subtracted (before addition of compounds) and normalized to maximum fluorescence obtained after addition of Triton X-100. Values represent means ± SD ($n = 3$). (d) Correlation of anti-HIV IC_{50} values from (b) and EC_{50} measured in the liposome leakage assays (c). Derivates g and h were excluded, as 50% leakage was not reached, and thus no EC_{50} was calculated.

not see any aggregation of virus-like particles induced by CLR01, CLR03, CLR05, or PC (Supplementary Figure 10). By contrast, SEVI fibrils induced aggregation of viral particles as expected (Supplementary Figure 10). These findings suggest that CLR01 and CLR05 disrupt viral membranes without inducing aggregation of the virus.

CLR01 and CLR05 are Broad-Spectrum Antivirals. If tweezers act against viral membranes, they should be generally active against enveloped viruses. Indeed, we found that CLR05 abrogated infection of pseudoviruses carrying the glycoproteins of Marburg, Ebola, rabies, or SARS-coronavirus 1 (Supplementary Figure 11a), as previously shown for CLR01.[24] Moreover, we found that both tweezers inhibited infection by pseudoviruses harboring the spike glycoprotein of SARS-CoV-2, the causative agent of the ongoing COVID-19 pandemic, whereas PC had a modest effect at high concentrations (Supplementary Figure 11b). CLR01 and CLR05 also inhibited infection of replication-competent ZIKV, HSV-1, HSV-2, measles virus (MV), and influenza virus (Figure 6b) with a mean IC_{50} of 19.3 μM for CLR01 and 38.1 μM for CLR05. The clip did not affect infectivity of any of these viruses except for a modest effect on MV (Figure 6b). Importantly, neither CLR01 nor CLR05 reduced infection by nonenveloped adenovirus (Supplementary Figure 11c) or encephalomyocarditis virus (Figure 6b). Thus, our results indicate that CLR01 and CLR05 are both broad-spectrum inhibitors of pathogenic enveloped

https://dx.doi.org/10.1021/jacs.0c06400
J. Am. Chem. Soc. XXXX, XXX, XXX−XXX

viruses. We cannot exclude at this point that CLR01 binding to lysine-rich tracts of viral proteins may also influence virus attachment to the host cell and thereby decrease infectivity. However, the structure of these glycoproteins varies greatly between different viruses, and interference with protein interactions usually requires higher affinities than those displayed by CLR01 (>20 μM). Furthermore, electron microscopy demonstrates a direct destabilization of the viral envelope by CLR01 (Figure 6a).[14] Indeed, there has so far been no exception from the empirical rule that molecular tweezers disrupt the membrane of all enveloped viruses but are inactive against nonenveloped viruses.

Additional Lipid Anchors Significantly Improve the Antiviral Activity of CLR01. If the mechanistic picture of membrane destabilization by direct tweezer docking onto lipid head groups is correct, additional lipid anchors on the tweezer should enhance this interaction and yield more potent scaffolds. In a first series of advanced tweezers, we introduced a wide range of aliphatic ester arms into each phosphate group of CLR01 (Figure 7a). These modifications were accomplished by activation of the phosphoric acid with trichloroacetontrile (TCA), which can be controlled in pyridine to occur only once.[14] The length of these additional lipid anchors was varied between C1 and C16 chains, and initial antiviral activities were assessed with the same experiments on HIV-1 as described for CLR01, CLR05, and PC. Intriguingly, most tweezer derivatives are more effective than their parent compound CLR01 (Figure 7b). The most efficient esters carried unbranched C4 units (CLR01-e and -f) and inhibit HIV-1 infection at ∼4−5-fold lower concentrations than CLR01. The CLR01 analogue with C18 chains, CLR01-i, was highly cytotoxic (Figure 7b and Supplementary Figure 12). The selectivity index of the modified tweezers confirmed that the advanced tweezers with lipid anchors, in particular CLR01-e and -f, are indeed superior to their ancestor CLR01 (Supplementary Figure 12b). The only exception was CLR01-i, which was cytotoxic (Supplementary Figure 12b). Liposomal dye-leakage assays demonstrated that most CLR01 derivatives induced a more rapid and more effective membrane disruption than the parent CLR01 (Figure 7c, Supplementary Figure 7d). Moreover, we observed a statistically significant ($p < 0.05$) correlation between the anti-HIV activity and potency in liposome disruption, supporting the above-detailed mechanism (Figure 7d). These findings show one way for improving efficacy of tweezers, namely by the introduction of membrane-active components to the parent tweezer unit. We are now performing a broad screening of such modified tweezers to identify powerful nontoxic candidates.

DISCUSSION

The molecular tweezer CLR01 is a well-established inhibitor of abnormal protein self-assembly and has been found to inhibit the formation of toxic oligomers and aggregates of multiple disease-associated proteins, including those involved in Alzheimer's disease[38,39] and Parkinson's disease.[10,40,41] Moreover, CLR01 also blocks formation of seminal amyloid fibrils[14] that are potent enhancers of Ebola virus and HIV-1 infection.[15,21] The antiamyloid activity is achieved by reversible inclusion of positively charged amino acid residues inside the tweezer cavity, primarily Lys and to a lower extent Arg.[14] More recently, we demonstrated that CLR01 also acts as broad-spectrum inhibitor of enveloped viruses, including HIV-1, ZIKV and Ebola virus.[24] The exact mechanism underlying the antiviral activity of CLR01 was, however, unclear.

We show here that the antiamyloid and the antiviral activity are separable functions of CLR01. CLR05, a tweezer derivative that carries methylene carboxylates instead of phosphates, does not encapsulate Lys/Arg residues and consequently displays no antiamyloid activity. However, like CLR01, CLR05 suppresses virus infection in a dose-dependent manner. This finding demonstrates that Lys/Arg inclusion is not necessary for virus inhibition. On the other hand, the phosphate clip PC, a structurally related phosphorylated derivative with a modified open cavity, was devoid of both activities, indicating that the closed horseshoe-shaped cavity of the tweezers plays a key role in viral membrane destabilization by CLR01 and CLR05. In agreement with these results, only CLR01, but not CLR05 and PC, effectively prevented complex formation between seminal fibrils and virions, and abrogated infectivity-enhancement. We conclude that the antiamyloid activity relies on Lys/Arg inclusion inside the tweezer cavity. This inclusion leads to a neutralized zeta potential of the fibrils, and eliminates their potential to carry virions to the cell membrane.

How do CLR01 and CLR05 destabilize and eventually disrupt the viral membrane? Through a combination of biomolecular simulations, model titrations (^{1}H NMR, fluorescence) and liposome experiments, we discovered that CLR01, CLR05, and PC all engage lipid head groups at the surface of biological and synthetic membranes. This supramolecular process involves encapsulation of the trimethylammonium moiety of the choline of DOPC or SM inside the cavities of the ligands, which only occurs close to the membrane surface. Here, even the amphiphilic CLR05 orients its methylene carboxylate arms toward the bulk water and thus exposes its cavity. Antiviral tweezers CLR01 and CLR05 induce a horizontal lipid orientation inside their closed cavities, which favors their insertion in the polar region of the outer leaflet and raises the local stress of the membrane. This rearrangement ultimately ruptures viral membranes—as visualized by cryo-TEM of CLR01-exposed HCMV particles—and diminishes viral infectivity. By contrast, the open PC cavity allows stress-free lipid insertion from below and hence does not affect viral membrane integrity, explaining the lack of antiviral activity.

Experiments with fluorescent GUVs and liposomes suggest a profound difference between DOPC membranes, which remain intact after tweezer or clip exposure, and DOPC liposomes containing SM and Chol, which imitate the composition of viral membranes and are quickly disrupted at their phase boundaries between DOPC and lipid rafts when tweezers are added. We explain this difference by the elevated surface tension already present in lipid rafts, which is further increased after CLR01 or CLR05 insertion. Our findings also explain the minimal cytotoxicity of tweezers[14] because the surface tension of the ordinary cellular plasma membrane is much lower than that of small nanometer-sized liposomal or viral membranes, which are disrupted by CLR01 or CLR05. In addition, we show by QM/MM calculations and NMR experiments that the inclusion complexes with SM are intrinsically more stable than those with DOPC, which is rationalized by a reduced competition between electrostatic and dispersion forces and solvation effects in SM.

CLR01 showed a modestly increased antiviral activity as compared to CLR05. Leakage assays revealed that CLR01 lyses DOPC/SM/Chol liposomes more rapidly and more effectively than CLR05. Computational modeling and NMR titrations showed that CLR05 is able to bind the trimethylammonium cation of the choline head group also outside the cavity by way of a chelate complex between its carboxylate tips. This binding

https://dx.doi.org/10.1021/jacs.0c06400
J. Am. Chem. Soc. XXXX, XXX, XXX−XXX

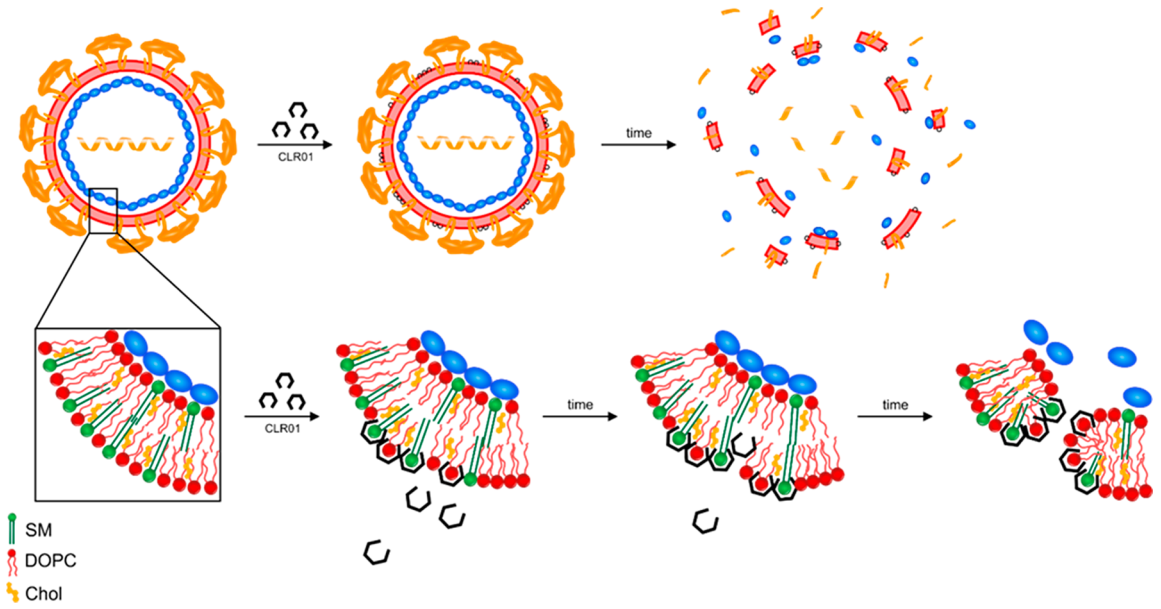

Figure 8. Schematic representation of virus disruption by molecular tweezers. Tweezer molecules encapsulate the phosphocholine head groups of DOPC and SM in the outer lipid leaflet of the viral membrane, thereby increasing the mechanical stress in the outer leaflet, which initiates the rupture of the viral membrane and consequently loss of viral infectivity.

mode is weaker, does not exert any strain on the lipids inside the membrane, and thus lowers the membrane destabilization efficiency. Collectively, these data suggest that tweezer architecture and the direct inclusion of the choline head group inside the tweezer cavity are required for their biological effect. Importantly, additional lipid anchor groups on the phosphate moieties further strengthen this effect (Figure 7).

We also observed that some viruses need a larger amount of tweezers than others in order to be disrupted. For example, CLR01 was more effective against HSV-2 than IAV (Figure 6b). This difference could be caused by distinct capsid/envelope packaging of various viruses, the overall virion architecture, the membrane curvature and/or tension, or the accessibility of the viral membrane because of the incorporation of viral and cellular proteins. Another explanation is that the total number of infectious, subinfectious, or noninfectious particles as well as the absolute infectious titer can vary greatly between different stocks of the same virus and even more between different virus families. In the light of these differences, it is actually surprising that all IC_{50} values determined so far (in independent studies with different viruses) were always between 5 and 50 μM.[14,24] These findings further underline the proposed universal antiviral mode of action: the direct interaction and disruption of the viral membrane by the tweezer. The micromolar IC_{50} values may reflect the large number of lipids in the membrane which must be occupied by molecular tweezers before rupture occurs. An indication for this possibility comes from elevated IC_{50} levels observed when viral preparations contain large amounts of cellular fragments (data not shown). However, CLR01 binds very weakly to choline head groups (mM K_d range) and in a fully reversible manner with fast exchange (averaged NMR signals). Only when the surface tension exceeds the critical threshold is the viral membrane disrupted irreversibly.

In conclusion, CLR01 and CLR05 specifically target enveloped viruses by destroying the integrity of the viral membrane (Figure 8). Both tweezers do not affect "naked" EMCV or adenovirus infection but are active against all analyzed enveloped viruses, including not only well-known pathogens such as herpesviruses or HIV-1 but also emerging or reemerging viruses, including Ebola and Zika virus. A series of two-armed new tweezers was synthesized based on this mechanistic insight, which display significantly improved antiviral activities. Their additional lipid anchors increase viral membrane destabilization, and opens the path for structural optimization to more potent scaffolds. Our findings may be particularly useful for prevention and treatment of viruses, where no specific antiviral therapy exists as with the ongoing SARS-CoV-2/COVID-19 pandemic. Moreover, the apparent lack of toxicity in animal models render molecular tweezers very promising lead compounds for a novel class of potential broad-spectrum antivirals.[40,42−46]

Safety. To the best of our knowledge, there are no unexpected, new, or significant hazards or risks associated with the reported work.

■ ASSOCIATED CONTENT

Supporting Information

This material is available free of charge on the ACS Web site () The Supporting Information is available free of charge at https://pubs.acs.org/doi/10.1021/jacs.0c06400.

Materials and methods, supplementary figures and tables, and references of materials and methods (PDF)

■ AUTHOR INFORMATION

Corresponding Authors

Jan Münch − *Institute of Molecular Virology, Ulm University Medical Center, 89081 Ulm, Germany;* orcid.org/0000-0001-7316-7141; Email: jan.muench@uni-ulm.de

Elsa Sanchez-Garcia − *Computational Biochemistry, Center of Medical Biotechnology, University of Duisburg-Essen, 45117 Essen, Germany;* orcid.org/0000-0002-9211-5803; Email: elsa.sanchez-garcia@uni-due.de

James Shorter − *Cell and Molecular Biology Graduate Group and Department of Biochemistry and Biophysics, Perelman School of Medicine at the University of Pennsylvania, Philadelphia,*

https://dx.doi.org/10.1021/jacs.0c06400
J. Am. Chem. Soc. XXXX, XXX, XXX−XXX

Pennsylvania 19104, United States; orcid.org/0000-0001-5269-8533; Email: jshorter@pennmedicine.upenn.edu
Thomas Schrader − *Faculty of Chemistry, University of Duisburg-Essen, 45117 Essen, Germany;* orcid.org/0000-0002-7003-6362; Email: thomas.schrader@uni-due.de

Authors

Tatjana Weil − *Institute of Molecular Virology, Ulm University Medical Center, 89081 Ulm, Germany;* orcid.org/0000-0003-0925-2426
Rüdiger Groß − *Institute of Molecular Virology, Ulm University Medical Center, 89081 Ulm, Germany*
Annika Röcker − *Institute of Molecular Virology, Ulm University Medical Center, 89081 Ulm, Germany*
Kenny Bravo-Rodriguez − *Computational Biochemistry, Center of Medical Biotechnology, University of Duisburg-Essen, 45117 Essen, Germany*
Christian Heid − *Faculty of Chemistry, University of Duisburg-Essen, 45117 Essen, Germany*
Andrea Sowislok − *Faculty of Chemistry, University of Duisburg-Essen, 45117 Essen, Germany*
My-Hue Le − *Faculty of Chemistry, University of Duisburg-Essen, 45117 Essen, Germany*
Nelli Erwin − *Physical Chemistry I−Biophysical Chemistry, Faculty of Chemistry and Chemical Biology, TU Dortmund University, 44227 Dortmund, Germany*
Mridula Dwivedi − *Physical Chemistry I−Biophysical Chemistry, Faculty of Chemistry and Chemical Biology, TU Dortmund University, 44227 Dortmund, Germany*
Stephen M. Bart − *Department of Microbiology and Cell and Molecular Biology Graduate Group, Perelman School of Medicine at the University of Pennsylvania, Philadelphia, Pennsylvania 19104, United States*
Paul Bates − *Department of Microbiology and Cell and Molecular Biology Graduate Group, Perelman School of Medicine at the University of Pennsylvania, Philadelphia, Pennsylvania 19104, United States*
Lukas Wettstein − *Institute of Molecular Virology, Ulm University Medical Center, 89081 Ulm, Germany*
Janis A. Müller − *Institute of Molecular Virology, Ulm University Medical Center, 89081 Ulm, Germany*
Mirja Harms − *Institute of Molecular Virology, Ulm University Medical Center, 89081 Ulm, Germany*
Konstantin Sparrer − *Institute of Molecular Virology, Ulm University Medical Center, 89081 Ulm, Germany*
Yasser B. Ruiz-Blanco − *Computational Biochemistry, Center of Medical Biotechnology, University of Duisburg-Essen, 45117 Essen, Germany;* orcid.org/0000-0001-5400-4427
Christina M. Stürzel − *Institute of Molecular Virology, Ulm University Medical Center, 89081 Ulm, Germany*
Jens von Einem − *Institute of Virology, Ulm University Medical Center, 89081 Ulm, Germany*
Sina Lippold − *Institute of Virology, Ulm University Medical Center, 89081 Ulm, Germany*
Clarissa Read − *Institute of Virology, Ulm University Medical Center, 89081 Ulm, Germany; Central Facility for Electron Microscopy, Ulm University, 89081 Ulm, Germany*
Paul Walther − *Central Facility for Electron Microscopy, Ulm University, 89081 Ulm, Germany*
Marco Hebel − *Max Planck Institute for Polymer Research, 55128 Mainz, Germany; Institute of Inorganic Chemistry I, Ulm University, 89081 Ulm, Germany*
Florian Kreppel − *Center for Biomedical Education and Research, University of Witten/Herdecke, 58453 Witten, Germany*
Frank-Gerrit Klärner − *Faculty of Chemistry, University of Duisburg-Essen, 45117 Essen, Germany*
Gal Bitan − *Department of Neurology, David Geffen School of Medicine, Brain Research Institute, and Molecular Biology Institute, University of California, Los Angeles, Los Angeles, California 90095, United States;* orcid.org/0000-0001-7046-3754
Michael Ehrmann − *Microbiology II, Center of Medical Biotechnology, University of Duisburg-Essen, 45117 Essen, Germany;* orcid.org/0000-0002-1927-260X
Tanja Weil − *Max Planck Institute for Polymer Research, 55128 Mainz, Germany; Institute of Inorganic Chemistry I, Ulm University, 89081 Ulm, Germany;* orcid.org/0000-0002-5906-7205
Roland Winter − *Physical Chemistry I−Biophysical Chemistry, Faculty of Chemistry and Chemical Biology, TU Dortmund University, 44227 Dortmund, Germany;* orcid.org/0000-0002-3512-6928

Complete contact information is available at: https://pubs.acs.org/10.1021/jacs.0c06400

Author Contributions

▲T.W., R.G., A.R., and K.B.-R. contributed equally.

Notes

All data were analyzed using GraphPad Prism version 7.03 for Windows, GraphPad Software, La Jolla California USA (www.graphpad.com). Significance levels were calculated using one-way analysis of variance (ANOVA) (nonparametric, grouped), followed by Bonferroni's or Dunnett's multiple comparison test (indicated in figure legends). p-Values of <0.01 were considered significant (*, $p < 0.01$ **, $p < 0.001$ ***, $p < 0.0001$). In some cases, unpaired t tests (parametric, two-tailored) were used to compare a buffer control to compound-treated conditions.
The authors declare the following competing financial interest(s): A.R., C.H., A.S., T.S., G.B., and J.M. are inventors on the provisional patent application 62/692,479 New Molecular Tweezers against Neurological Disorders and Viral Infections. J.S. is a consultant for Dewpoint Therapeutics.

■ ACKNOWLEDGMENTS

M.H., T.W., L.W. and R.G. are part of the International Graduate School in Molecular Medicine Ulm. R.G. was funded by a scholarship from the International Graduate School in Molecular Medicine Ulm. P.W., J.M., and E.S.-G. acknowledge funding by the DFG CRC1279. J.S. was supported by a Bill and Melinda Gates Foundation Grand Challenges Explorations Award and NIH grant R21HD074510. J.M. acknowledges funding by the Volkswagen Foundation and the EU's Horizon 2020 research and innovation programme (Fight-nCoV, 101003555). J.A.M. is funded by a grant from the Medical Faculty of Ulm University and indebted to the Baden-Württemberg Stiftung for the financial support of this research project by the Eliteprogramme for Postdocs. A.S, C.H., and T.S. as well as K.B.R. and E.S-G. gratefully acknowledge funding by the DFG CRC 1093 "Supramolecular Chemistry on Proteins" (A3 and A8). E.S-G. and R.W. acknowledge the Deutsche Forschungsgemeinschaft (DFG, German Research Foundation) under Germany's Federal and State Excellence Strategy EXC-2033 Projektnummer 390677874. E.S-G. also acknowledges the Boehringer Ingelheim Foundation (Plus-3 grant) and the

computational time provided by the Computing and Data Facility of the Max Planck Society and the supercomputer magnitUDE of the University of Duisburg-Essen. G.B. acknowledges support from NIH/NIA grant R01AG050721. We thank Stefan Pöhlmann for providing the SARS-CoV-2 spike expression plasmid.

REFERENCES

(1) Jackman, J. A.; Shi, P. Y.; Cho, N. J. Targeting the Achilles Heel of Mosquito-Borne Viruses for Antiviral Therapy. *ACS Infect. Dis.* **2019**, *5* (1), 4−8.

(2) Vigant, F.; Santos, N. C.; Lee, B. Broad-Spectrum Antivirals against Viral Fusion. *Nature Reviews Microbiology*; Nature Publishing Group: 2015; pp 426−437.

(3) Liao, M.; Kielian, M. Domain III from Class II Fusion Proteins Functions as a Dominant-Negative Inhibitor of Virus Membrane Fusion. *J. Cell Biol.* **2005**, *171* (1), 111−120.

(4) Koehler, J. W.; Smith, J. M.; Ripoll, D. R.; Spik, K. W.; Taylor, S. L.; Badger, C. V.; Grant, R. J.; Ogg, M. M.; Wallqvist, A.; Guttieri, M. C.; Garry, R. F.; Schmaljohn, C. S. A Fusion-Inhibiting Peptide against Rift Valley Fever Virus Inhibits Multiple, Diverse Viruses. *PLoS Neglected Trop. Dis.* **2013**, *7* (9), e2430.

(5) Diwaker, D.; Mishra, K. P.; Ganju, L. Potential Roles of Protein Disulphide Isomerase in Viral Infections. *Acta Virol.* **2013**, *57* (3), 293−304.

(6) Badani, H.; Garry, R. F.; Wimley, W. C. Peptide Entry Inhibitors of Enveloped Viruses: The Importance of Interfacial Hydrophobicity. *Biochim. Biophys. Acta, Biomembr.* **2014**, *1838*, 2180−2197.

(7) Pollock, S.; Nichita, N. B.; Bohmer, A.; Radulescu, C.; Dwek, R. A.; Zitzmann, N. Polyunsaturated Liposomes Are Antiviral against Hepatitis B and C Viruses and HIV by Decreasing Cholesterol Levels in Infected Cells. *Proc. Natl. Acad. Sci. U. S. A.* **2010**, *107* (40), 17176−17181.

(8) St. Vincent, M. R.; Colpitts, C. C.; Ustinov, A. V.; Muqadas, M.; Joyce, M. A.; Barsby, N. L.; Epand, R. F.; Epand, R. M.; Khramyshev, S. A.; Valueva, O. A.; Korshun, V. A.; Tyrrell, D. L. J.; Schang, L. M. Rigid Amphipathic Fusion Inhibitors, Small Molecule Antiviral Compounds against Enveloped Viruses. *Proc. Natl. Acad. Sci. U. S. A.* **2010**, *107* (40), 17339−17344.

(9) Hollmann, A.; Castanho, M. A. R. B.; Lee, B.; Santos, N. C. Singlet Oxygen Effects on Lipid Membranes: Implications for the Mechanism of Action of Broad-Spectrum Viral Fusion Inhibitors. *Biochem. J.* **2014**, *459* (1), 161−170.

(10) Sinha, S.; Lopes, D. H. J.; Du, Z.; Pang, E. S.; Shanmugam, A.; Lomakin, A.; Talbiersky, P.; Tennstaedt, A.; McDaniel, K.; Bakshi, R.; Kuo, P. Y.; Ehrmann, M.; Benedek, G. B.; Loo, J. A.; Klärner, F. G.; Schrader, T.; Wang, C.; Bitan, G. Lysine-Specific Molecular Tweezers Are Broad-Spectrum Inhibitors of Assembly and Toxicity of Amyloid Proteins. *J. Am. Chem. Soc.* **2011**, *133* (42), 16958−16969.

(11) Attar, A.; Bitan, G. Disrupting Self-Assembly and Toxicity of Amyloidogenic Protein Oligomers by " Molecular Tweezers" - from the Test Tube to Animal Models. *Curr. Pharm. Des.* **2014**, *20* (15), 2469−2483.

(12) Schrader, T.; Bitan, G.; Klärner, F. G. Molecular Tweezers for Lysine and Arginine-Powerful Inhibitors of Pathologic Protein Aggregation. *Chem. Commun.* **2016**, *52* (76), 11318−11334.

(13) Hadrovic, I.; Rebmann, P.; Klärner, F.-G.; Bitan, G.; Schrader, T. Molecular Lysine Tweezers Counteract Aberrant Protein Aggregation. *Front. Chem.* **2019**, *7*, 657.

(14) Lump, E.; Castellano, L. M.; Meier, C.; Seeliger, J.; Erwin, N.; Sperlich, B.; Stürzel, C. M.; Usmani, S.; Hammond, R. M.; Von Einem, J.; Gerold, G.; Kreppel, F.; Bravo-Rodriguez, K.; Pietschmann, T.; Holmes, V. M.; Palesch, D.; Zirafi, O.; Weissman, D.; Sowislok, A.; Wettig, B.; Heid, C.; Kirchhoff, F.; Weil, T.; Klärner, F. G.; Schrader, T.; Bitan, G.; Sanchez-Garcia, E.; Winter, R.; Shorter, J.; Munch, J. A Molecular Tweezer Antagonizes Seminal Amyloids and HIV Infection. *eLife* **2015**, *4* (August), 1−33.

(15) Münch, J.; Rücker, E.; Ständker, L.; Adermann, K.; Goffinet, C.; Schindler, M.; Wildum, S.; Chinnadurai, R.; Rajan, D.; Specht, A.; Giménez-Gallego, G.; Sánchez, P. C.; Fowler, D. M.; Koulov, A.; Kelly, J. W.; Mothes, W.; Grivel, J. C.; Margolis, L.; Keppler, O. T.; Forssmann, W. G.; Kirchhoff, F. Semen-Derived Amyloid Fibrils Drastically Enhance HIV Infection. *Cell* **2007**, *131* (6), 1059−1071.

(16) Roan, N. R.; Müller, J. A.; Liu, H.; Chu, S.; Arnold, F.; Stürzel, C. M.; Walther, P.; Dong, M.; Witkowska, H. E.; Kirchhoff, F.; Münch, J.; Greene, W. C. Peptides Released by Physiological Cleavage of Semen Coagulum Proteins Form Amyloids That Enhance HIV Infection. *Cell Host Microbe* **2011**, *10* (6), 541−550.

(17) Usmani, S. M.; Zirafi, O.; Müller, J. A.; Sandi-Monroy, N. L.; Yadav, J. K.; Meier, C.; Weil, T.; Roan, N. R.; Greene, W. C.; Walther, P.; Nilsson, K. P. R.; Hammarström, P.; Wetzel, R.; Pilcher, C. D.; Gagsteiger, F.; Fändrich, M.; Kirchhoff, F.; Münch, J. Direct Visualization of HIV-Enhancing Endogenous Amyloid Fibrils in Human Semen. *Nat. Commun.* **2014**, *5* (1), 3508.

(18) Kim, K. A.; Yolamanova, M.; Zirafi, O.; Roan, N. R.; Staendker, L.; Forssmann, W. G.; Burgener, A.; Dejucq-Rainsford, N.; Hahn, B. H.; Shaw, G. M.; Greene, W. C.; Kirchhoff, F.; Münch, J. Semen-Mediated Enhancement of HIV Infection Is Donor-Dependent and Correlates with the Levels of SEVI. *Retrovirology* **2010**, *7* (1), 55.

(19) Castellano, L. M.; Shorter, J. The Surprising Role of Amyloid Fibrils in HIV Infection. *Biology* **2012**, 58−80.

(20) Torres, L.; Ortiz, T.; Tang, Q. Enhancement of Herpes Simplex Virus (HSV) Infection by Seminal Plasma and Semen Amyloids Implicates a New Target for the Prevention of HSV Infection. *Viruses* **2015**, *7* (4), 2057−2073.

(21) Bart, S. M.; Cohen, C.; Dye, J. M.; Shorter, J.; Bates, P. Enhancement of Ebola Virus Infection by Seminal Amyloid Fibrils. *Proc. Natl. Acad. Sci. U. S. A.* **2018**, *115* (28), 7410−7415.

(22) Roan, N. R.; Munch, J.; Arhel, N.; Mothes, W.; Neidleman, J.; Kobayashi, A.; Smith-McCune, K.; Kirchhoff, F.; Greene, W. C. The Cationic Properties of SEVI Underlie Its Ability To Enhance Human Immunodeficiency Virus Infection. *J. Virol.* **2009**, *83* (1), 73−80.

(23) Arnold, F.; Schnell, J.; Zirafi, O.; Sturzel, C.; Meier, C.; Weil, T.; Standker, L.; Forssmann, W.-G.; Roan, N. R.; Greene, W. C.; Kirchhoff, F.; Munch, J. Naturally Occurring Fragments from Two Distinct Regions of the Prostatic Acid Phosphatase Form Amyloidogenic Enhancers of HIV Infection. *J. Virol.* **2012**, *86* (2), 1244−1249.

(24) Röcker, A. E.; Müller, J. A.; Dietzel, E.; Harms, M.; Krüger, F.; Heid, C.; Sowislok, A.; Riber, C. F.; Kupke, A.; Lippold, S.; von Einem, J.; Beer, J.; Knöll, B.; Becker, S.; Schmidt-Chanasit, J.; Otto, M.; Vapalahti, O.; Zelikin, A. N.; Bitan, G.; Schrader, T.; Münch, J. The Molecular Tweezer CLR01 Inhibits Ebola and Zika Virus Infection. *Antiviral Res.* **2018**, *152*, 26−35.

(25) Dutt, S.; Wilch, C.; Gersthagen, T.; Talbiersky, P.; Bravo-Rodriguez, K.; Hanni, M.; Sánchez-García, E.; Ochsenfeld, C.; Klärner, F. G.; Schrader, T. Molecular Tweezers with Varying Anions: A Comparative Study. *J. Org. Chem.* **2013**, *78* (13), 6721−6734.

(26) Talbiersky, P.; Bastkowski, F.; Klärner, F. G.; Schrader, T. Molecular Clip and Tweezer Introduce New Mechanisms of Enzyme Inhibition. *J. Am. Chem. Soc.* **2008**, *130* (30), 9824−9828.

(27) Polkowska, J.; Bastkowski, F.; Schrader, T.; Klärner, F.-G.; Zienau, J.; Koziol, F.; Ochsenfeld, C. A Combined Experimental and Theoretical Study of the PH-Dependent Binding Mode of NAD+ by Water-Soluble Molecular Clips. *J. Phys. Org. Chem.* **2009**, *22* (8), 779−790.

(28) Jasper, C.; Schrader, T.; Panitzky, J.; Klärner, F.-G. Selective Complexation of N-Alkylpyridinium Salts: Recognition of NAD+ in Water. *Angew. Chem., Int. Ed.* **2002**, *41* (8), 1355−1358.

(29) Schrader, T.; Fokkens, M.; Klärner, F.-G.; Polkowska, J.; Bastkowski, F. Inclusion of Thiamine Diphosphate and S-Adenosylmethionine at Their Chemically Active Sites. *J. Org. Chem.* **2005**, *70* (25), 10227−10237.

(30) French, K. C.; Makhatadze, G. I. Core Sequence of Papf39 Amyloid Fibrils and Mechanism of Ph-Dependent Fibril Formation: The Role of Monomer Conformation. *Biochemistry* **2012**, *51* (51), 10127−10136.

https://dx.doi.org/10.1021/jacs.0c06400
J. Am. Chem. Soc. XXXX, XXX, XXX−XXX

(31) Lorizate, M.; Sachsenheimer, T.; Glass, B.; Habermann, A.; Gerl, M. J.; Kräusslich, H. G.; Brügger, B. Comparative Lipidomics Analysis of HIV-1 Particles and Their Producer Cell Membrane in Different Cell Lines. *Cell. Microbiol.* **2013**, *15* (2), 292−304.
(32) Thaa, B.; Siche, S.; Herrmann, A.; Veit, M. Acylation and Cholesterol Binding Are Not Required for Targeting of Influenza A Virus M2 Protein to the Hemagglutinin-Defined Budozone. *FEBS Lett.* **2014**, *588* (6), 1031−1036.
(33) Takahashi, T.; Suzuki, T. Function of Membrane Rafts in Viral Lifecycles and Host Cellular Response. *Biochem. Res. Int.* **2011**, *2011*, 1.
(34) Bavari, S.; Bosio, C. M.; Wiegand, E.; Ruthel, G.; Will, A. B.; Geisbert, T. W.; Hevey, M.; Schmaljohn, C.; Schmaljohn, A.; Javad Aman, M. Lipid Raft Microdomains: A Gateway for Compartmentalized Trafficking of Ebola and Marburg Viruses. *J. Exp. Med.* **2002**, *195* (5), 593−602.
(35) Brügger, B.; Glass, B.; Haberkant, P.; Leibrecht, I.; Wieland, F. T.; Kräusslich, H. G. The HIV Lipidome: A Raft with an Unusual Composition. *Proc. Natl. Acad. Sci. U. S. A.* **2006**, *103* (8), 2641−2646.
(36) Chan, R.; Uchil, P. D.; Jin, J.; Shui, G.; Ott, D. E.; Mothes, W.; Wenk, M. R. Retroviruses Human Immunodeficiency Virus and Murine Leukemia Virus Are Enriched in Phosphoinositides. *J. Virol.* **2008**, *82* (22), 11228−11238.
(37) Van Genderen, I. L.; Brandimarti, R.; Torrisi, M. R.; Campadelli, G.; Van Meer, G. The Phospholipid Composition of Extracellular Herpes Simplex Virions Differs from That of Host Cell Nuclei. *Virology* **1994**, *200* (2), 831−836.
(38) Sinha, S.; Du, Z.; Maiti, P.; Klärner, F. G.; Schrader, T.; Wang, C.; Bitan, G. Comparison of Three Amyloid Assembly Inhibitors: The Sugar Scyllo- Inositol, the Polyphenol Epigallocatechin Gallate, and the Molecular Tweezer CLR01. *ACS Chem. Neurosci.* **2012**, *3* (6), 451−458.
(39) Zheng, X.; Liu, D.; Klärner, F. G.; Schrader, T.; Bitan, G.; Bowers, M. T. Amyloid β-Protein Assembly: The Effect of Molecular Tweezers CLR01 and CLR03. *J. Phys. Chem. B* **2015**, *119* (14), 4831−4841.
(40) Prabhudesai, S.; Sinha, S.; Attar, A.; Kotagiri, A.; Fitzmaurice, A. G.; Lakshmanan, R.; Ivanova, M. I.; Loo, J. A.; Klärner, F. G.; Schrader, T.; Stahl, M.; Bitan, G.; Bronstein, J. M. A Novel "Molecular Tweezer" Inhibitor of α-Synuclein Neurotoxicity in Vitro and in Vivo. *Neurotherapeutics* **2012**, *9* (2), 464−476.
(41) Acharya, S.; Lapidus, L. J.; Safaie, B. M.; Attar, A.; Bitan, G.; Wongkongkathep, P.; Loo, J. A.; Ivanova, M. I.; Klärner, F.-G.; Schrader, T. Molecular Basis for Preventing α-Synuclein Aggregation by a Molecular Tweezer. *J. Biol. Chem.* **2014**, *289* (15), 10727−10737.
(42) Attar, A.; Chan, W. T. C.; Klärner, F. G.; Schrader, T.; Bitan, G. Safety and Pharmacological Characterization of the Molecular Tweezer CLR01-A Broad-Spectrum Inhibitor of Amyloid Proteins' Toxicity. *BMC Pharmacol. Toxicol.* **2014**, *15* (1), 23.
(43) Attar, A.; Ripoli, C.; Riccardi, E.; Maiti, P.; Li Puma, D. D.; Liu, T.; Hayes, J.; Jones, M. R.; Lichti-Kaiser, K.; Yang, F.; Gale, G. D.; Tseng, C. -h.; Tan, M.; Xie, C.-W.; Straudinger, J. L.; Klarner, F.-G.; Schrader, T.; Frautschy, S. A.; Grassi, C.; Bitan, G. Protection of Primary Neurons and Mouse Brain from Alzheimer's Pathology by Molecular Tweezers. *Brain* **2012**, *135* (12), 3735−3748.
(44) Ferreira, N.; Pereira-Henriques, A.; Attar, A.; Klärner, F. G.; Schrader, T.; Bitan, G.; Gales, L.; Saraiva, M. J.; Almeida, M. R. Molecular Tweezers Targeting Transthyretin Amyloidosis. *Neurotherapeutics* **2014**, *11* (2), 450−461.
(45) Fogerson, S. M.; van Brummen, A. J.; Busch, D. J.; Allen, S. R.; Roychaudhuri, R.; Banks, S. M. L.; Klärner, F. G.; Schrader, T.; Bitan, G.; Morgan, J. R. Reducing Synuclein Accumulation Improves Neuronal Survival after Spinal Cord Injury. *Exp. Neurol.* **2016**, *278*, 105−115.
(46) Lulla, A.; Barnhill, L.; Bitan, G.; Ivanova, M. I.; Nguyen, B.; O'Donnell, K.; Stahl, M. C.; Yamashiro, C.; Klärner, F. G.; Schrader, T.; Sagasti, A.; Bronstein, J. M. Neurotoxicity of the Parkinson Disease-Associated Pesticide Ziram Is Synuclein-Dependent in Zebrafish Embryos. *Environ. Health Perspect.* **2016**, *124* (11), 1766−1775.

https://dx.doi.org/10.1021/jacs.0c06400
J. Am. Chem. Soc. XXXX, XXX, XXX−XXX

Supplementary Information: Supramolecular Mechanism of Viral Envelope Disruption by Molecular Tweezers

Tatjana Weil[1#], Rüdiger Groß[1#], Annika Röcker[1#], Kenny Bravo-Rodriguez[2#], Christian Heid[3], Andrea Sowislok[3], My-Hue Le[3], Nelli Erwin[4], Mridula Dwivedi[4], Stephen M. Bart[5,6], Paul Bates[5,6], Lukas Wettstein[1], Janis A. Müller[1], Mirja Harms[1], Konstantin Sparrer[1], Yasser B. Ruiz-Blanco,[2] Christina M. Stürzel[1], Jens von Einem[7], Sina Lippold[7], Clarissa Read[7,8], Paul Walther[8], Marco Hebel[9,10], Florian Kreppel[11], Frank-Gerrit Klärner[3], Gal Bitan[12], Michael Ehrmann[13], Tanja Weil[9,10], Roland Winter[4], Thomas Schrader[3*], James Shorter[6,14*], Elsa Sanchez-Garcia[2*] and Jan Münch[1*]

[1]Institute of Molecular Virology, Ulm University Medical Center, 89081 Ulm, Germany;
[2]Computational Biochemistry, Center of Medical Biotechnology, University of Duisburg-Essen, 45117 Essen, Germany;
[3]Faculty of Chemistry, University of Duisburg-Essen, 45117 Essen, Germany;
[4]Physical Chemistry I—Biophysical Chemistry, Faculty of Chemistry and Chemical Biology, TU Dortmund University, 44227 Dortmund, Germany;
[5]Department of Microbiology, Perelman School of Medicine at the University of Pennsylvania, Philadelphia, Pennsylvania 19104, U.S.A.;
[6]Cell and Molecular Biology Graduate Group, Perelman School of Medicine at the University of Pennsylvania, Philadelphia, Pennsylvania 19104, U.S.A.;
[7]Institute of Virology, Ulm University Medical Center, 89081 Ulm, Germany;
[8]Central Facility for Electron Microscopy, Ulm University, 89081 Ulm, Germany;
[9]Max Planck Institute for Polymer Research, 55128 Mainz, Germany;
[10]Institute of Inorganic Chemistry I, Ulm University, 89081 Ulm, Germany;
[11]Center for Biomedical Education and Research, University of Witten/Herdecke, 58453 Witten, Germany;
[12]Department of Neurology, David Geffen School of Medicine, Brain Research Institute, and Molecular Biology Institute, University of California, Los Angeles, California 90095, U.S.A.;
[13]Microbiology II, Center of Medical Biotechnology, University of Duisburg-Essen, 45117 Essen, Germany;
[14]Department of Biochemistry and Biophysics, Perelman School of Medicine at the University of Pennsylvania, Philadelphia, Pennsylvania 19104, U.S.A.

# equal contribution
*For correspondence:
jan.muench@uni-ulm.de; elsa.sanchez-garcia@uni-due.de;
jshorter@pennmedicine.upenn.edu; thomas.schrader@uni-due.de;

Table of Contents

1. Materials and Methods

Computational details

Free energy perturbation (FEP)[1] and extended-system Adaptive Biasing Force[2] (eABF) calculations were used to study the binding of **CLR05** to PAP248-286. The FEP included the alchemical transformation of **CLR01** to **CLR05** while forming an inclusion complex with Lys/Arg residues in PAP248-286 to evaluate the relative binding affinity of **CLR05** with respect to **CLR01.** Molecular dynamics (MD) simulations of the only-DOPC and mixed (54:30:36 DOPC:PSM:Chol) bilayers in the presence of nine ligand molecules (**CLR01**, **CLR05** or **PC**) were performed in explicit water with the tweezers and clip molecules initially placed 4 Å over the membrane. Three independent replicas of 110 ns each were performed for all systems where the first 10 ns were not considered in the analysis of the results. The insertion of **CLR01**/**CLR05**/**PC** into the bilayers was studied using the eABF scheme.[2] These calculations were done with NAMD2.9[3] and the CHARMM36 force field[4]. The parameters for **CLR01**/**CLR05**/**PC** were obtained using the Swissparam server[5] and validated by us. The total simulated time reported in this study was above 7.7 μs.

*REMD simulation of the interaction between PAP248-286 and **CLR05***

The interactions of $PAP_{248-286}$ with the molecular tweezer **CLR05** were investigated using Replica Exchange Molecular Dynamics (REMD) simulations[6,7] performed with Gromacs 4.6[8] and the CHARMM27 force field (FF)[9,10]. In total, 37 replicas were simulated during 75 ns, following a setup analogous to the previously reported for **CLR01**[11].

Free Energy calculations of PAP248-286 with tweezers

The interactions of $PAP_{248-286}$ with the molecular tweezers **CLR01** and **CLR05** were also investigated using free energy calculations. The NAMD2.9 code[3] was used with the CHARMM22 force field (including CMAP corrections)[10,12] and the TIP3P model for water[13]. The parameters for **CLR01** and **CLR05** were obtained using the Swissparam server[5] and have been previously validated by us[14,15]. The initial coordinates of $PAP_{248-286}$ were taken from the Protein Data Bank, code 2L3H[16]. For each Lys and Arg (except Lys272, which is only accessible in certain conformations) the relative free energy change for the binding of **CLR01** and **CLR05** was calculated considering inclusion complexes with a 1:1 ratio of $PAP_{248-286}$ and molecular tweezers. The alchemical transformation was performed using NAMD2.9[3] and Free Energy Perturbation theory[1] (FEP). Only the substituents in the tweezers were alchemically transformed. The temperature was set to 300 K. The alchemical transformation was accomplished using 60 windows. In each window, $4 \cdot 10^5$ time steps of MD simulation (including $1 \cdot 10^5$time steps of equilibration) were performed to generate a representative ensemble. The forward and backward transformations were performed to estimate the error in the free energy values using the Bennett acceptance ratio estimator[17].

In addition, the extended-system Adaptive Biasing Force (eABF)[18], as implemented in NAMD2.9, was used to estimate if the tweezers form an inclusion complex with each of the seven considered residues. Two collective variables were selected (Fig. S1b). The collective

variable representing the distance between the included amino acid and the tweezers was explored from 0 Å to 12 Å with a 0.5 Å width, while the angle measuring the degree of inclusion of the amino acid in the cavity of the tweezers was explored from 0º to 180º with a 10º width. In the inclusion complex, the optimal values of the collective variables are approximately 0.25 Å and 90º. For each bin, 100 samples were taken before the application of the biasing force. The timestep of the simulations was set to 1 fs and the total simulated time was 100 ns. The temperature was set to 300 K.

Molecular dynamics simulations of the ligands in model membranes

Two model lipid bilayers were used for the study of the interaction of **CLR01**, **CLR05** and **PC** with membranes. We built a DOPC bilayer containing 120 DOPC lipids per leaflet and a mixed bilayer containing 54, 30 and 36 molecules per leaflet of DOPC, SM and CHL, respectively. Both bilayers were built using the CHARMM–GUI interface.[19,20]

The interaction of each molecule with the model membranes was studied using three independent molecular dynamics (MD) simulations containing nine molecules of **CLR01**, **CLR05** or **PC**. The molecules were initially placed 4 Å over the membrane. The membrane was oriented perpendicular to the z-axis and the center of mass of the nitrogen atoms in both leaflets was harmonically restrained to the coordinates' origin to prevent the membrane drifting along the z-axis. A harmonic potential was used to prevent **CLR01**, **CLR05** or **PC** to cross the boundary of the simulated cell in the +z direction.

MD simulations were performed with the NAMD2.9 program using the CHARMM36 force field.[3,4] The systems were solvated using the TIP3P water model and ions added to reach 0.1 M concentration.[13] A timestep of 2 fs was used. The temperature was set to 300 K. Before the production runs, the bilayers were equilibrated for 50 ns. In all cases, 110 ns of production MD were performed, and the initial 10 ns were discarded. The total MD simulated time was nearly 1 μs for each ligand.

*Free energy calculations of **CLR01**/**CLR05**/**PC** in bilayers*

The PMF profiles for the insertion of **CLR01**, **CLR05** and **PC** in the bilayers were calculated using the eABF method[18]. The z projection of the center of mass of the tweezers was taken as the collective variable. The collective variable was divided in 22 windows of 2 Å widths. Each window was simulated for 10 ns. In each bin, 200 samples were collected before starting to apply the biasing force. The initial geometry for each window was taken from a Steered Molecular Dynamic (SMD) simulation[21,22] in which a force in the –z direction was applied to **CLR01** to accelerate the insertion of **CLR01** in the membrane. The SMD was performed under the same conditions as described for the standard MD simulations. In addition, a constant velocity regime was used with a speed of 0.0005 Å timestep^{-1} and a force constant of 7 kcal mol^{-1} Å^{-1}.

QM/MM calculations

The inclusion complexes of **CLR01** with DOPC and SM were studied using QM/MM optimizations. To this end, randomly selected snapshots from the MD simulations of **CLR01** with or without the mixed bilayer in explicit water were optimized at the B3LYP-D3/def2-

SVP//CHARMM36[4,23–25] level of theory using ChemShell v3.5.[26] For each complex, five snapshots were selected. An electrostatic embedding scheme[27] was employed together with a charge shift scheme.[28,29] The active region consisted of a 20 Å region around **CLR01** and the lipid forming the inclusion complex. The tweezer together with the trimethylammonium part of the lipid head were chosen as the QM region, which was calculated with Turbomole v6.6[24] while DL_POLY[30] was used for the MM region. All atoms within the active region were allowed to freely move in each optimization step.

Small molecules, peptides and seminal amyloids

CLR01, **CLR05** and **PC** were prepared as described previously[15,31–33] and 1.3-7.4 mM stock solutions were prepared in PBS (for **CLR01** and **PC**) or diluted NaOH/water/10 mM NaH_2PO_4 pH = 7.6 (for **CLR05**). Synthetic peptides PAP248-286, PAP85-120, and SEM1(45-107) were purchased from Keck Biotechnology Resource Laboratory, Shanghai Hanhong Chemical Company or Celtek peptides. For fibril formation, peptides were reconstituted and assembled as previously described[34–36].

Amyloid detection assay

For assembly experiments, reconstituted peptides PAP248-286 (1 mM), PAP85-120 (1 mM) ore SEM1(45-107) (0.5 mM) were incubated with **CLR01**, **CLR05** or **PC** and agitated at 37°C at 1400 rpm. At various time points, aliquots (1 µl) were removed and added to 25 µM ThT in PBS (200 µl). Changes in fluorescence (excitation: 440 nm, emission: 482 nm) were measured using a Tecan Safire2 microplate reader. Alternatively, reactions were processed for TEM as described[11].

For amyloid-remodeling experiments, fibrils (20 µM, based on peptide monomer concentrations) were diluted into an assay buffer (25 mM HEPES, 150 mM KOAc, 10 mM $Mg(OAc)_2$, pH 7.4) in the presence of ATP (5 mM) and incubated with either **CLR01**, **CLR05** or **PC**. After 2 h, aliquots (5 µl) were removed and added to 25 µM ThT in PBS (55 µl) before ThT fluorescence was measured. Alternatively, reactions were processed for TEM as described[11].

Confocal microscopy

Fibrils (200 µg/ml in PBS) were stained with Proteostat Amyloid Plaque Detection Kit (Enzo Life Sciences, Plymouth Meeting, PA). Then, fibrils were treated with a 20-fold excess **CLR01**, **CLR05** or **PC** and mixed 1:2 with MLV-Gag-YFP virions. Samples were transferred to µ-slides VI0.4 (Ibidi, Munich, Germany) and imaged with a Zeiss LSM confocal microscope.

Effect of tweezer on HIV infection and amyloid-mediated enhancement

The reporter cell line TZM-bl was obtained through the NIH ARRRP and cultured as described[11]. Virus stocks of the R5-tropic HIV-1 NL4-3 92TH014 derivative were generated by transient transfection of 293T cells as described[35]. Stocks were analyzed by p24 antigen ELISA and stored at -80°C. To compare the antiviral effects of **CLR05** and **PC** to **CLR01**, 3-fold dilution series of the compounds were prepared before R5-tropic HIV-1 NL4-3 92TH014 was added (20 ng/ml p24 antigen), resulting in **CLR01**/**CLR05**/**PC** concentrations of 0-150 µM. After incubation for 10 min at 37°C, the mixtures were resuspended and added to 10^4

TZM-bl cells in 180 µl medium seeded in 96-well flat-bottom plates the day before infection. Infection rates were determined 3 days post infection by detecting β-galactosidase activity in cellular lysates using the Tropix Gal-Screen kit (Applied Biosystems) and the Orion microplate luminometer (Berthold). All values represent reporter gene activities (relative light units per second; RLU/s) derived from triplicate infections minus background activities derived from uninfected cells. To assess the effect of **CLR01**, **CLR05** and **PC** on amyloid-mediated enhancement of HIV-1 infection, 200 µg/ml fibrils (44 µM SEVI, 45 µM PAP85-120 fibrils, 28 µM SEM1(45-107) fibrils) were treated with a 20-fold molar excess of **CLR05** or **CLR01** for 10 min at room temperature. The mixtures were serially diluted 5-fold before R5-tropic HIV-1 NL4-3 92TH014 was added (1 ng/ml p24 antigen). After 5 min, 20 µl of these mixtures were added to 10^4 TZM-bl cells and infection rates were determined 3 days post infection.

Giant unilamellar vesicles

Giant unilamellar vesicles (GUVs) were prepared by electroformation on optically transparent and electrically conductive indium tin oxide (ITO)-coated glass slides in a preparation chamber consisting of a closed bath imaging chamber RC-21B affixed to a P-2 platform topped with a flow-through temperature block. A solution of pure DOPC (1,2-dioleoyl-sn-glycero-3-phosphocholine) containing 0.2 mol% N-Rh-DHPE (N-(lissamine rhodamine B sulfonyl)-1,2-dihexadecanoyl-sn-glycero-3-phosphoethanolamine) or a lipid mixture of 45 mol% DOPC, 25 mol% sphingomyelin (SM), and 30 mol% cholesterol (Chol) containing 0.2 mol% N-Rh-DHPE and 0.1 mol% Bodipy-Chol (23-(dipyrrometheneboron difluoride)-24-norcholesterol) in chloroform was spread on an ITO-coated cover slip (20 µL, 1 mg/mL), spin-coated at 800 rpm for 1 min, and subsequently dried under vacuum for at least 2 h. Then, the lipids were hydrated in 10 mM NaH2PO4 buffer (pH 7.6) containing the water-soluble fluorophore ATTO 647 (5 µM) within the preparation chamber. The electroformation of pure DOPC and the DOPC/SM/Chol mixture was performed at RT and 60°C, respectively, by applying a frequency-alternating current field (500 Hz, 100 mV for 10 min, 1 V for 20 min, and 1.6 V for 2.5 h) to the ITO electrodes by a TG315 function generator. The preparation chamber was cooled down to RT in case of the lipid mixture and carefully rinsed with 10 mM NaH_2PO_4 buffer to remove the water-soluble ATTO 647 that was not enclosed in the interior of the vesicles. 150 µM **CLR05** or **PC** dissolved in 10 mM NaH_2PO_4 buffer were added to the samples and imaged after different incubation times using a Biorad confocal microscope coupled via a side port to an inverted Nikon microscope enabling fluorescence excitation in the focal plane of a Nikon objective. Fluorescence of Bodipy-Chol, N-Rh-DHPE, and ATTO 647 was acquired using a Kr/Ar laser. Analysis of the data was performed using the Fiji software.

Liposome dye leakage

Liposomes for dye-leakage assay were prepared by thin-film hydration & extrusion. DOPC (1,2-dioleoyl-sn-glycero-3-phosphocholine), sphingomyelin (Egg SM) and cholesterol (ovine wool) dissolved in chloroform (Avanti Polar Lipids, Alabaster, USA) were mixed at 45/25/30 mol% ratio in a glass round-bottom flask. The solvent was then evaporated by slowly applying a vacuum at a Schlenk line. The vacuum was held for 2 h and then purged with argon. The lipid film was then hydrated by adding 50 mM 5(6)-carboxyfluorescein prepared in 50% PBS (resulting in a solution isoosmolar to PBS) and adjusted to pH 7.4 with NaOH, yielding a total lipid concentration of 5 mM. The flasks were shaken at 60°C, 180 rpm, for 1h. Small

unilamellar vesicles were then prepared by 25x extrusion through 0.2 µM polycarbonate membranes (Nuclepore Track-Etched Membrane, Whatman, Maidstone, USA) in a Mini Extruder (Avanti Polar Lipids) on a heating platform at 60°C. Free dye was removed by 2x size-exclusion filtration using PD midiTrap Sephadex G-25 columns (GE Healthcare, Buckinghamshire, UK) and liposomes then quantified by nanoparticle tracking analysis (NTA) using a ZetaView (ParticleMetrix, Inning, Germany). For assay in 96-well format, liposome preparations were diluted in PBS and 2.25*10^9/well added to plates in 90 µl volume. Fluorescence intensity was read in a Cytation 3 plate reader (Biotek, Winooski, USA). Baseline was established by measuring fluorescence for 5 min, 10 µl of compounds then added and plates incubated for 30 min more with measurements every 1 min. Maximum intensity (100% dye release) was then measured by adding Triton X-100 to 1% final concentration and again measuring for 5 min.

Atomic force microscopy

Stock solutions (10 mg/mL) of every single lipid in chloroform were mixed to obtain the desired composition and amount. After most of the solvent was removed with a nitrogen steam, remaining chloroform was evaporated under vacuum for at least 2 h. The dried lipid mixture was hydrated with 20 mM Tris (pH 7.4) and 5 mM $MgCl_2$. After extensive vortexing and sonification in a water bath at a temperature above the melting temperature of the respective lipid mixture and applying five freeze-thaw cycles, large unilamellar vesicles with a pore size of 100 nm size were obtained by extrusion trough a polycarbonate membrane (Avanti Polar Lipids, Alabaster USA). Vesicle fusion on mica was carried out by depositing 70 µL of the large unilamellar vesicles solution on freshly cleaved mica and incubation in a wet chamber at 70 °C for 2 h. After vesicle fusion, the samples were rinsed carefully with Tris buffer to remove unspread vesicles. For the tweezer-membrane interaction studies, 200 µL of the tweezer (at the desired concentrations) were injected into the AFM fluid cell. Measurements were performed on a MultiMode scanning probe microscope with a Nano- Scope IIIa controller (Digital Instruments, Santa Barbara, CA) and use of a J-Scanner (scan size 125 µm). Images were obtained by applying the tapping mode in liquid with oxide-sharpened silicon nitride (DNP-S) or sharp nitride lever (SNL) probes mounted in a fluid cell (MTFML, Veeco (now Bruker), Karlsruhe, Germany). Tips with nominal force constants of 0.24 Nm^{-1} were used at driving frequencies around 9 kHz and drive amplitudes between 200 and 800 mV. Scan frequencies were between 1.0 and 1.94 Hz. Height and phase images of sample regions were acquired with resolutions of 512 × 512 pixels. All measurements were carried out at room temperature and analyzed by using the analysis and processing software NanoScope version 5 and Origin 9.1 (OriginLab Corporation, Northampton, MA, USA).

Cryo-TEM

For cryo-TEM of HCMV extracellular virions, 1.5 ml cell-free supernatant of HCMV infected cells virions was centrifuged at 14,000 rpm for 30 min. Pelleted virions were resuspended in 20 µl serum-free medium and subsequently treated with serum-free medium or 50 µM **CLR01** for 30 min at 37°C. Then, 3.5 µl of the virus preparations were applied to a freshly glow-discharged C-flat holey carbon grid (CF-2/2-4C, Protochips) and then vitrified in liquid ethane by a Vitrobot type FP 5350/60 (FEI). Images with a pixel size of 0.187 nm were acquired using the

JEM2100F (Jeol) microscope at an acceleration voltage of 200 kV. For this, a direct electron camera type DE12 (Direct Electron) and the SerialEM software version 3.5.3 were used.

Comparative NMR studies

1:1 complexes and 3:1 complexes between **CLR01**, **CLR05** and **PC** and the lipids DOPC and SM were prepared in deuterated methanol (CD_3OD) for homogeneous solubility at 0.33 mM lipid concentration and 0.33 mM as well as 1.00 mM host concentration. Chemical shift changes to higher field for the NMe_3 signals of the choline head-group were monitored as quantitative relative indicators for their potential inclusion inside the host cavities. T = 298 K.

NMR Titrations

A lipid guest solution (c = 0.33 mmol/L) was prepared in deuterated methanol CD_3OD. 600 µL of this solution were placed in an NMR tube and a spectrum was recorded. The **CLR01** host solution (c = 10 mmol/L) was prepared using the guest solution to keep the guest concentration constant during the titration. Increasing amounts of host solution were added and the resulting NMR spectra were recorded. The resulting **CLR01** concentrations were: 0.16 mM, 0.32 mM, 0.48 mM, 0.62 mM, 0.91 mM, 1.18 mM, 1.43 mM, 1.89 mM, 2.31 mM, 2.85 mM, 3.33 mM. Hence the final host guest ratio was higher than 10:1. For the determination of binding constants, the chemical shift changes of the N**(Me)$_3$**, the P-O-**CH_2**-CH_2 and the P-O-CH_2-**CH_2** protons were monitored during the titration. From the resulting binding isotherms, 1:1 affinities and $\Delta\delta_{max}$ values between 1.06 ppm and 4.36 ppm were calculated by non-linear regression. NMR titrations were performed for **CLR01**, **CLR05** and **PC** with both lipids DOPC and SM.

Cell viability

The effect of **CLR05** on the metabolic activity of TZM-bl cells was analyzed using CellTiter-Glo assay (Promega). After 3 days of incubation, supernatant was discarded and 50 µl PBS and 50 µl CellTiter-Glo Reagent were added to the cells. After incubation and gentle shaking for ten minutes at room temperature, luminescence in the cell-free supernatant was determined via the Orion microplate luminometer (Berthold). The luminescence signal is proportional to the amount of ATP and thus, the number of viable cells present.

p24 release assay

HIV-1 NL4-3 92TH014 was incubated for 10 min at 37°C with buffer, or 100 µM **CLR01**, **CLR05** or **PC** before the mixtures were centrifuged at 20,000×g and 4°C for 1 h. The p24 content of the supernatant and pellet was determined using an in house p24-antigen ELISA.

RNA release assay

ZIKV MR766 (8.89x107 TCID50/ml) was purified via sucrose cushion spin. To this end, 500 µl virus stock were added on top of a 200 µl 20% sucrose solution and centrifuged for 2 h at 20,000×g. After discarding the supernatant, the virus pellet was resuspended in 100 µl PBS, resulting in a 5-fold concentration of viral particles. For the preparation of controls, the supernatant of uninfected Vero E6 cells was treated equally. Purified virus or cell supernatant were then incubated with PBS, 1.5-150 µM **CLR01**, **PC**, 150 µM Triton X-100 or 15-300 µM **CLR05** for 30 min at 37 °C. Then, the samples were UV-inactivated for 1 h. 10 µl of each sample were used to quantify the RNA concentration using a QuantiFluor® RNA System and

a Quantus Fluorometer (Promega) according to the manufacturer's instructions. From each sample, the signal of PBS treated ZIKV was subtracted to obtain the actually released RNA concentrations.

Aggregation of virus-like particles (VLPs)

Virus-like-particles of murine leukemia virus tagged with YFP (MLVgag-YFP VLPs) were produced by transfection of HEK293T cells with pcDNA3_MLV Gag-YFP using Transit LT-1 (Mirus). 2 days post-transfection, supernatants were harvested, clarified by centrifugation, aliquoted and frozen at -80°C until use. Thawed supernatants were diluted in PBS and analyzed by fluorescent nanoparticle tracking analysis (F-NTA) using a ZetaView TWIN (Particle Metrix). To study aggregation of VLPs, pre-diluted VLPs were incubated with compounds (or PBS only) for 30 or 120 min at room temperature and then injected into the ZetaView. Particles were then tracked using the following settings: 25°C fixed temperature, 488 nm excitation laser, 500 nm fluorescence filter, 11 positions, 2s/video per position, sensitivity 95, shutter 250, 15 fps, 3 acquisitions with 20 µl PBS pumped between measurements. Tracked particle size distributions were analyzed in FlowJo 10.7.1 and gated to reveal free VLPs based on the tracking data of untreated particles. The number of free particles was averaged per tracked position. Note that in fluorescence mode, only VLPs but no fibrils/other macromolecules are visualized and tracked. Aggregation is inferred from apparent size changes due to reduced diffusion speed of particles.

Antiviral assays

Herpes simplex virus 1 (HSV-1) and HSV-2: Dilution series of **CLR01**, **CLR05** and **PC** were prepared in serum free minimal essential medium (MEM, Invitrogen, Germany). HSV-1 (strain R 10.2) was added corresponding to infection rates of about 50%, resulting in final compound concentrations of 0-150 µM. After incubation for 30 min at 37°C, mixtures were added to $1.7x10^4$ Vero E6 cells per well in a 96-well flat-bottom plate and incubated for 1 h at 37°C. Then, media were changed, and cells were overlayed with 0.6% methylcellulose. 12 hours post infection (hpi) cells were fixed and infection rates were determined by indirect immunofluorescence staining for HSV-1 infected cell protein 0 (ICP0) antigen.

Human Adenovirus type 5 (HAdV5): The E1-deleted replication-deficient human adenovirus type 5-based vector containing a HCMV promoter-controlled EGFP expression cassette was produced, purified and characterized as described[11]. To assess effects of **CLR01** and **CLR05** on HAdV5 infectivity, the vector was titrated with 0–100 µM **CLR01** or **CLR05** and incubated 10 min at 37°C in 50 mM HEPES, 150 mM NaCl, pH 7.17. $1×10^5$ A549 cells per well were seeded 1 day prior to infection in 24-well plates and infected with 200 MOI of the pretreated virus. EGFP expression was analyzed 1 day post transduction using a Beckman–Coulter Gallios flow cytometer.

Zika virus (ZIKV): Virus stocks of ZIKV strain MR766 (kindly provided by J. Schmidt-Chanasit, Bernhard Nocht Institute for Tropical Medicine, Hamburg) was propagated as described previously[11,37] in Vero E6 cells (Cercopithecus aethiops derived epithelial kidney, also kindly provided by J. Schmidt-Chanasit). Virus titers were determined via the Reed-Muench method[38] and stored at -80°C. To investigate the effect of **CLR01** and **CLR05** on

ZIKV infection, ZIKV MR766 at an MOI of 0.2 was incubated for 30 min at 37°C with buffer or 0.2-150 µM **CLR01**, **CLR05** or **PC**. Then, these mixtures were added to 6×10^3 Vero E6 cells seeded the day before into 96-well plates. After 2 days, a cell-based ZIKV immunodetection assay was performed as described[39,40].

Pseudotyped lentiviral particles: Lentiviral pseudotypes harboring glycoproteins from Ebola, Marburg, SARS and Rabies virus were obtained as described previously[39,40]. Viral pseudotypes were incubated with **CLR05** or **PC** for 10 min at 37°C and used to infect 10^4 Huh-7 cells. After 3 days, infection rates were determined by quantifying firefly luciferase activity using the Luciferase Assay System (Promega, Madison, USA). All values represent reporter gene activities (relative light units per second; RLU/s) derived from triplicate infections minus background activities derived from uninfected cells.

Lentiviral-SARS-COV-2 pseudoparticle: For pseudoparticle generation $3x10^6$ HEK293T cells were seeded in 10 cm dishes one day prior to transfection. The next day medium was changed, and cells were transfected with TransIT-LT1 (Mirus Bio) according to the manufacturer's instructions. A total DNA amount of 30 µg DNA was transfected comprising 2 % pCG1-SARS-2-S (encoding the SARS-CoV-2 Wuhan Hu-1 Spike protein, kindly provided by Stefan Pöhlmann) as well as pSEW-luc2 (encoding a firefly luciferase gene) and pCMVdR8.91 (encoding an *env* deficient lentiviral backbone) at a 1:1 ratio. At 8 h post transfection, medium was replaced with DMEM supplemented with 2.5% FCS. At 48 h post transfection, the virus stock was harvested and clarified by centrifugation (5 min, 1500rpm) and virus containing supernatants were stored at 4 °C.

For inhibition assay of the tweezer, lentiviral-SARS-COV-2pp were incubated for 30 minutes at 37°C with 150 µM - 1.17 µM **CLR01**, **CLR05**, **CLR03** and **PC.** Afterwards the tweezer-pseudoparticle mixture was added on CaCo2 cells in 96 well plate. At 48 h post transduction, the infection rates were assessed by measuring firefly luciferase activity using Firefly luciferase assay kit from Promega. Therefore, supernatant was removed, and cells were washed once with PBS. PBS was discarded and cells were lysed with 40 µl lysis-buffer per well. 30 µl of these lysates were transferred to a 96-well Nunclon-delta white microwell plate and mixed with 50 µl of Luciferase Assay substrate. Values represent % luciferase activities (relative light units per second; RLU/s) derived from triplicate infections and normalized to values obtained for transduced cells in absence of tweezer.

Encephalomyocarditis virus (EMCV): Murine encephalomyocarditis virus (EMC strain) was obtained from ATCC and propagated in Vero E6 cells[41]. The virus was incubated for 30 min at 37°C either with buffer or 0.2-150 µM **CLR01**, **CLR05** or **PC** before adding it to 2×10^4 HFF cells in 96-well plates (MOI 0.1). 48 h post infection the cytopathic effect was quantified using the 3-[4,5-dimethyl-2-thiazolyl]-2,5-diphenyl-2H-tetrazolium bromide-(MTT)-based cell viability assay[37]. To determine infection rates, sample values were subtracted from untreated controls that were set to 100% viability.

Influenza virus (IAV): Influenza strain A/PR/8/34 (H1N1; PR8) was purchased from ATCC and propagated in MDCK cells as previously reported[41]. For inhibition assays, virus was diluted

in serum-free medium supplemented with 1 µg/mL TPCK treated trypsin (Sigma) and was incubated with 0-150 µM **CLR01**, **CLR05** or **PC** for 30 min at 37°C before the mixtures were used to infect 2×10^4 A549 cells (MOI 0.2). After 1 h incubation at 37°C, cells were washed three times with PBS before 100 µl fresh growth medium containing 0.1% FCS and TPCK treated trypsin were added. After 48 hours, infectivity rates were determined by measuring neuramidase activity in cellular lysates (MUNANA assay). Therefore, cells were lysed for 30 min in 10% Triton-X100 and lysates were diluted 1:2 in MES buffer (containing 32.5 mM MES monohydrate and 4 mM $CaCl_2$ dihydrate). 20 µl of each sample were transferred to black 96-well plates and 30 µl 10 µM 20-(4-methylumbelliferyl)-a-D-N-acetylneuraminic acid (MUNANA) were added. After 4 h of incubation at 37°C and gentle shaking, reaction was stopped with 150 µl stop solution containing 0.1 M glycine and 25% ethanol. Neuramidase-dependent cleavage of the substrate to the fluorescent product methylumbelliferone was quantified at an excitation of 360 nm and an emission at 455 nm was measured on a Cytation 3 Cell Imaging Multi-Mode Reader (BioTek, USA). Background from uninfected cells was subtracted and relative enzyme activity was used to quantify infection rates.

Measles virus (MV): Measles virus strain Schwarz was obtained from the lab of Karl-Klaus Conzelmann and propagated in Vero E6 cells as previously published[42]. Virus was diluted in serum-free medium and a viral dose corresponding to MOI 0.5 was added to 0-150 µM dilutions of **CLR01**, **CLR05** or **PC** for 30 min at 37°C before the mixtures were added to 2×10^4 A549 cells seeded the day before into black 96-well plates with a clear bottom (Corning Costar, USA). After 4 h, cells were washed 3x with PBS and fresh medium containing 10% FCS was added to the cells. 48 hours post infection, supernatants were discarded, cells were washed 1x with PBS and fixed with 70% acetone for 20 min at 4°C. After discarding the acetone, plates were allowed to dried completely before 50 µl FITC-coupled mouse anti-measles antibody (Millipore, USA), 1:2000 diluted in PBS were added to each well. The plates were incubated in the dark overnight at 4°C. After 3 washing steps with PBS, fluorescence at 528 nm (excitation at 485 nm) was quantified on a Cytation 3 Cell Imaging Multi-Mode Reader (BioTek, USA).

Supplementary Figures

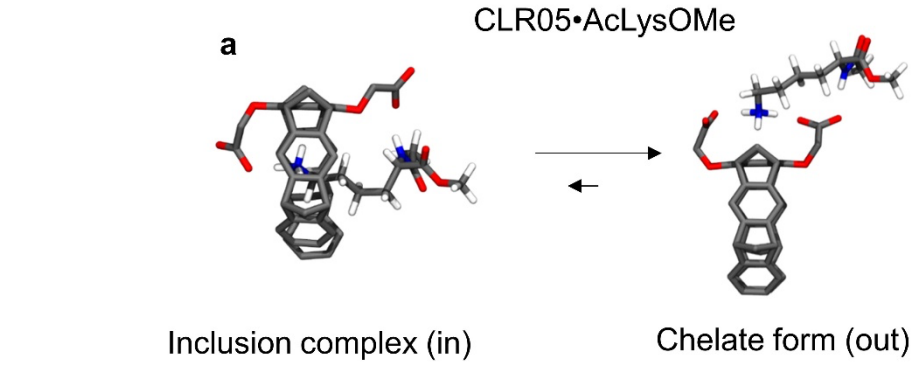

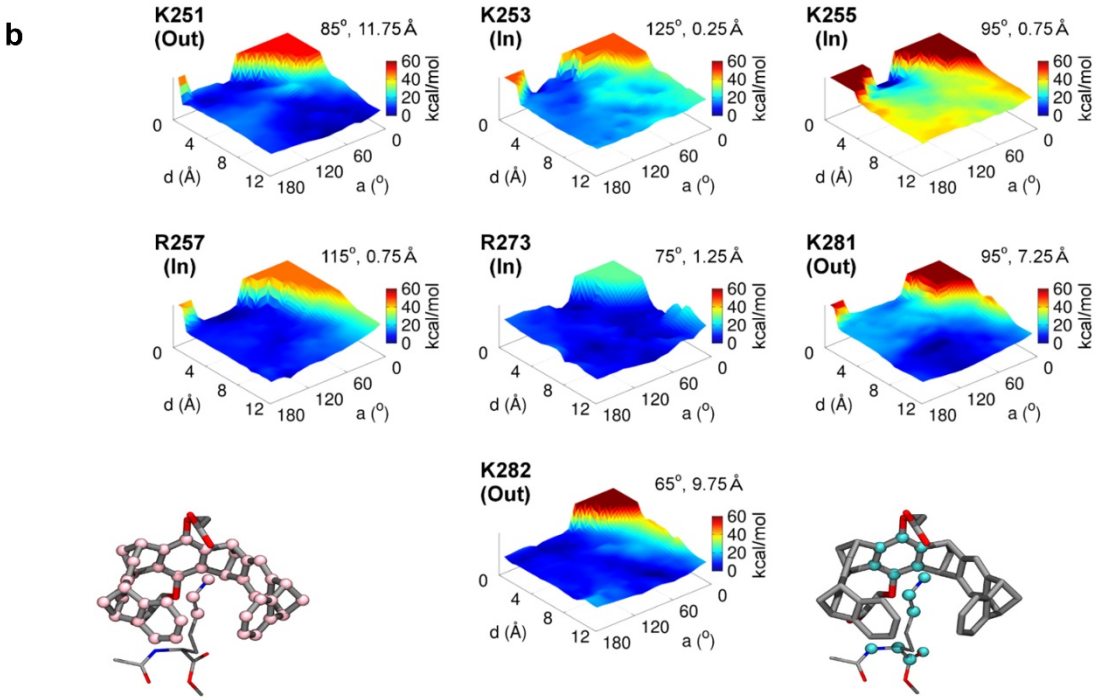

c

	Distance (Å)		Angle (°)	
Residue	**eABF**	**Reference value[1]**	**eABF**	**Reference value[1]**
Lys_{251}	11.75	1.0 ± 0.33	85	97 ± 14
Lys_{253}	0.25	1.1 ± 0.37	125	85 ± 15
Lys_{255}	0.75	1.1 ± 0.56	95	93 ± 16
Arg_{257}	0.75	1.7 ± 0.75	115	79 ± 17
Arg_{273}	1.25	1.8 ± 0.67	75	72 ± 15
Lys_{281}	7.25	1.0 ± 0.59	95	104 ± 17
Lys_{282}	9.75	1.0 ± 0.54	65	103 ± 18

[1]Reference values, which indicate inclusion, were obtained in REMD simulations of the inclusion complexes

d

Lys/Arg	ΔΔG (kcal/mol)
K251	-1.9 ± 0.3
K253	-4.8 ± 0.2
K255	-3.9 ± 0.2
R257	-3.1 ± 0.2
R273	1.3 ± 0.3
K281	-2.8 ± 0.2
K282	-3.2 ± 0.2

Supplementary Fig. 1. CLR05 has diminished ability (with respect to CLR01) to form inclusion complexes with lysine and arginine residues in PAP248-286. (**a**) Structures of complexes between **CLR05** and the lysine derivative AcLysOMe optimized by QM/MM

calculations (QM(B3LYP-D2/SVP) / CHARMM22) in explicit water (**b**) The free energy surfaces indicate that binding of **CLR05** to residues at the N-and C-terminal regions of PAP248-286 is not favored. This unfavorable binding is the case for K251, K281 and K282, as indicated by absence of a deep global minimum on the potential energy surfaces. For K253, K255, R257 and R273, the inclusion complex could be formed as shown by the major global minima. However, in K253 and R257, the interaction angles largely deviate from the reference REMD values in inclusion complexes. The collective variables used in these calculations were: *i*) the distance (d) between the center of mass (COM) of the pink atoms in **CLR05** and the COM of the pink atoms in the lateral chain of Lys/Arg and, *ii)* the angle (a) between the COM of the cyan backbone atoms of Lys/Arg, the COM of the cyan atoms in the lateral chain of Lys/Arg and the COM of the cyan atoms in **CLR05**. (**c**) Values of the collective variables shown in the panel **b** based on eABF calculations and REMD simulations (2.7 μs) as reference. The collective variables capture the extent of the inclusion of the Lys or Arg residues inside the tweezers' cavity. (**d**) Alchemical transformation calculations indicate that **CLR01** forms more stable inclusion complexes than **CLR05** for all residues, except R273. The relative stability of the inclusion complex of **CLR05** with R273 is related to the position of R273, which makes possible additional extended hydrophobic interactions with the surrounding aliphatic residues.

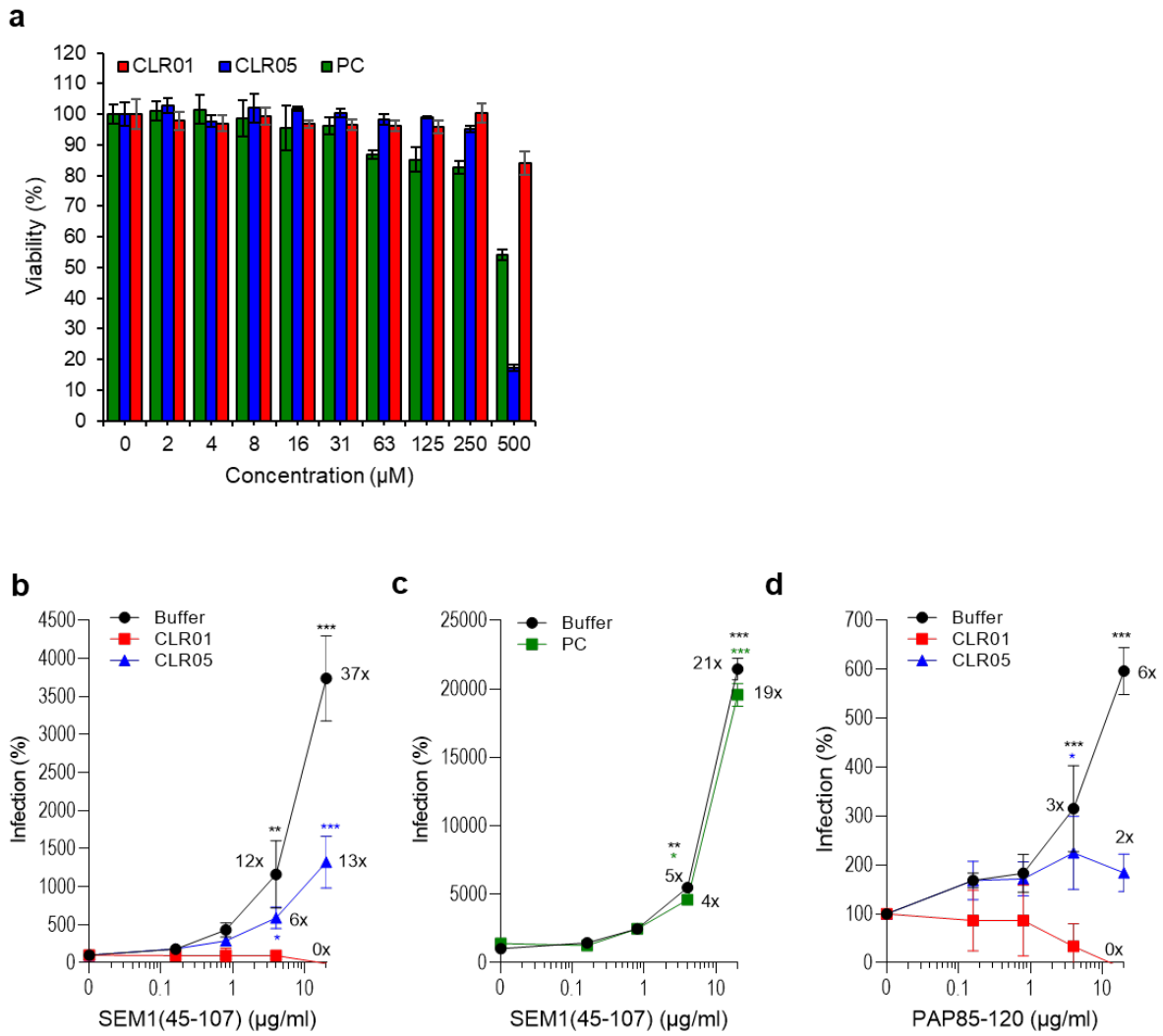

e

	IC_{50} (µM)	CC_{50} (µM)	SI
CLR01	17.76	> 500	> 26.15
CLR05	41.61	260.1	6.25
PC	~ 116.8	> 500	> 4.28

Supplementary Fig. 2. CLR05 and PC are non-toxic, CLR05 decreases the HIV-1 enhancing activity of seminal amyloids. (**a**) **CLR01**, **CLR05** and **PC** are non-cytotoxic in the applied concentrations in cell culture. TZM-bl cells ($1x10^4$ per well) were seeded one day before incubation with the indicated **CLR01**, **CLR05** and **PC** concentrations. After two days, metabolic activity of cells was assessed using CellTiter-Glo assay. Values were normalized to untreated cells and to determine % viability. Mean values from biological triplicates ±SD are shown. SEM1(45-107) (**b** and **c**) or PAP85-120 (**d**) fibrils were incubated with buffer or a 20-fold molar excess of **CLR01**, **CLR05** or **PC** for 10 min at room temperature. After preparing 5-fold dilution series of the mixtures, CCR5-tropic HIV-1 (1 ng/ml p24 antigen) was added and TZM-bl cells were inoculated with these samples. Values represent % β-galactosidase activities (mean) compared to cells infected with virus only and are obtained from triplicate infections ± SEM (n=9). Numbers above the symbols indicate n-fold enhancement of infection**. (e)** The half maximal inhibitory concentration (IC_{50}), half maximal cytotoxic concentration (CC_{50}) and the

selectivity index (SI, i.e. CC_{50}/IC_{50}) values of CLR01, CLR05 and phosphate clip PC for experiments shown in Fig 2c and Supplementary Fig 2a.

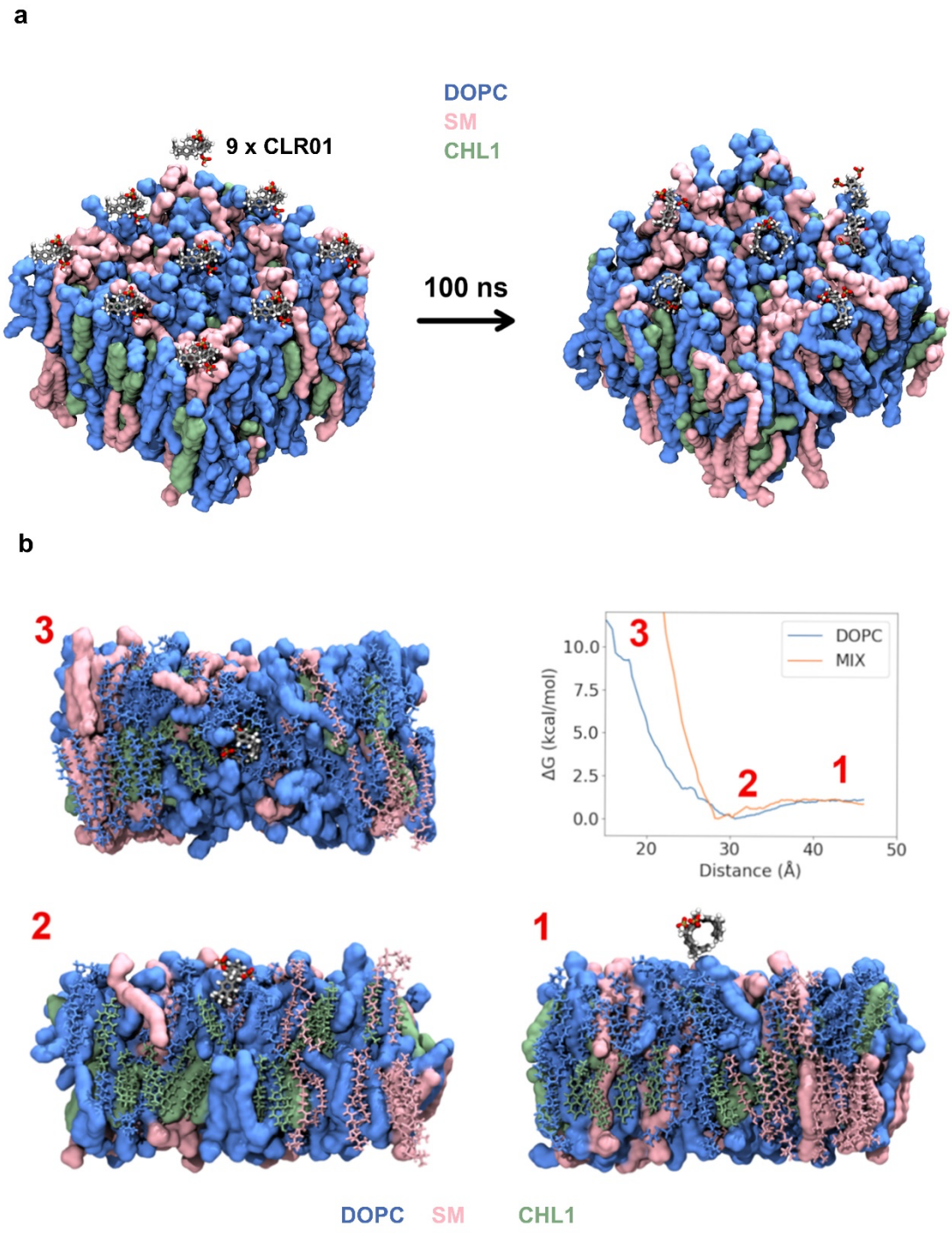

Supplementary Fig. 3. Several inclusion complexes are formed by CLR01 during the MD simulations with DOPC and mixed bilayers. (a) Initial and final snapshot of one of the replicas of the MD simulation performed with **CLR01** and the mixed bilayer. **CLR01** molecules are initially placed 4 Å over the bilayer. **(b)** Free energy changes along the insertion of **CLR01** in the DOPC and mixed bilayer models (MIX). Snapshots of the highlighted positions **1**, **2** and **3** in the curves are shown. **1** corresponds to the tweezers in water, in **2** the tweezers are forming an inclusion complex with a head-group of a lipid (DOPC) located at the surface of the membrane and in **3**, the tweezers are inside the bilayer. The color scheme is the same as in a) and the mixed bilayer is depicted.

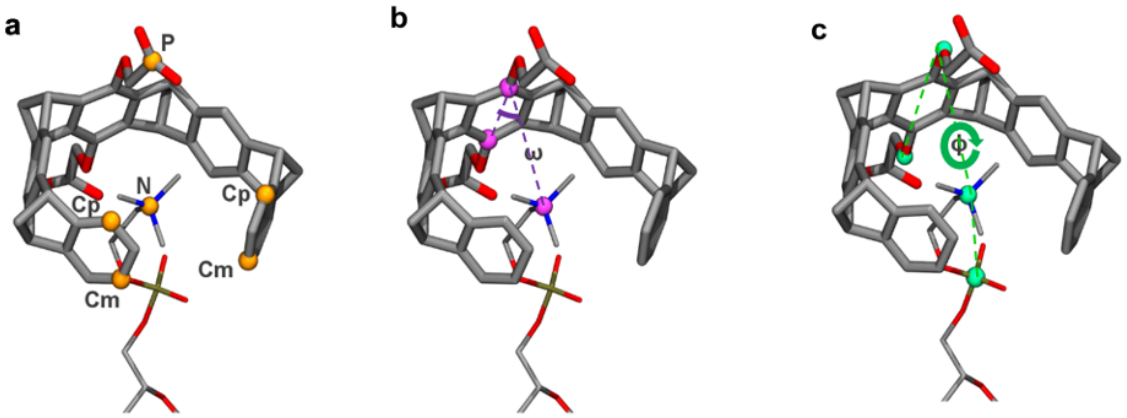

Supplementary Fig. 4. Angles and distances describing the tweezers/lipid interactions. Selected distances and angles used to characterize the inclusion complexes of **CLR01**, **CLR05** and **PC** with amino acids/lipids. **a**) Distances Cp – Cp, Cm – Cm and P – N. Cp – Cp and Cm – Cm distances indicate how distorted the tweezers are upon complexation, while the P – N distance indicates how inserted is the side chain or the lipid head-group inside the tweezers' cavity. **b**) The angle ω is formed by the three atoms highlighted in pink and indicates the degree of penetration of the side chain/lipid inside the tweezer's cavity. **c**) The angle Φ is the dihedral formed by the atoms highlighted in green in **CLR05** and the atoms highlighted in green in DOPC. Φ (not to be confused with Φz, the angle with respect to the z-axis shown in Fig. 3) indicates the relative orientation of the central benzene ring of **CLR01**/**CLR05**/**PC** with respect to the lipid's head-group.

a

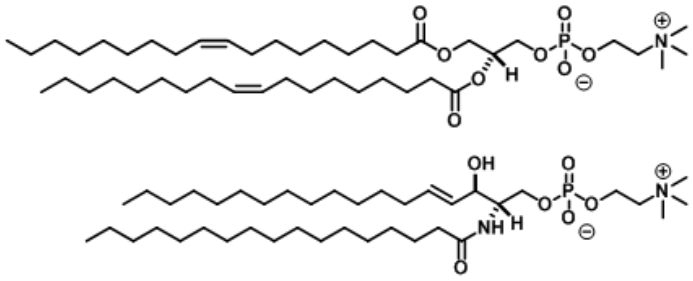

b

Complex	Relative Energy (QM region, kcal/mol) (In membrane)	Relative Energy (QM region, kcal/mol) (In water)
CLR01 – SM	0 ± 5	0 ±5.2
CLR01 – DOPC	28 ± 7	24 ±3.4

c

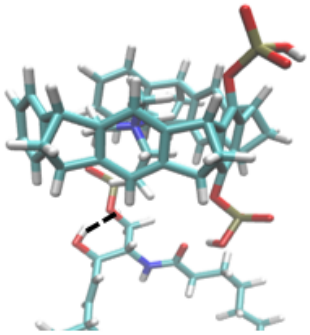

Supplementary Fig. 5. The results of QM/MM calculations predict a more stable complex of CLR01 with SM than with DOPC. (a) Chemical structure of DOPC and SM. (**b**) Relative QM energies from QM/MM calculations of the optimized complexes between **CLR01** and DOPC or SM, both in the membrane and in water. (**c**) Inclusion complex of **CLR01** with SM, highlighting the intramolecular hydrogen bond in SM.

a NMR titration Sphingomyelin and **CLR01**:

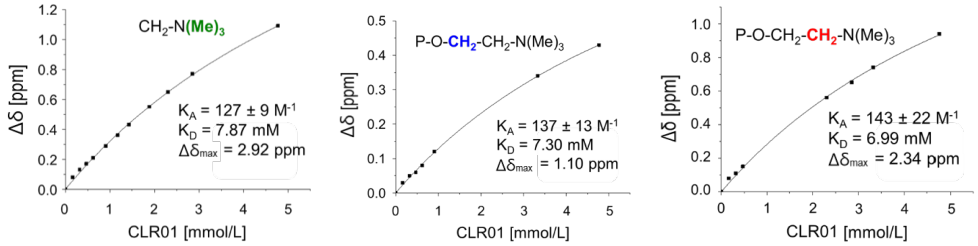

b NMR titration DOPC and **CLR01**:

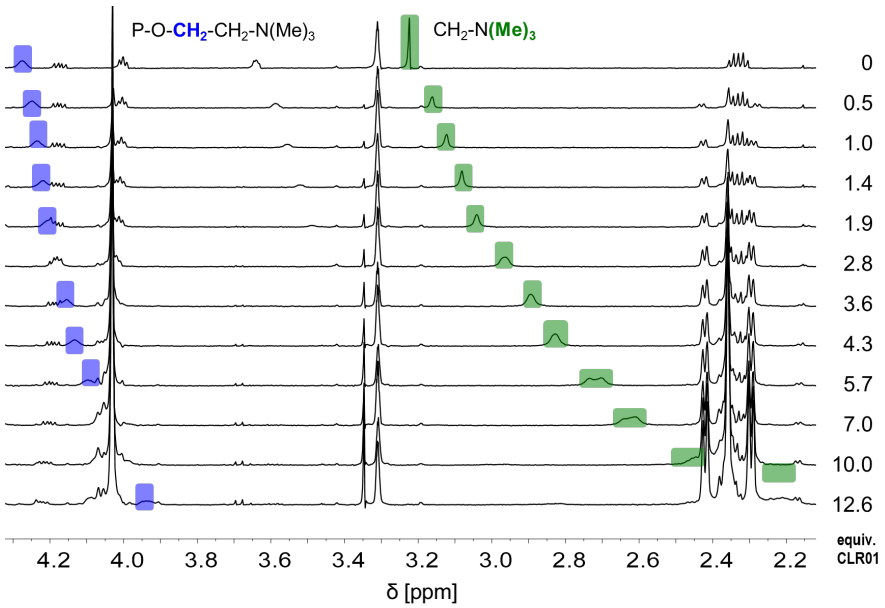

Binding curves DOPC and **CLR01**:

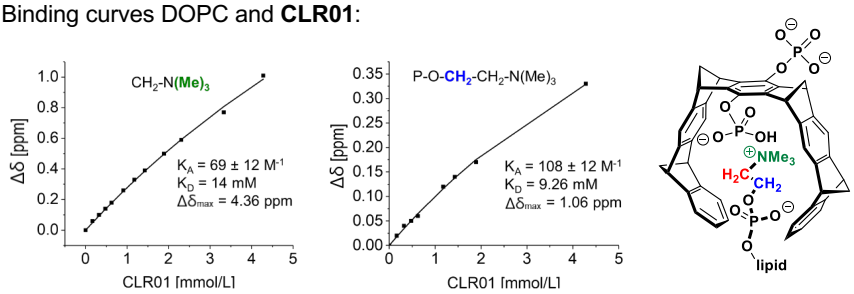

c NMR titration Sphingomyelin and **PC**:

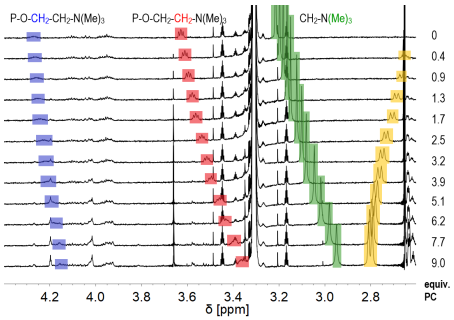

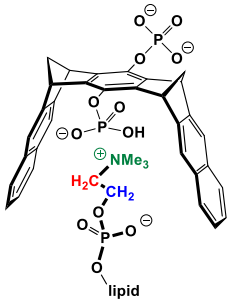

Binding curves Sphingomyelin and **PC**:

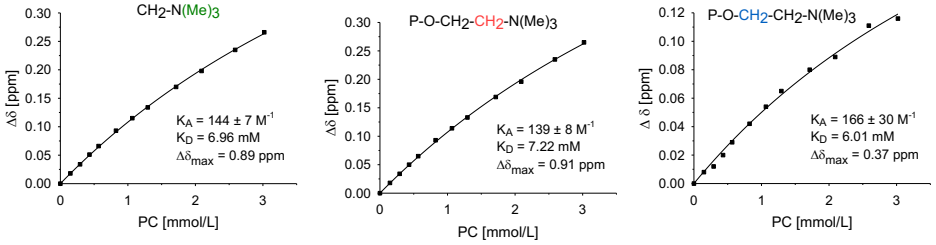

d NMR titration DOPC and **PC**:

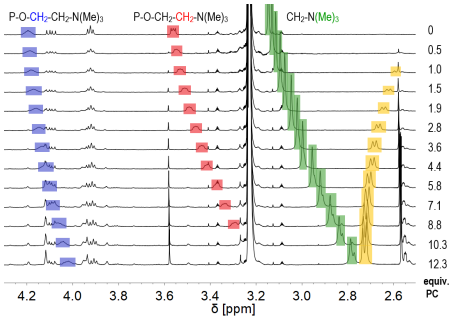

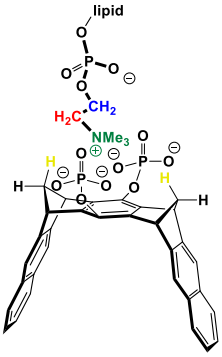

Binding curves DOPC and **PC**:

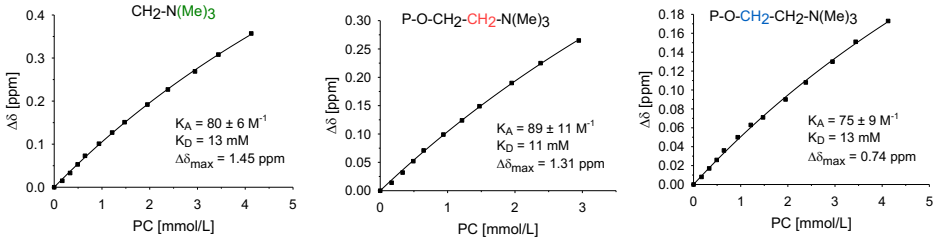

e NMR titration Sphingomyelin and **CLR05**:

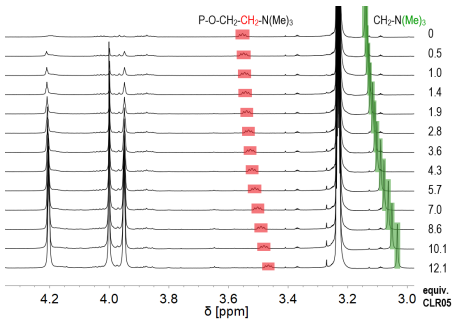

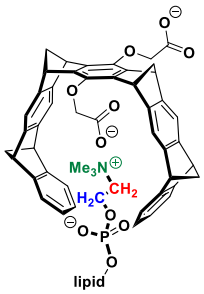

Binding curves Sphingomyelin and **CLR05**:

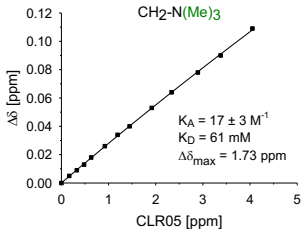

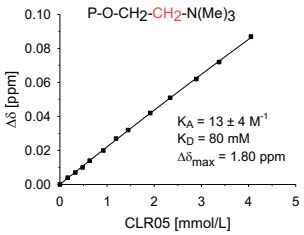

f NMR titration DOPC and **CLR05**:

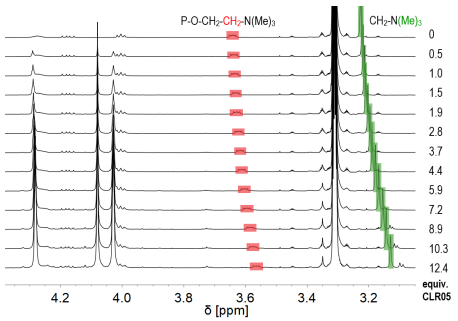

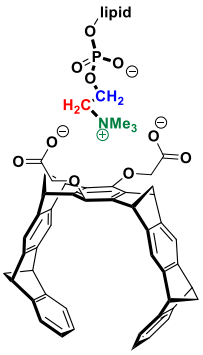

Binding curves DOPC and **CLR05**:

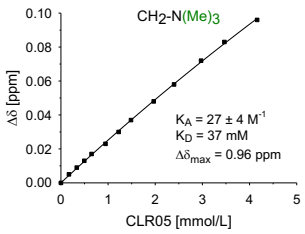

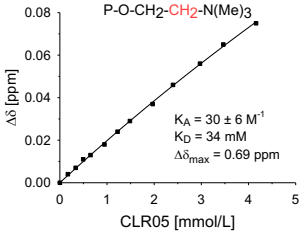

Supplementary Fig. 6. NMR titrations in d$_4$-methanol between tweezers, clip and lipids. (**a**) Complex formation between **CLR01** and phosphosphingomyelin **(SM)** monitored by NMR spectroscopy, continued from Fig. 4: corresponding binding curves for the $N(Me)_3^+$ and both ethoxy methylene groups with the resulting affinity (K_A/K_D) and $\Delta\delta_{max}$ value obtained from nonlinear regression. (**b**) NMR titration between **CLR01** and DOPC: Stacked plot with upfield shifting signals in green and blue, resulting binding curves with corresponding affinities and maximum chemical shift changes as well as Lewis structure illustrating the proposed binding

mode; (**c**) NMR titration between **PC** and SM; **(d)** NMR titration between **PC** and DOPC; **(e)** NMR titration between **CLR05** and SM; **(f)** NMR titration between **CLR05** and DOPC.

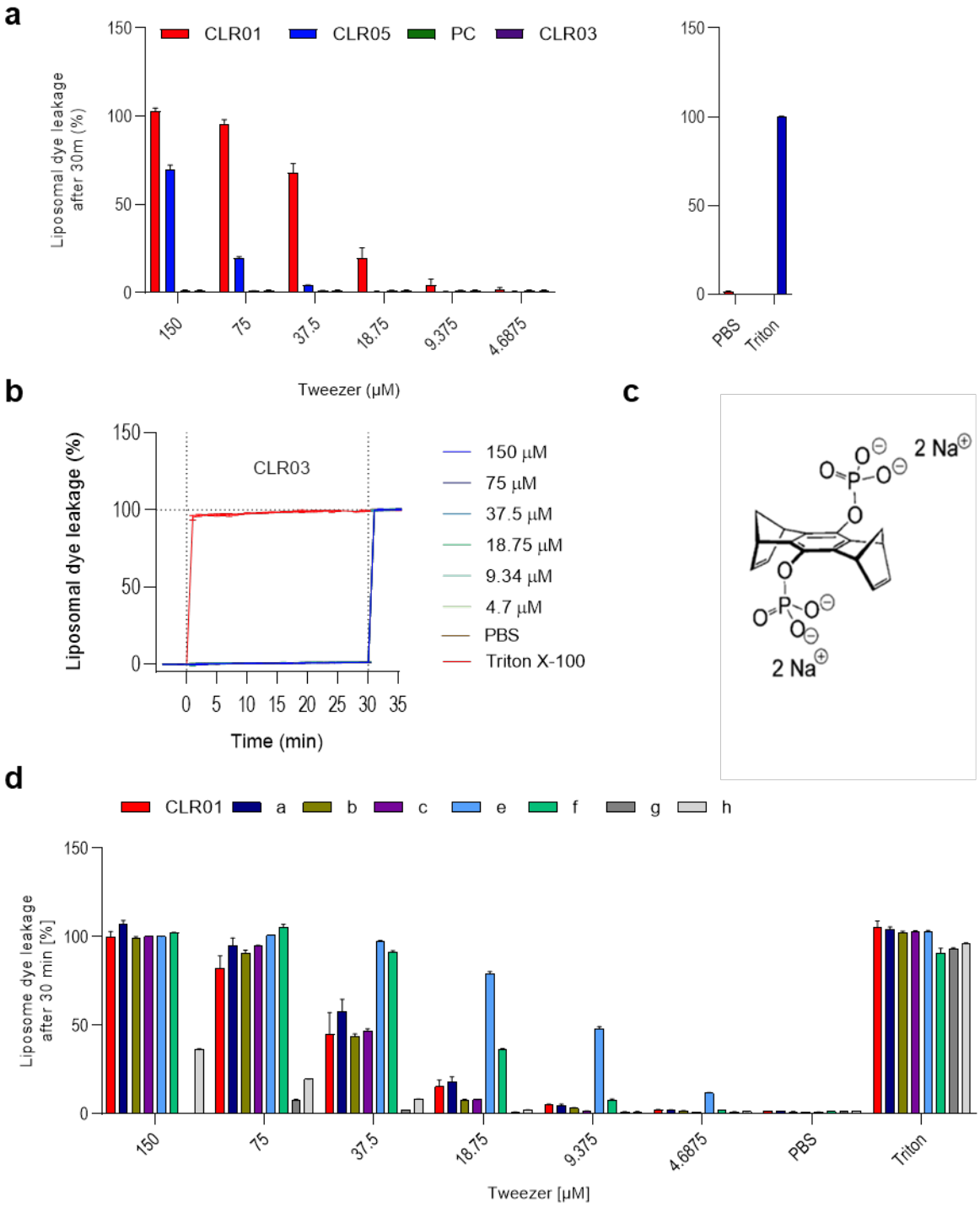

Supplementary Fig. 7 Peak dye leakage from liposomes incubated with tweezers for 30 min. (a) Dose-dependent liposome leakage induced by **CLR01**, **CLR05**, **PC** and **CLR03** shown as the maximum reached after 30 min before addition for Triton X-100. Data shows means ± SDs from two individual experiments, each performed in triplicates. **(b)** Time-dependent leakage experiment with previously reported **CLR03** performed in analogy to experiments shown in Fig. 5c. **(d)** Dose-dependent liposome leakage induced by **CLR01** and advanced molecular tweezer derivatives shown as the maximum reached after 30 min before addition for Triton X-100. Data shows means ± SDs from two individual experiments, each performed in triplicates.

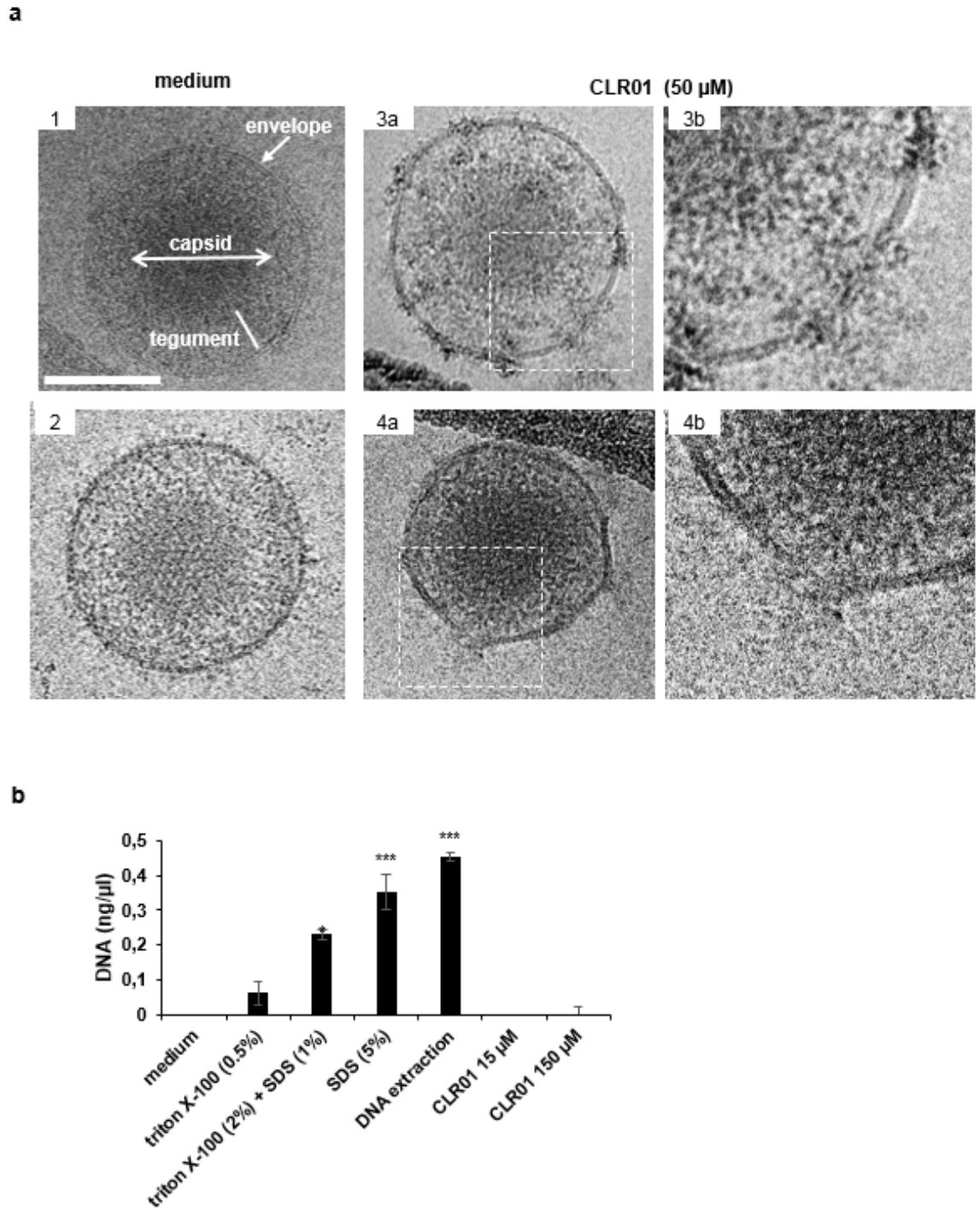

Supplementary Fig. 8. CLR01 interacts with the viral envelope of HCMV particles but does not destroy virion architecture. (a) Cryo-TEM of HCMV virions (strain TB40/E) after treatment with medium (1-2) or 50 µM **CLR01** (3a and 4a, higher magnifications in 3b and 4b) for 30 min at 37°C. Important virion structures are indicated in image 1. Note that **CLR01**-treated virions show a discontinuous envelope and are decorated with electron-dense material at these sites. Scale bar is 100 nm. **(b)** Cell-free supernatants of HCMV (strain TB40/E) were either subjected to DNA extraction or treated with indicated conditions for 30 min at 37°C prior to DNA quantification. Means ± SDs from two individual experiments, each performed in triplicate. DNA measurements of identically treated cell supernatants of uninfected cells were subtracted to determine the DNA released from virus particles.

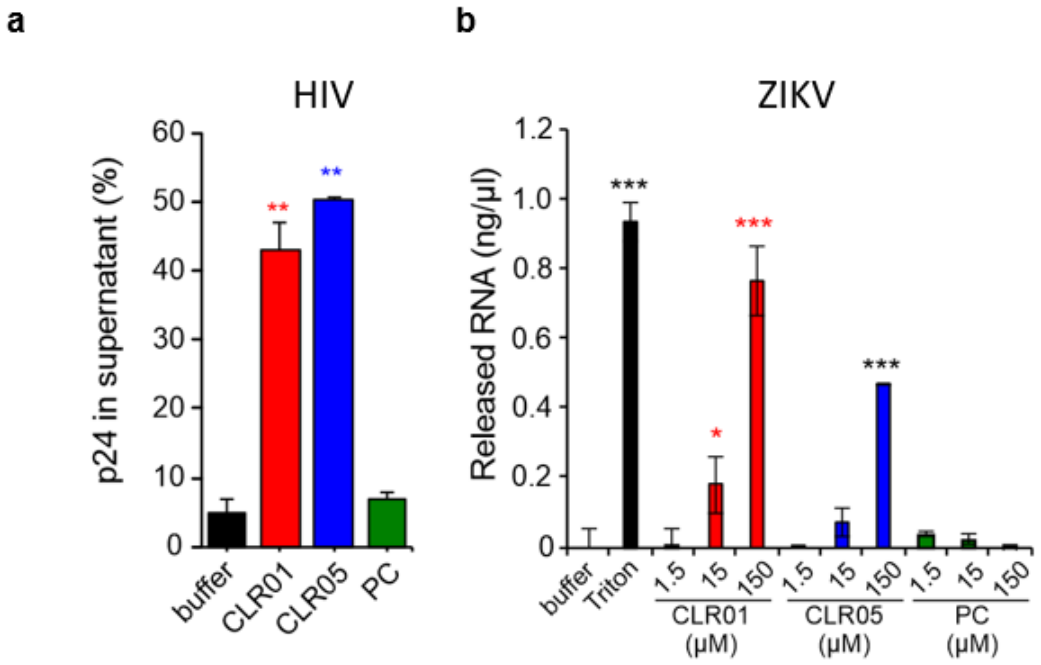

Supplementary Fig. 9. Tweezers destroy HIV and ZIKV particles. (**a**) **CLR05** releases p24 capsid antigen from HIV particles. HIV-1 was incubated with buffer, 100 µM **CLR05**, or 100 µM **CLR01**, centrifuged, and the supernatant assayed for p24 antigen. Values represent means ±SD (n=3). Unpaired t-tests were applied to compare the buffer control to the **CLR05** or **CLR01** condition (** denotes $p<0.01$). (**b**) **CLR05** releases viral RNA. ZIKV MR766 was incubated with PBS, 150 µM Triton X-100, 1.5-150 µM **CLR01** or **PC** or 15-300 µM **CLR05** for 30 min at 37 °C. RNA concentrations of the samples were quantified using the QuantiFluor® RNA System and a Quantus Fluorometer. RNA levels of virus stock incubated with PBS were subtracted. Values represent means ±SD (n=3). One-way ANOVA (non-parametric, grouped), followed by Bonferroni's multiple comparison tests were applied to compare the buffer control to the different **CLR01**, **CLR05** or **PC** conditions.

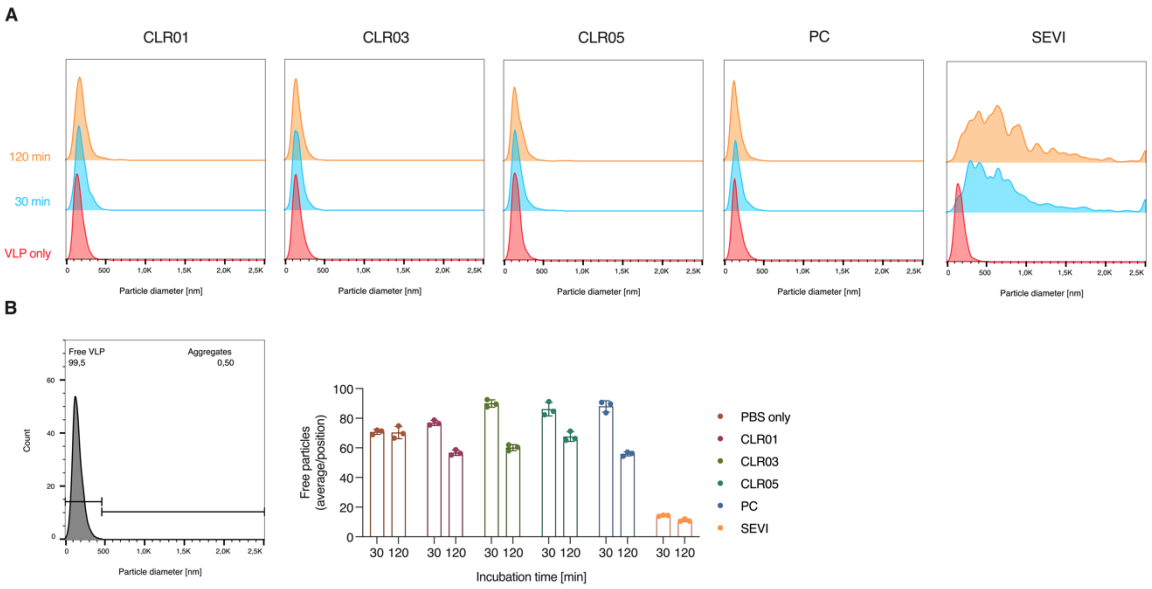

Supplementary Fig. 10. Molecular tweezers do not induce aggregation of virus-like particles (VLPs). (a) Representative size-distribution histograms acquired by F-NTA of YFP-labeled virus-like lentiviral particles after incubation with indicated compounds (Tweezers: 150 µM, SEVI 100 µg/ml) compared with VLPs diluted in PBS only. **(b)** Gating of free VLPs (left) and quantification of samples treated with compounds (right) after 30 and 120 minutes of incubation. Values represent means ± SD (n=3).

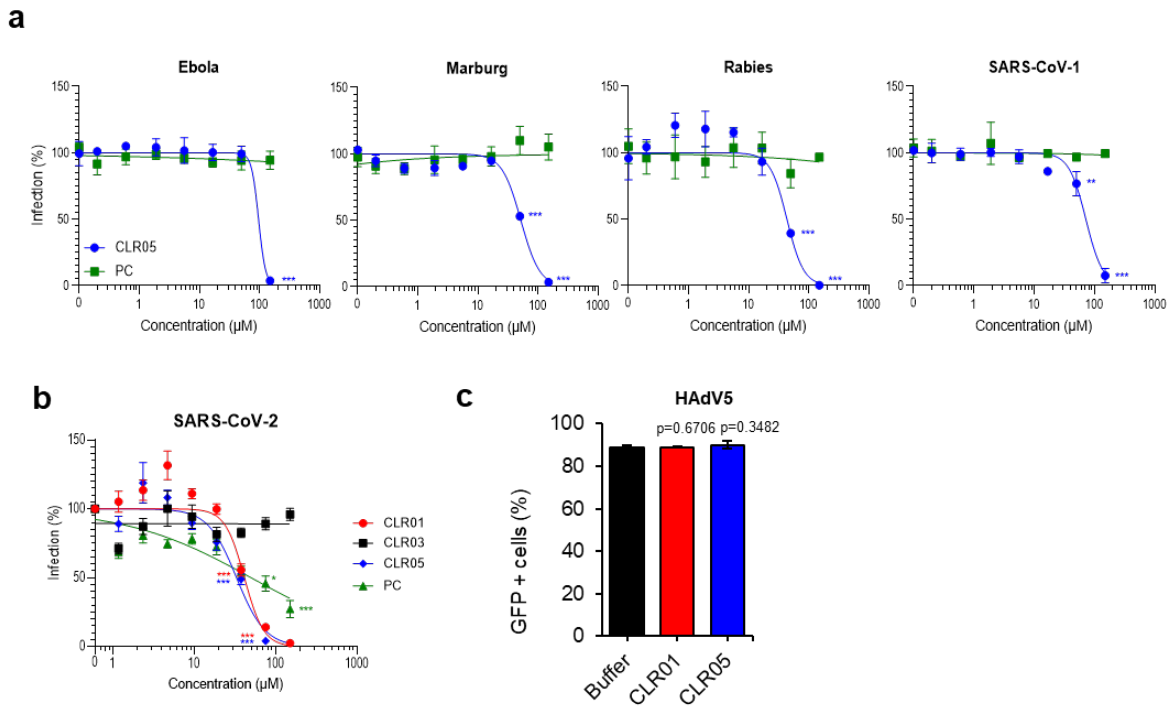

Supplementary Fig. 11. CLR05 inhibits pseudovirions but not Adenovirus. (**a**) **CLR05** inhibits lentiviral particles pseudotyped with envelope proteins of Marburg, Ebola, Rabies virus and SARS-CoV-1. Pseudoparticles were incubated with **CLR05** and **PC** and used to infect Huh-7 cells. After three days, infection rates were determined by quantifying firefly luciferase activity. Values represent % reporter gene activities derived from triplicate infections (minus background activities derived from uninfected cells) normalized to values obtained for cells infected in the absence of compounds. Data of CLR01 and CLR03 inhibition on Marburg, Ebola, Rabies, SARS-CoV-1 pseudoparticle were recently published[40]. (**b**) **CLR01** and **CLR05** inhibit SARS-CoV-2 pseudoparticles. Virions were incubated with **CLR01**, **CLR05**, **CLR03** and **PC** and used to infect CaCo2 cells. After two days, infection rates were determined by quantifying firefly luciferase activity. Values represent % reporter gene activities derived from triplicate infections (minus background activities derived from uninfected cells) normalized to values obtained for cells infected in the absence of compounds. Values represent means ± SEM (n = 3). (**c**) **CLR05** has no effect on adenovirus. HAdV5 vector containing an EGFP expression cassette was titrated with buffer, 100 µM **CLR01** or **CLR05** and incubated for 10 min at 37°C before A549 cells were infected with the pretreated virus. EGFP expression was analyzed one day post transduction using a Beckman–Coulter Gallios flow cytometer.

a

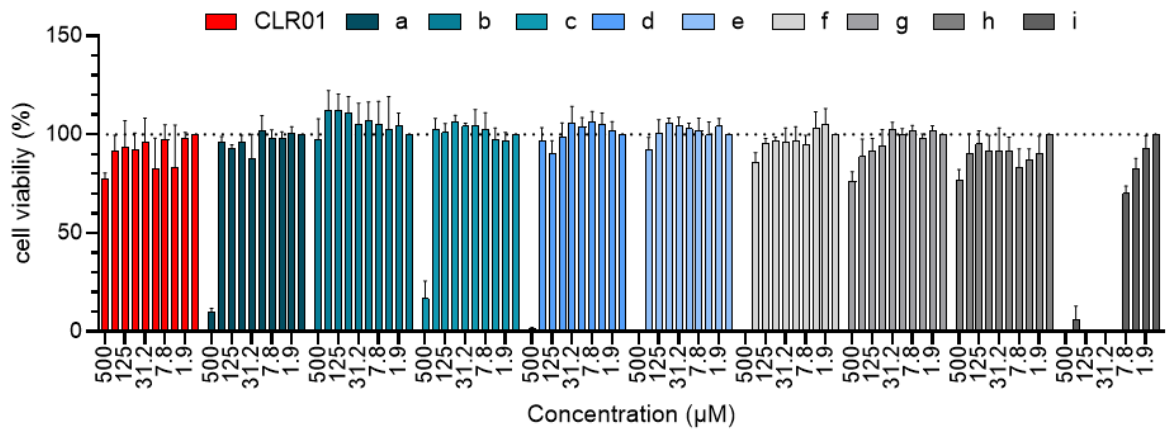

b

	IC_{50} (µM)	CC_{50} (µM)	SI
CLR01	35.44	> 500	> 14.10
a	21.56	~ 376.6	~17.46
b	21.10	> 500	> 23.69
c	12.02	~464.0	~ 38.60
d	28.72	~ 342.4	~ 11.92
e	8.78	~ 299.6	~ 34.08
f	6.64	~ 294.1	~ 44.29
g	26.85	> 500	> 18.62
h	27.04	> 500	> 18.49
i	77.62	8.98	0.115

Supplementary Fig. 12. Advanced molecular tweezer derivatives with two aliphatic ester arms display improved activity against HIV-1 infection. (a) Effect of tweezer on cells was observed by CellTiterGlo. Therefore, tweezers were added to TZM-bl cells (1.95 – 500 µM) and 2 days post treatment cell viability was quantified by measuring ATP amount. Values represent % cell viability derived from triplicate treatment normalized to values obtained for cells in the absence of compounds. Data shows means ± SD from one individual experiment, performed in triplicates. **(b)** The half maximal inhibitory concentration (IC_{50}), half maximal cytotoxic concentration (CC_{50}) and the selectivity index (SI, i.e. CC_{50}/IC_{50}) values of tweezer CLR01 and advanced molecular tweezer derivates a – i of experiments illustrated in Fig. 7b and Supplementary Fig. 12a.

Supplementary Tables

Supplementary Table 1. Binding events of **CLR01**, **CLR05** and **PC** to the membranes.

		max. number of binding events per replica of the simulation		
Membrane composition	Number of molecules	**CLR01**	**CLR05**	**PC**
DOPC	9	8	4	9
DOPC/SM/Chol	9	6	4	9

Supplementary Table 2. Distances and angles used to characterize the binding of the lipids to **CLR01** during the MD simulations. Figure S4 illustrates the geometrical parameters listed below.

Replica	Binding events	Lipid	Cp – Cp (Å)	Cm – Cm (Å)	P – N (Å)	ω (°)	Φ (°)
DOPC Bilayer							
1	8	DOPC	7.03 ± 0.61	5.80 ± 0.60	6.86 ± 0.91	68.0 ± 9.5	20.4 ± 12.0
			6.98 ± 0.68	5.81 ± 0.64	7.12 ± 1.21	67.6 ± 11.3	19.2 ± 11.9
			6.44 ± 0.99	5.01 ± 1.14	9.39 ± 3.19	54.0 ± 27.3	34.9 ± 24.3
			7.19 ± 0.45	5.93 ± 0.51	6.81 ± 0.54	71.9 ± 7.0	16.8 ± 8.3
			7.27 ± 0.52	6.00 ± 0.52	6.89 ± 0.79	71.4 ± 7.2	15.5 ± 9.5
			7.23 ± 0.58	5.95 ± 0.63	6.50 ± 1.38	70.7 ± 11.8	21.0 ± 20.0
			7.07 ± 0.77	5.89 ± 0.65	7.55 ± 0.51	63.5 ± 8.7	23.8 ± 9.9
			7.06 ± 0.59	5.87 ± 0.57	6.66 ± 1.02	67.4 ± 8.3	17.4 ± 8.1
2	6	DOPC	7.33 ± 0.49	6.05 ± 0.56	7.00 ± 0.90	71.9 ± 8.8	19.8 ± 12.7
			7.40 ± 0.43	6.06 ± 0.50	5.54 ± 0.85	73.4 ± 5.5	16.2 ± 9.0
			7.43 ± 0.50	6.19 ± 0.54	7.13 ± 0.44	69.2 ± 6.6	23.6 ± 13.7
			7.41 ± 0.51	6.14 ± 0.55	7.25 ± 0.79	70.2 ± 7.1	20.7 ± 12.2
			7.32 ± 0.48	6.04 ± 0.51	6.17 ± 0.99	70.2 ± 7.1	20.7 ± 12.2
			7.11 ± 0.58	5.85 ± 0.65	6.94 ± 1.00	68.7 ± 10.1	20.2 ± 14.0
3	6	DOPC	6.47 ± 1.03	5.03 ± 1.19	9.10 ± 3.29	89.1 ± 31.8	58.2 ± 46.9
			7.54 ± 0.65	6.39 ± 0.70	6.34 ± 2.42	65.9 ± 6.8	28.4 ± 26.8
			7.36 ± 0.46	6.08 ± 0.50	6.49 ± 0.97	71.1 ± 7.1	17.1 ± 9.0
			7.07 ± 0.69	5.90 ± 0.72	7.35 ± 1.42	64.4 ± 15.1	23.5 ± 16.3
			7.42 ± 0.50	6.12 ± 0.51	6.42 ± 0.99	71.7 ± 6.3	18.9 ± 8.8
			7.05 ± 0.73	5.74 ± 0.81	6.87 ± 1.91	70.8 ± 14.7	26.7 ± 27.7
Mixed Bilayer							
1	6	DOPC	7.38 ± 0.44	6.01 ± 0.48	5.07 ± 0.51	73.7 ± 6.9	18.7 ± 8.2
		DOPC	7.08 ± 0.54	5.85 ± 0.52	6.95 ± 0.72	68.9 ± 8.3	17.7 ± 8.5
		SM	7.29 ± 0.44	5.99 ± 0.49	5.81 ± 1.01	70.9 ± 6.7	19.6 ± 8.8
		SM	7.23 ± 0.69	5.98 ± 0.75	7.36 ± 1.78	63.5 ± 14.2	29.8 ± 25.3
		DOPC	7.38 ± 0.42	6.07 ± 0.48	6.56 ± 0.74	74.4 ± 5.9	16.9 ± 7.5
		DOPC	6.92 ± 0.92	5.67 ± 0.94	6.48 ± 0.86	61.7 ± 16.7	29.2 ± 26.4
2	4	DOPC	6.96 ± 0.74	5.81 ± 0.67	7.63 ± 0.60	61.5 ± 9.5	24.1 ± 12.5
		DOPC	7.26 ± 0.40	6.02 ± 0.44	6.06 ± 0.89	71.3 ± 5.5	18.3 ± 7.7
		DOPC	7.42 ± 0.39	6.11 ± 0.42	7.11 ± 0.32	72.5 ± 5.1	17.6 ± 6.1
		DOPC	7.29 ± 0.52	6.05 ± 0.56	6.60 ± 1.37	69.0 ± 8.4	23.1 ± 11.5
3	5	DOPC	7.29 ± 0.58	6.00 ± 0.61	7.01 ± 0.87	70.4 ± 9.5	17.5 ± 12.7
		SM	7.48 ± 0.39	6.25 ± 0.39	7.09 ± 0.41	72.1 ± 6.2	16.3 ± 8.6
		DOPC	8.02 ± 0.89	6.84 ± 1.00	6.18 ± 1.77	64.7 ± 9.8	45.8 ± 18.1
		DOPC	6.62 ± 1.04	5.16 ± 1.16	8.30 ± 3.29	90.4 ± 26.8	38.7 ± 32.9
		DOPC	7.67 ± 0.82	6.41 ± 0.94	5.69 ± 0.56	65.7 ± 6.1	36.6 ± 16.2

Supplementary Table 3. Distances and angles used to characterize the binding of the lipids to **CLR05** during the MD simulations. Figure S4 illustrates the geometrical parameters listed below.

Replica	Binding events	Lipid	Cp – Cp (Å)	Cm – Cm (Å)	P – N (Å)	ω (º)	Φ (º)
DO**PC** Bilayer							
1	4	DOPC	7.41 ± 0.55	6.12 ± 0.62	6.59 ± 1.48	71.1 ± 8.1	23.9 ± 18.8
			7.25 ± 0.72	5.95 ± 0.79	7.01 ± 2.18	68.7 ± 20.8	31.3 ± 23.5
			7.27 ± 0.57	5.94 ± 0.63	6.65 ± 1.51	69.3 ± 12.2	22.7 ± 14.9
			7.20 ± 0.63	5.90 ± 0.69	7.03 ± 1.38	72.0 ± 16.8	22.8 ± 25.1
2	1	DOPC	7.27 ± 0.73	5.95 ± 0.83	7.08 ± 2.05	74.3 ± 19.2	57.7 ± 56.4
3	3	DOPC	7.42 ± 0.65	6.16 ± 0.75	6.58 ± 1.59	68.8 ± 13.1	29.8 ± 21.2
			7.29 ± 0.76	5.98 ± 0.86	6.90 ± 1.70	73.8 ± 18.2	23.9 ± 20.2
			7.40 ± 0.49	6.11 ± 0.52	6.27 ± 0.71	69.0 ± 6.0	20.5 ± 10.4
Mixed Bilayer							
1	4	DOPC	7.42 ± 0.53	6.14 ± 0.56	6.66 ± 0.94	67.5 ± 6.7	25.4 ± 13.5
		DOPC	7.44 ± 0.51	6.20 ± 0.55	6.47 ± 0.83	68.6 ± 6.4	24.8 ± 14.3
		DOPC	7.41 ± 0.50	6.12 ± 0.53	6.38 ± 0.77	68.7 ± 6.1	19.9 ± 10.6
		DOPC	7.44 ± 0.47	6.15 ± 0.50	6.23 ± 0.74	69.1 ± 5.5	20.3 ± 11.0
2	3	DOPC	9.17 ± 0.75	8.57 ± 0.87	6.84 ± 0.77	64.1 ± 5.1	30.0 ± 11.9
		DOPC	7.36 ± 0.47	6.09 ± 0.52	6.75 ± 0.82	69.0 ± 6.3	18.5 ± 8.0
		DOPC	7.35 ± 0.51	6.04 ± 0.54	6.51 ± 0.86	68.3 ± 6.6	22.4 ± 10.0
3	3	DOPC	7.37 ± 0.48	6.07 ± 0.54	6.29 ± 0.70	69.9 ± 6.1	19.7 ± 9.5
		DOPC	7.36 ± 0.55	6.09 ± 0.62	6.54 ± 1.23	67.4 ± 9.8	24.3 ± 17.4
		SM	7.46 ± 0.47	6.15 ± 0.51	6.34 ± 0.75	68.7 ± 5.5	18.9 ± 9.7

Supplementary Table 4. Distances and angles used to characterize the binding of the lipids to **PC** during the MD simulations. Figure S4 illustrates the geometrical parameters listed below.

Replica	Binding events	Lipid	Cp – Cp (Å)	Cm – Cm (Å)	P – N (Å)	ω (º)	Φ (º)
DOPC Bilayer							
1	9	DOPC	9.06 ± 0.41	9.96 ± 0.50	6.87 ± 0.47	72.3 ± 7.1	86.8 ± 49.1
			8.99 ± 0.38	9.83 ± 0.49	6.89 ± 0.58	74.9 ± 6.6	115.0 ± 30.8
			9.08 ± 0.45	9.99 ± 0.52	7.22 ± 0.45	67.9 ± 7.3	61.3 ± 23.6
			9.07 ± 0.55	9.96 ± 0.68	9.17 ± 3.02	63.8 ± 24.3	83.3 ± 43.2
			9.12 ± 0.43	10.01 ± 0.54	6.84 ± 0.49	73.4 ± 7.6	92.6 ± 42.3
			9.02 ± 0.43	9.97 ± 0.53	6.95 ± 0.51	72.2 ± 7.4	70.2 ± 32.7
			9.11 ± 0.43	10.04 ± 0.54	6.89 ± 0.70	72.6 ± 8.8	78.3 ± 39.6
			9.09 ± 0.42	9.99 ± 0.53	6.85 ± 0.49	73.4 ± 8.5	109.1 ± 41.1
			9.17 ± 0.48	10.08 ± 0.56	7.20 ± 0.66	68.1 ± 10.2	67.4 ± 30.8
2	9	DOPC	9.04 ± 0.43	9.89 ± 0.53	6.89 ± 0.78	74.1 ± 8.2	86.2 ± 41.9
			9.12 ± 0.43	10.04 ± 0.53	6.66 ± 0.67	72.6 ± 6.8	96.3 ± 37.4
			9.11 ± 0.44	10.02 ± 0.55	6.88 ± 0.77	73.2 ± 9.5	83.7 ± 36.2
			9.10 ± 0.47	10.05 ± 0.55	7.35 ± 0.65	65.1 ± 7.1	45.9 ± 20.0
			9.10 ± 0.42	10.02 ± 0.52	6.81 ± 0.51	72.7 ± 7.1	78.4 ± 49.7
			9.10 ± 0.43	9.98 ± 0.53	6.70 ± 0.86	76.1 ± 8.3	95.6 ± 22.5
			9.03 ± 0.42	9.91 ± 0.54	6.92 ± 0.58	73.1 ± 8.2	110.6 ± 52.5
			9.09 ± 0.43	9.97 ± 0.54	6.85 ± 0.48	73.6 ± 7.1	92.2 ± 46.7
			8.96 ± 0.41	9.85 ± 0.52	6.88 ± 0.45	73.5 ± 7.8	36.4 ± 29.7
3	9	DOPC	9.04 ± 0.51	9.92 ± 0.63	9.28 ± 2.89	76.2 ± 26.5	87.3 ± 40.8
			9.02 ± 0.45	9.95 ± 0.55	7.03 ± 0.99	72.4 ± 9.04	92.3 ± 33.5
			9.03 ± 0.43	9.92 ± 0.52	7.26 ± 0.48	66.9 ± 7.9	67.5 ± 55.6
			9.05 ± 0.43	9.95 ± 0.54	6.93 ± 0.48	73.0 ± 7.5	71.5 ± 37.5
			9.08 ± 0.46	9.97 ± 0.57	6.91 ± 1.19	73.1 ± 9.8	102.6 ± 32.4
			9.07 ± 0.48	9.95 ± 0.57	7.16 ± 1.03	69.5 ± 8.5	61.0 ± 31.2
			9.02 ± 0.44	9.93 ± 0.55	6.91 ± 0.60	72.2 ± 8.2	106.1 ± 42.6
			9.12 ± 0.41	10.02 ± 0.52	6.68 ± 0.60	73.7 ± 7.2	95.7 ± 39.3
			9.12 ± 0.41	10.02 ± 0.52	6.78 ± 0.47	74.1 ± 7.4	91.0 ± 43.9

Supplementary Table 4 (cont.)

Replica	Binding events	Lipid	Cp – Cp (Å)	Cm – Cm (Å)	P – N (Å)	ω (º)	Φ (º)
Mixed Bilayer							
1	7	SM	8.93 ± 0.49	9.86 ± 0.58	7.66 ± 0.93	62.7 ± 8.7	50.3 ± 17.9
		SM	9.16 ± 0.43	10.07 ± 0.53	6.92 ± 0.48	71.6 ± 7.3	105.3 ± 38.2
		SM	9.10 ± 0.42	10.00 ± 0.52	6.68 ± 0.76	73.1 ± 7.0	75.0 ± 39.4
		DOPC	9.01 ± 0.53	9.93 ± 0.66	9.58 ± 2.83	88.1 ± 27.7	77.2 ± 48.3
		DOPC	9.04 ± 0.41	9.90 ± 0.50	6.91 ± 0.48	72.7 ± 7.1	87.5 ± 36.0
		SM	9.11 ± 0.42	10.00 ± 0.53	6.88 ± 0.50	72.4 ± 7.6	110.0 ± 40.4
		DOPC	9.03 ± 0.48	9.92 ± 0.60	6.92 ± 0.80	74.1 ± 9.05	62.6 ± 37.0
2	6	DOPC	9.04 ± 0.45	9.93 ± 0.57	6.98 ± 1.09	74.0 ± 11.3	85.9 ± 41.9
		SM	9.14 ± 0.43	10.05 ± 0.54	9.58 ± 3.11	93.6 ± 40.4	78.4 ± 37.2
		SM	9.06 ± 0.41	9.90 ± 0.50	9.80 ± 3.11	50.5 ± 26.9	86.9 ± 47.5
		DOPC	9.06 ± 0.42	9.91 ± 0.52	6.86 ± 0.54	72.6 ± 8.7	110.3 ± 50.3
		DOPC	9.13 ± 0.43	10.07 ± 0.53	6.82 ± 0.48	73.4 ± 7.3	79.9 ± 32.9
		DOPC	9.13 ± 0.43	10.08 ± 0.52	6.72 ± 0.64	71.9 ± 6.8	65.8 ± 31.6
3	9	SM	9.07 ± 0.43	9.96 ± 0.54	6.81 ± 0.54	73.7 ± 7.3	74.5 ± 51.8
		DOPC	9.00 ± 0.44	9.92 ± 0.54	6.91 ± 0.64	73.1 ± 7.6	74.7 ± 61.0
		DOPC	9.07 ± 0.45	10.00 ± 0.54	6.92 ± 0.72	72.0 ± 7.2	74.9 ± 26.1
		DOPC	9.05 ± 0.41	9.93 ± 0.50	6.93 ± 0.45	72.0 ± 7.0	96.4 ± 39.5
		DOPC	9.11 ± 0.41	10.03 ± 0.51	6.71 ± 0.58	73.6 ± 6.6	80.5 ± 31.3

DOPC	9.13 ± 0.45	10.03 ± 0.55	6.97 ± 0.48	71.5 ± 7.1	65.7 ± 35.4
SM	9.01 ± 0.48	9.91 ± 0.58	6.89 ± 1.25	71.6 ± 9.6	42.3 ± 28.0
PSM	8.95 ± 0.42	9.82 ± 0.50	6.99 ± 0.55	72.7 ± 6.8	53.1 ± 27.8
DOPC	9.10 ± 0.42	10.00 ± 0.51	6.77 ± 0.63	71.6 ± 6.9	84.1 ± 34.3

Comment on Tables 2-4: The complexes established between the tweezers (**CLR01** and **CLR05**) and a lipid significantly differ from those that **PC** establishes with the lipids (see also Figure S4c) regarding the orientation of the lipid's head-group with respect to the central unit of the tweezers and clip as measured by the angle Φ. While complexes between **CLR01/CLR05** and DOPC/SM featured, in general, Φ values of around 10° – 30° with an overall standard deviation of about 15°, the respective **PC** complexes showed much larger Φ values (mostly in the 60° – 90° range) and larger standard deviations. We note that, although the tweezer's complexes with SM are more stable than with DOPC, the number of binding events to DOPC is higher due to the larger amount of these lipids in the mixed bilayer.

Supplementary Table 5.

Quantification of cryo-TEM images of CLR01 treated HCMV virions. Quantified from at least three individual experiments via blind assignment. n: number of virions

sample	n	distorted envelope	intact envelope
CLR01	39	33 (84.6%)	6 (15.4%)
medium	32	7 (21.9%)	25 (78.1%)

Supplementary References

(1) Zwanzig, R. W. High-Temperature Equation of State by a Perturbation Method. I. Nonpolar Gases. *J. Chem. Phys.* **1954**, *22* (8), 1420–1426. https://doi.org/10.1063/1.1740409.

(2) Comer, J.; Gumbart, J. C.; Hénin, J.; Lelièvre, T.; Pohorille, A.; Chipot, C. The Adaptive Biasing Force Method: Everything You Always Wanted To Know but Were Afraid To Ask. *J. Phys. Chem. B* **2015**, *119* (3), 1129–1151. https://doi.org/10.1021/jp506633n.

(3) Phillips, J. C.; Braun, R.; Wang, W.; Gumbart, J.; Tajkhorshid, E.; Villa, E.; Chipot, C.; Skeel, R. D.; Kalé, L.; Schulten, K. Scalable Molecular Dynamics with NAMD. *Journal of Computational Chemistry*. Wiley Subscription Services, Inc., A Wiley Company December 2005, pp 1781–1802. https://doi.org/10.1002/jcc.20289.

(4) Vanommeslaeghe, K.; MacKerell, A. D. CHARMM Additive and Polarizable Force Fields for Biophysics and Computer-Aided Drug Design. *Biochim. Biophys. Acta, Gen. Subj.* **2015**, *1850* (5), 861–871. https://doi.org/10.1016/j.bbagen.2014.08.004.

(5) Zoete, V.; Cuendet, M. A.; Grosdidier, A.; Michielin, O. SwissParam: A Fast Force Field Generation Tool for Small Organic Molecules. *J. Comput. Chem.* **2011**, *32* (11), 2359–2368. https://doi.org/10.1002/jcc.21816.

(6) Sugita, Y.; Okamoto, Y. Replica-Exchange Molecular Dynamics Method for Protein Folding. *Chem. Phys. Lett.* **1999**, *314* (1–2), 141–151. https://doi.org/10.1016/S0009-2614(99)01123-9.

(7) Okabe, T.; Kawata, M.; Okamoto, Y.; Mikami, M. Replica-Exchange Monte Carlo Method for the Isobaric–Isothermal Ensemble. *Chem. Phys. Lett.* **2001**, *335* (5–6), 435–439. https://doi.org/10.1016/S0009-2614(01)00055-0.

(8) Hess, B.; Kutzner, C.; van der Spoel, D.; Lindahl, E. GROMACS 4: Algorithms for Highly Efficient, Load-Balanced, and Scalable Molecular Simulation. *J. Chem. Theory Comput.* **2008**, *4* (3), 435–447. https://doi.org/10.1021/ct700301q.

(9) Bjelkmar, P.; Larsson, P.; Cuendet, M. A.; Hess, B.; Lindahl, E. Implementation of the CHARMM Force Field in GROMACS: Analysis of Protein Stability Effects from Correction Maps, Virtual Interaction Sites, and Water Models. *J. Chem. Theory Comput.* **2010**, *6* (2), 459–466. https://doi.org/10.1021/ct900549r.

(10) Mackerell, A. D.; Feig, M.; Brooks, C. L. Extending the Treatment of Backbone Energetics in Protein Force Fields: Limitations of Gas-Phase Quantum Mechanics in Reproducing Protein Conformational Distributions in Molecular Dynamics Simulations. *J. Comput. Chem.* **2004**, *25* (11), 1400–1415. https://doi.org/10.1002/jcc.20065.

(11) Lump, E.; Castellano, L. M.; Meier, C.; Seeliger, J.; Erwin, N.; Sperlich, B.; Stürzel, C. M.; Usmani, S.; Hammond, R. M.; Von Einem, J.; Gerold, G.; Kreppel, F.; Bravo-Rodriguez, K.; Pietschmann, T.; Holmes, V. M.; Palesch, D.; Zirafi, O.; Weissman, D.; Sowislok, A.; Wettig, B.; Heid, C.; Kirchhoff, F.; Weil, T.; Klärner, F. G.; Schrader, T.; Bitan, G.; Sanchez-Garcia, E.; Winter, R.; Shorter, J.; Munch, J. A Molecular Tweezer Antagonizes Seminal Amyloids and HIV Infection. *Elife* **2015**, *4* (AUGUST2015), 1–33. https://doi.org/10.7554/eLife.05397.

(12) MacKerell, A. D. J.; Bashford, D.; Bellott, M.; Dunbrack, R. L.; Evanseck, J. D.; Field, M. J.; Fischer, S.; Gao, J.; Guo, H.; Ha, S.; Joseph-McCarthy, D.; Kuchnir, L.; Kuczera, K.; Lau, F. T.; Mattos, C.; Michnick, S.; Ngo, T.; Nguyen, D. T.; Prodhom, B.; Reiher, W. E.; Roux, B.; Schlenkrich, M.; Smith, J. C.; Stote, R.; Straub, J.; Watanabe, M.; Wiórkiewicz-Kuczera, J.; Yin, D.; Karplus, M. All-Atom Empirical Potential for Molecular Modeling and Dynamics Studies of Proteins. *J. Phys. Chem. B* **1998**, *102* (18), 3586–3616. https://doi.org/10.1021/jp973084f.

(13) Jorgensen, W. L.; Chandrasekhar, J.; Madura, J. D.; Impey, R. W.; Klein, M. L. Comparison of Simple Potential Functions for Simulating Liquid Water. *J. Chem. Phys.* **1983**, *79* (2), 926–935. https://doi.org/10.1063/1.445869.
(14) Bier, D.; Rose, R.; Bravo-Rodriguez, K.; Bartel, M.; Ramirez-Anguita, J. M.; Dutt, S.; Wilch, C.; Klärner, F.-G.; Sanchez-Garcia, E.; Schrader, T.; Ottmann, C. Molecular Tweezers Modulate 14-3-3 Protein–Protein Interactions. *Nat. Chem.* **2013**, *5* (3), 234–239. https://doi.org/10.1038/nchem.1570.
(15) Dutt, S.; Wilch, C.; Gersthagen, T.; Talbiersky, P.; Bravo-Rodriguez, K.; Hanni, M.; Sánchez-García, E.; Ochsenfeld, C.; Klärner, F. G.; Schrader, T. Molecular Tweezers with Varying Anions: A Comparative Study. *J. Org. Chem.* **2013**, *78* (13), 6721–6734. https://doi.org/10.1021/jo4009673.
(16) Nanga, R. P. R.; Brender, J. R.; Vivekanandan, S.; Popovych, N.; Ramamoorthy, A. NMR Structure in a Membrane Environment Reveals Putative Amyloidogenic Regions of the SEVI Precursor Peptide PAP248−286. *J. Am. Chem. Soc.* **2009**, *131* (49), 17972–17979. https://doi.org/10.1021/ja908170s.
(17) Bennett, C. H. Efficient Estimation of Free Energy Differences from Monte Carlo Data. *J. Comput. Phys.* **1976**, *22* (2), 245–268. https://doi.org/10.1016/0021-9991(76)90078-4.
(18) Darve, E.; Rodríguez-Gómez, D.; Pohorille, A. Adaptive Biasing Force Method for Scalar and Vector Free Energy Calculations. *J. Chem. Phys.* **2008**, *128* (14), 144120. https://doi.org/10.1063/1.2829861.
(19) Jo, S.; Kim, T.; Iyer, V. G.; Im, W. CHARMM-GUI: A Web-Based Graphical User Interface for CHARMM. *J. Comput. Chem.* **2008**, *29* (11), 1859–1865. https://doi.org/10.1002/jcc.20945.
(20) Wu, E. L.; Cheng, X.; Jo, S.; Rui, H.; Song, K. C.; Dávila-Contreras, E. M.; Qi, Y.; Lee, J.; Monje-Galvan, V.; Venable, R. M.; Klauda, J. B.; Im, W. CHARMM-GUI Membrane Builder toward Realistic Biological Membrane Simulations. *J. Comput. Chem.* **2014**, *35* (27), 1997–2004. https://doi.org/10.1002/jcc.23702.
(21) Grubmüller, H.; Heymann, B.; Tavan, P. Ligand Binding: Molecular Mechanics Calculation of the Streptavidin-Biotin Rupture Force. *Science (80-.).* **1996**, *271* (5251), 997–999. https://doi.org/10.1126/science.271.5251.997.
(22) Park, S.; Khalili-Araghi, F.; Tajkhorshid, E.; Schulten, K. Free Energy Calculation from Steered Molecular Dynamics Simulations Using Jarzynski's Equality. *J. Chem. Phys.* **2003**, *119* (6), 3559–3566. https://doi.org/10.1063/1.1590311.
(23) Lee, C.; Yang, W.; Parr, R. G. Development of the Colle-Salvetti Correlation-Energy Formula into a Functional of the Electron Density. *Phys. Rev. B* **1988**, *37* (2), 785–789. https://doi.org/10.1103/PhysRevB.37.785.
(24) Ahlrichs, R.; Bär, M.; Häser, M.; Horn, H.; Kölmel, C. Electronic Structure Calculations on Workstation Computers: The Program System Turbomole. *Chem. Phys. Lett.* **1989**, *162* (3), 165–169. https://doi.org/10.1016/0009-2614(89)85118-8.
(25) Grimme, S.; Ehrlich, S.; Goerigk, L. Effect of the Damping Function in Dispersion Corrected Density Functional Theory. *J. Comput. Chem.* **2011**, *32* (7), 1456–1465. https://doi.org/10.1002/jcc.21759.
(26) Metz, S.; Kästner, J.; Sokol, A. A.; Keal, T. W.; Sherwood, P. ChemShell-a Modular Software Package for QM/MM Simulations. *Wiley Interdiscip. Rev. Comput. Mol. Sci.* **2014**, *4* (2), 101–110. https://doi.org/10.1002/wcms.1163.
(27) Bakowies, D.; Thiel, W. Hybrid Models for Combined Quantum Mechanical and Molecular Mechanical Approaches. *J. Phys. Chem.* **1996**, *100* (25), 10580–10594. https://doi.org/10.1021/jp9536514.
(28) de Vries, A. H.; Sherwood, P.; Collins, S. J.; Rigby, A. M.; Rigutto, M.; Kramer, G. J. Zeolite Structure and Reactivity by Combined Quantum-Chemical−Classical

Calculations. *J. Phys. Chem. B* **2002**, *103* (29), 6133–6141. https://doi.org/10.1021/jp9913012.
(29) Antes, I.; Thiel, W. On the Treatment of Link Atoms in Hybrid Methods. In *Combined Quantum Mechanical and Molecular Mechanical Methods*; ACS Symposium Series; American Chemical Society, 2009; Vol. 712, pp 50–65. https://doi.org/10.1021/bk-1998-0712.ch004.
(30) Todorov, I. T.; Smith, W. DL_POLY_3: The CCP5 National UK Code for Molecular-Dynamics Simulations. *Philosophical Transactions: Mathematical, Physical and Engineering Sciences*. Royal Society 2004, pp 1835–1852. https://doi.org/10.2307/4142464.
(31) Talbiersky, P.; Bastkowski, F.; Klärner, F. G.; Schrader, T. Molecular Clip and Tweezer Introduce New Mechanisms of Enzyme Inhibition. *J. Am. Chem. Soc.* **2008**, *130* (30), 9824–9828. https://doi.org/10.1021/ja801441j.
(32) Fokkens, M.; Jasper, C.; Schrader, T.; Koziol, F.; Ochsenfeld, C.; Polkowska, J.; Lobert, M.; Kahlert, B.; Klärner, F. G. Selective Complexation of N-Alkylpyridinium Salts: Binding of NAD + in Water. *Chem. - A Eur. J.* **2005**, *11* (2), 477–494. https://doi.org/10.1002/chem.200400603.
(33) Schrader, T.; Fokkens, M.; Klärner, F.-G.; Polkowska, J.; Bastkowski, F. Inclusion of Thiamine Diphosphate and S-Adenosylmethionine at Their Chemically Active Sites. *J. Org. Chem.* **2005**, *70* (25), 10227–10237. https://doi.org/10.1021/jo0511896.
(34) Arnold, F.; Schnell, J.; Zirafi, O.; Sturzel, C.; Meier, C.; Weil, T.; Standker, L.; Forssmann, W.-G.; Roan, N. R.; Greene, W. C.; Kirchhoff, F.; Munch, J. Naturally Occurring Fragments from Two Distinct Regions of the Prostatic Acid Phosphatase Form Amyloidogenic Enhancers of HIV Infection. *J. Virol.* **2012**, *86* (2), 1244–1249. https://doi.org/10.1128/jvi.06121-11.
(35) Münch, J.; Rücker, E.; Ständker, L.; Adermann, K.; Goffinet, C.; Schindler, M.; Wildum, S.; Chinnadurai, R.; Rajan, D.; Specht, A.; Giménez-Gallego, G.; Sánchez, P. C.; Fowler, D. M.; Koulov, A.; Kelly, J. W.; Mothes, W.; Grivel, J. C.; Margolis, L.; Keppler, O. T.; Forssmann, W. G.; Kirchhoff, F. Semen-Derived Amyloid Fibrils Drastically Enhance HIV Infection. *Cell* **2007**, *131* (6), 1059–1071. https://doi.org/10.1016/j.cell.2007.10.014.
(36) Roan, N. R.; Müller, J. A.; Liu, H.; Chu, S.; Arnold, F.; Stürzel, C. M.; Walther, P.; Dong, M.; Witkowska, H. E.; Kirchhoff, F.; Münch, J.; Greene, W. C. Peptides Released by Physiological Cleavage of Semen Coagulum Proteins Form Amyloids That Enhance HIV Infection. *Cell Host Microbe* **2011**, *10* (6), 541–550. https://doi.org/10.1016/j.chom.2011.10.010.
(37) Müller, J. A.; Harms, M.; Schubert, A.; Mayer, B.; Jansen, S.; Herbeuval, J. P.; Michel, D.; Mertens, T.; Vapalahti, O.; Schmidt-Chanasit, J.; Münch, J. Development of a High-Throughput Colorimetric Zika Virus Infection Assay. *Med. Microbiol. Immunol.* **2017**, *206* (2), 175–185. https://doi.org/10.1007/s00430-017-0493-2.
(38) Reed, L. J.; Muench, H. A Simple Method of Estimating Fifty per Cent Endpoints. *Am. J. Epidemiol.* **1938**, *27* (3), 493–497. https://doi.org/10.1093/oxfordjournals.aje.a118408.
(39) Schandock, F.; Riber, C. F.; Röcker, A.; Müller, J. A.; Harms, M.; Gajda, P.; Zuwala, K.; Andersen, A. H. F.; Løvschall, K. B.; Tolstrup, M.; Kreppel, F.; Münch, J.; Zelikin, A. N. Macromolecular Antiviral Agents against Zika, Ebola, SARS, and Other Pathogenic Viruses. *Adv. Healthc. Mater.* **2017**, *6* (23), 1700748. https://doi.org/10.1002/adhm.201700748.
(40) Röcker, A. E.; Müller, J. A.; Dietzel, E.; Harms, M.; Krüger, F.; Heid, C.; Sowislok, A.; Riber, C. F.; Kupke, A.; Lippold, S.; von Einem, J.; Beer, J.; Knöll, B.; Becker, S.; Schmidt-Chanasit, J.; Otto, M.; Vapalahti, O.; Zelikin, A. N.; Bitan, G.; Schrader, T.;

Münch, J. The Molecular Tweezer CLR01 Inhibits Ebola and Zika Virus Infection. *Antiviral Res.* **2018**, *152*, 26–35. https://doi.org/10.1016/j.antiviral.2018.02.003.
(41) Sparrer, K. M. J.; Gableske, S.; Zurenski, M. A.; Parker, Z. M.; Full, F.; Baumgart, G. J.; Kato, J.; Pacheco-Rodriguez, G.; Liang, C.; Pornillos, O.; Moss, J.; Vaughan, M.; Gack, M. U. TRIM23 Mediates Virus-Induced Autophagy via Activation of TBK1. *Nat. Microbiol.* **2017**, *2* (11), 1543–1557. https://doi.org/10.1038/s41564-017-0017-2.
(42) Runge, S.; Sparrer, K. M. J.; Lässig, C.; Hembach, K.; Baum, A.; García-Sastre, A.; Söding, J.; Conzelmann, K. K.; Hopfner, K. P. In Vivo Ligands of MDA5 and RIG-I in Measles Virus-Infected Cells. *PLoS Pathog.* **2014**, *10* (4), e1004081. https://doi.org/10.1371/journal.ppat.1004081.